



SATHYABAMA

**INSTITUTE OF SCIENCE AND TECHNOLOGY
(DEEMED TO BE UNIVERSITY)**

Accredited "A" Grade by NAAC | 12B Status by UGC | Approved by AICTE

www.sathyabama.ac.in

**SCHOOL OF MECHANICAL ENGINEERING
DEPARTMENT OF AUTOMOBILE ENGINEERING**

SAU1601 AUTOMOTIVE AERODYNAMICS

UNIT I INTRODUCTION TO AUTOMOTIVE AERODYNAMICS

I. Introduction

Automotive Aerodynamics is the study of air flows around and through the vehicle body. More generally, it can be labelled “Fluid Dynamics” because air is really just a very thin type of fluid. Above slow speeds, the air flow around and through a vehicle begins to have a more pronounced effect on the acceleration, top speed, fuel efficiency and handling.

Influence of flow characteristics and improvement of flow past vehicle bodies

- Reduction of fuel consumption
- More favourable comfort characteristics (mud deposition on body, noise, ventilating and cooling of passenger compartment)
- Improvement of driving characteristics (stability, handling, traffic safety)

Scope of Vehicle Aerodynamics

The Flow processes to which a moving vehicle is subjected fall into 3 categories:

1. Flow of air around the vehicle
2. Flow of air through the vehicle's body
3. Flow processes within the vehicle's machinery.



The flow of air through the engine compartment is directly dependent upon the flow field around the vehicle. Both fields must be considered together. On the other hand, the flow processes within the engine and transmission are not directly connected with the first two, and are not treated here. The external flow subjects the vehicle to forces and moments which greatly influence the vehicle's performance and directional stability.

These two effects, and has only lately focused on the need to keep the windows and lights free of dirt and accumulated rain water, to reduce wind noise, to prevent windscreen wipers lifting, and to cool the engine oil sump and brakes, etc. The streamlines follow the contour of the vehicle over long stretches, even in the area of sharp curves; the air flow separates at the rear edge of the roof, forming a large wake which can be observed by introducing smoke into the bubble behind the vehicle.

The aerodynamic drag D , as well as the other force components and moments, increases with the square of the vehicle speed V :

$$D \sim V^2$$

The scope for improving economy by reducing aerodynamic drag of the vehicle. For this reason drag remains the focal point of vehicle aerodynamics, whether the objective is speed or fuel economy.

$$D = c_D A \frac{\rho}{2} V^2$$

Where,

c_D is the non-dimensional drag coefficient;
 A is the projected frontal area of the vehicle
 ρ is the density of the surrounding air.

The drag D of a vehicle is determined by its frontal area A , and by its shape, the aerodynamic quality of which is described by the drag coefficient c_D . Generally the vehicle size, and frontal area, is determined by the design requirements, and efforts to reduce drag are concentrated on reducing the drag coefficient. The pressure difference between the upper and lower sides of the vehicle produces a resultant force, at right angles to the direction of motion, which is called lift. As a rule the lift is in the upward direction, i.e. it tends to lift the vehicle and therefore reduces effective wheel loads. It is coupled with a pitching moment, which differentially affects the wheel loads at the front and rear.

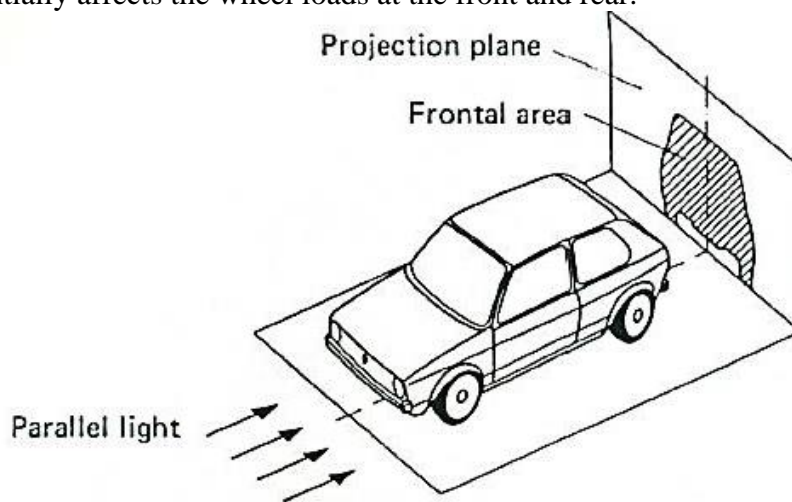


Fig. Frontal Area of a Vehicle

Cross-winds

The air flow around the vehicle is asymmetric to the longitudinal centre plane. The shape of the car must be such that the additional forces and moments remain so small that the directional stability is not greatly affected. First, the need to react to a cross-wind of varying intensity and direction is inconvenient, as the driver must continually apply steering corrections.

However, it is also important to prevent drivers from being surprised by side-wind gusts, and being unable to react quickly enough. Better design of roads and their surroundings can help to overcome this problem.

Soiling of the rear of the vehicle can be studied from the wake flow. Dust or dirty water is whirled up by the wheels, and dust particles and water droplets distributed throughout the entire wake region by turbulent mixing, and deposited on the rear of the vehicle. Since the flow pattern at the rear has a significant influence upon the aerodynamic drag.

History of the Vehicle Aerodynamics in passenger cars

Initial development concentrated exclusively on drag, and the problem of cross-wind sensitivity only arose with increasing driving speeds. Lately attempts have been made, by suitable shaping, to eliminate the deposition of dirt and water on the windows and lights.

This brief account of the history of automobile aerodynamics has two aims. The first is to show which work contributed to the development of automobile aerodynamics; the second illustrates how this knowledge was applied to automobile design. The many attempts to apply the growing aerodynamic knowledge to production cars
















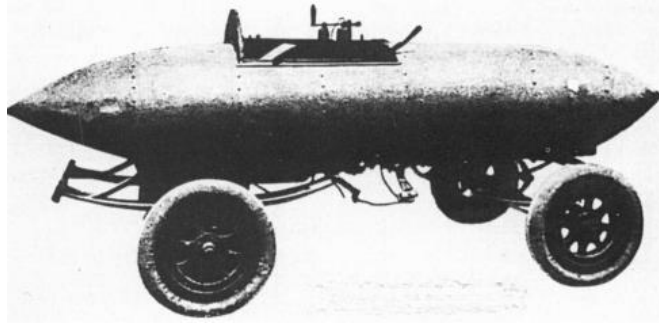
Basic shapes	1900 to 1930	   Torpedo Boat tail Air ship	
	1921 to 1923	 Rumpler	 Bugatti
Streamlined cars	1922 to 1939	  Jaray	
	1934 to 1939	 Kamm	 Schlör
	Since 1955	 Citroen	 NSU-Ro 80
Detail optimization	Since 1974	 VW-Scirocco I	 VW-Golf I
Shape optimization	Since 1983	 Audi 100 III	 Ford Sierra

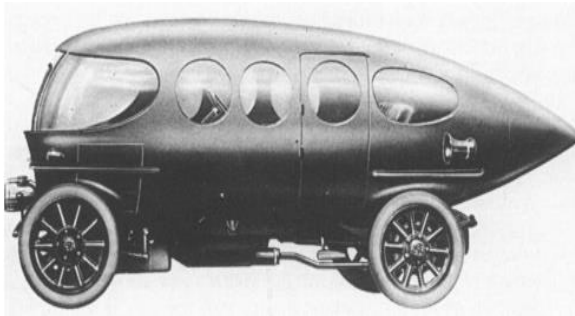
Fig: Four Primary Phases of Car Aerodynamics

a) Basic shapes

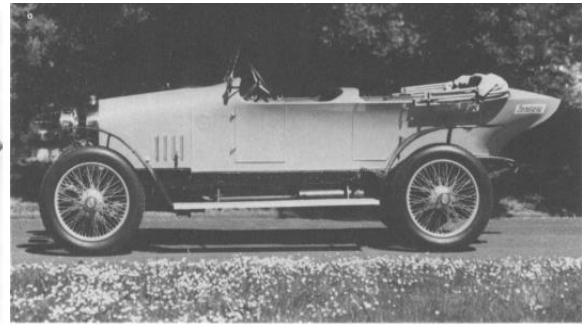
In the first phase, dating from the turn of the century, an attempt was made to apply to the automobile streamlined shapes from other disciplines such as naval architecture and airship engineering. They were little suited to the automobile, for instance the 'airship form', or ineffective, for instance the 'boat tail'. Due to the poor roads and low engine power, speeds were still so low that aerodynamic drag only played a subordinate role. Most cars derived from these basic shapes had one error in common: they neglected the fact that the flow past a body of revolution is no longer axially symmetrical when the body is close to the ground, and when wheels and axles are added. In spite of this, shapes represented great progress toward lower drag in comparison to shapes based on the horse-drawn carriage.



Record-breaking car from Camille Jenatton, 1899



Alfa-Romeo of Count Ricotti, 1913

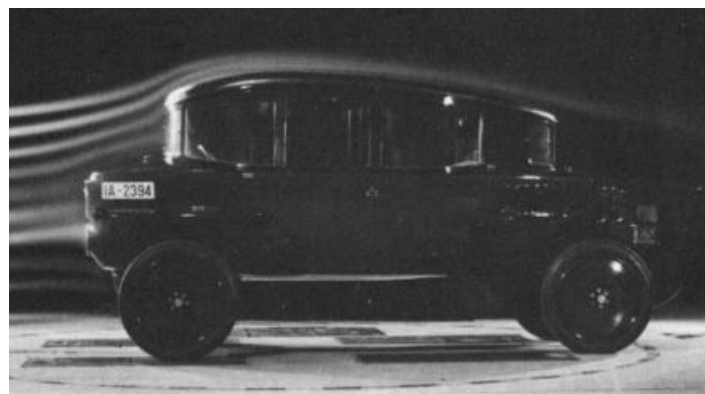


Boat-tailed 'Audi-Alpensieger', 1913

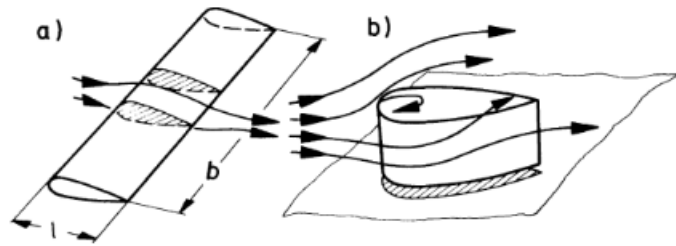
b) Streamlined shapes

The analysis of the tractive resistance of road vehicles carried out by Riedler in 1911 gave vehicle aerodynamics a rational basis. The more Prandtl and Eiffel worked out the nature of aerodynamic drag, the more this knowledge was used to explain the aerodynamic drag of cars; see for instance Aston. However, getting away from Newton's 'Impact Theory' was a very slow process.

After the First World War, the design of streamlined bodies started at a number of locations simultaneously. E. Rumpler, who had become well known through his successful aircraft, the 'Rumpler-Taube', developed several vehicles which he designated 'teardrop cars'. The most famous Rumpler limousine was shown in the figure. In order to make use of the narrow space in the rear of the vehicle, Rumpler decided on a rear engine configuration. Viewed from the top, his car has the shape of an aerofoil. But the roof is also well streamlined, thus proving that Rumpler was aware of the three-dimensional character of the flow field.



Rumpler Car model – streamline air flow



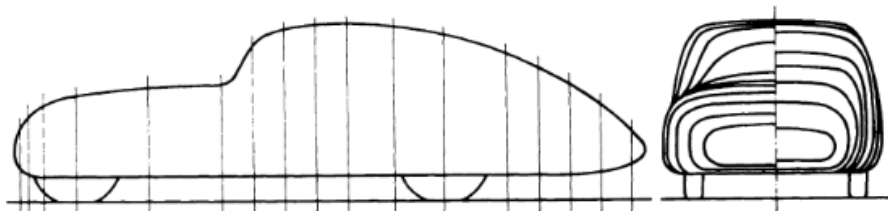
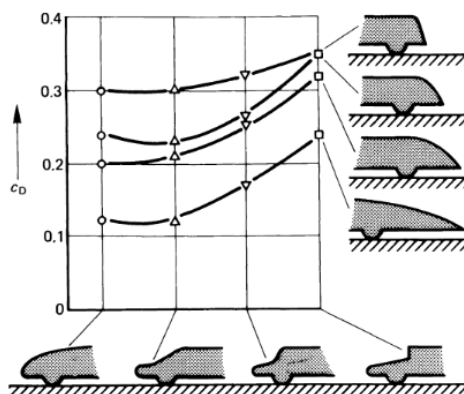
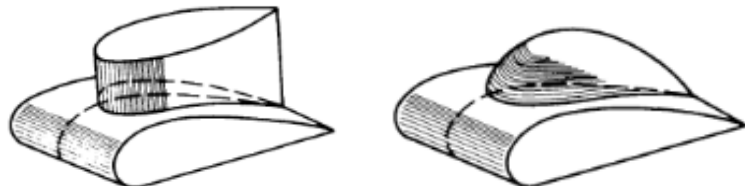
(a) Two-dimensional flow around a profile; (b) three-dimensional flow field around a profile section close to ground

An original Rumpler car provided by the Deutsches Museum in Munich, gave the following results:

Frontal area $A = 2.57 \text{ m}^2$; drag coefficient $c_D = 0.28$

On the Rumpler car the wheels are uncovered, resulting in an increase in drag, which becomes more significant as the aerodynamic quality of the vehicle body improves. The flow around a body of revolution, which has a very low drag coefficient in free air, is no longer axially symmetrical when close to the ground. As a result the drag increases, owing to the flow separation occurring at the rear upper side. The limit, where the ground clearance approaches zero, the optimum shape in terms of drag is a half-body, which forms a complete body of revolution together with its mirror image—produced through reflection from the roadway.

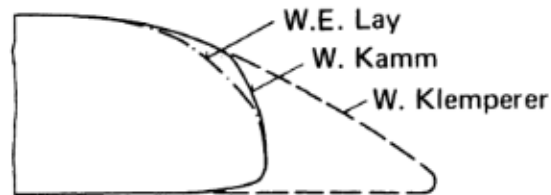
	$A_{1:1} [\text{m}^2]$	c_D
	2.99	0.64
Large Jaray cars	2.86	0.30
Small Jaray car	1.87	0.29
	2.99	
Half-body without wheels	front with sharp edges	0.13
	front edges rounded	0.09
Half-body with wheels		0.15



Lange car; length l to height h , $l/h = 3.52$; $C_D = 0.14$ to 0.16 , completely smooth model

Influence of main body parameters on the drag of a car and their interactions

The blunt rear end shape which first occurred in the work of Lay led to the development of the 'Kamm-back', which combined the advantage of greater headroom in the back seat with that of low drag. The Kamm-back, the Lay blunt back and Klemperer's long-tail design are compared. The low drag is achieved because the flow remains attached for as long as possible and is then forced to separate by cutting off the rear end at an already much diminished cross-sectional area. This results in a small wake. By tapering the body moderately, the flow is subjected to a pressure increase which ensures that the pressure at the rear of the vehicle, the 'base pressure', is comparatively high, which itself then reduces the overall drag.



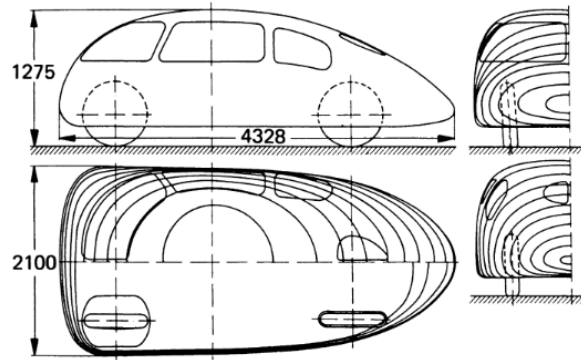
Comparison of three different rear end shapes

Type of measurement	Everling, 1938	Kamm K5, 1939	DB 170 V
Model Expected for full scale car	 $A = 2.24 \text{ m}^2$ $c_D = 0.15$	 $A = 2.17 \text{ m}^2$ $c_D = 0.24$	 $c_D = 0.48$
	$c_D = 0.24$		
Coast down	$c_D = 0.31$	$c_D = 0.24$	$c_D = 0.48$
Wind tunnel, full scale		$c_D = 0.37$	$0.52 < c_D < 0.55$ $\overline{c_D} = 0.55$

Vehicle aerodynamics initially concentrated on the drag in still air conditions (symmetrical oncoming flow), the problems of side wind as well as cooling and ventilation soon became apparent whose results showed that drag varied little with increasing yaw angle for 'sharp edged' cars which already had high aerodynamic drag, but decreased sharply—after a slight increase—with streamlined shapes.



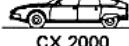
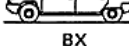
Author Year Scale	Optimized halfbody shape	Car for comparison
W.T. Fishleigh 1931 M 1:4	 drag-ratio 1:2.6	
R. H. Heald 1933 1:15	 $c_D = 0.24$ $c_D = 0.20$	 $c_D = 0.67$ $c_D = 0.74$ $c_D = 0.71$ $c_D = 0.55$
W.E. Lay 1933 1:8	 $c_D = 0.30 \ 0.24 \ 0.20 \ 0.13$	 $c_D = 0.61$
E.G. Reid 1935	 $c_D = 0.15 \div 0.20$	 $c_D = 0.61$

Bodies with low aerodynamic drag

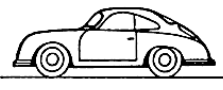
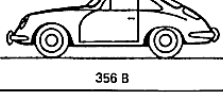
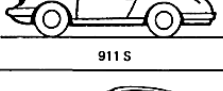
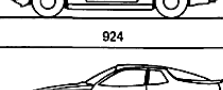
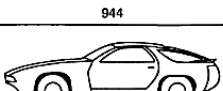
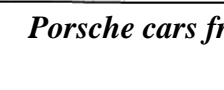


Plan and sectional elevation of scholar car

The development of streamlined automobiles was interrupted by the Second World War. Citroen and Panhard were the only car manufacturers resuming this development after the war the GS and the CX are more closely related to Kamm's ideas (cut-off rear end). All three models have an extremely low drag coefficient in comparison to their contemporary competitors.

	Model Year	A [m ²]	c _D
 ID 19	1956	2.14	0.38
 GS	1970	1.77	0.37
 CX 2000	1974	1.96	0.40
 BX	1982	1.89	0.33 – 0.34

Model line-up of citroen cars 1956 to 1982

	Model year	A [m ²]	c _D
 356 A	1950	1.61	0.34
 356 B	1959	1.61	0.38-0.40
 911 S	1976	1.77	0.40
 924	1975	1.79	0.33
 944	1981	1.82	0.35
 928 S	1977	1.95	0.38

Porsche cars from 1950 to present

c) Optimization of body details

The success of modern streamlined cars, aerodynamics has only recently become the dominating design criterion. Previously, ways were found of adapting aerodynamics to practical automotive engineering requirements of styling, packaging, safety, comfort and production. The method of optimizing body details were developed by Hucho, Janssen and Emmelmann.

The starting point for aerodynamic development is the stylistic design; modifications to the shape must be made within the styling concept. Details such as radii, curvature, taper, spoilers etc. are modified in sequence or where required, in combination, step by step, to prevent separation or to control the separation so that the drag is minimized. Practice has shown that in comparison to the initial shape considerable reductions in the drag can be achieved.

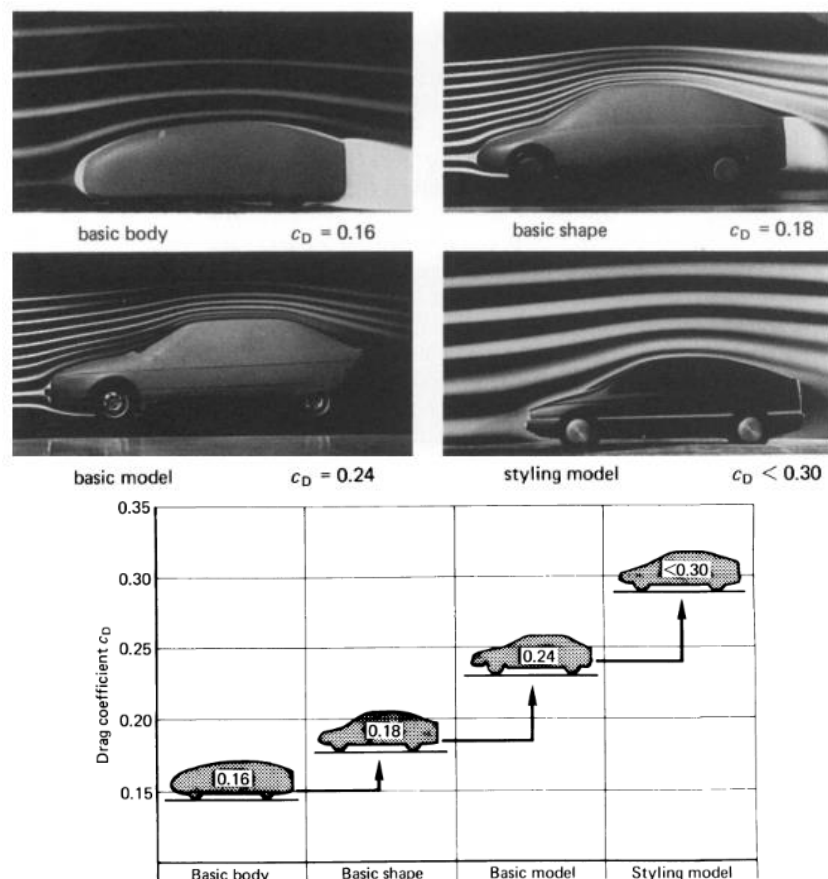
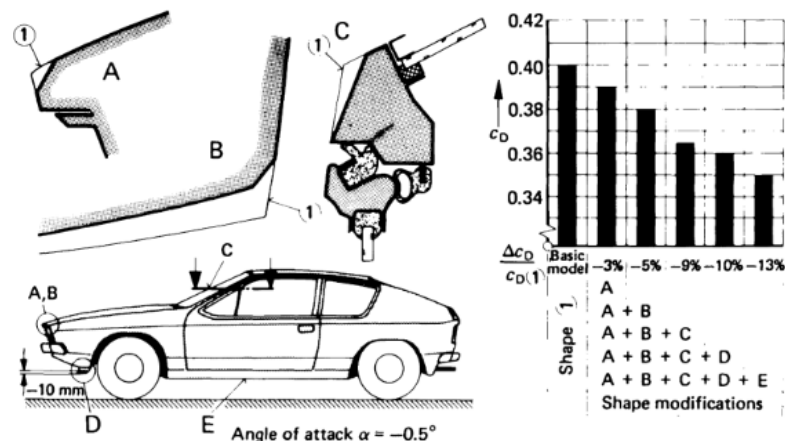


Fig. Development of low drag car body

Flow Phenomenon Related the Vehicles

- External flow (all details its surface)
- Internal flow (ducts, passenger compartment, engine compartment)

a) External flow:

The external flow around a vehicle is shown in Fig. In still air, the undisturbed velocity V_∞ is the road speed of the car. Provided no flow separation takes place, the viscous effect in the fluid are restricted to a thin layer of a few millimeters thickness, called the boundary layer. Beyond this layer the flow can be regarded as inviscid, and its pressure is imposed on the boundary layer. Within the boundary layer the velocity decreases from the value of the inviscid external flow at the outer edge of the boundary layer to zero at the wall, where the fluid fulfills a no-slip condition. When the flow separates the boundary layer is "dispersed" and the flow is entirely governed by viscous effects. Such regions are quite significant as compared to the characteristic length of the vehicle. At some distance from the vehicle there exists no velocity difference between the free stream and the ground. Therefore, in vehicle-fixed coordinates, the ground plane is a stream surface with constant velocity and at this surface there is no boundary layer present.

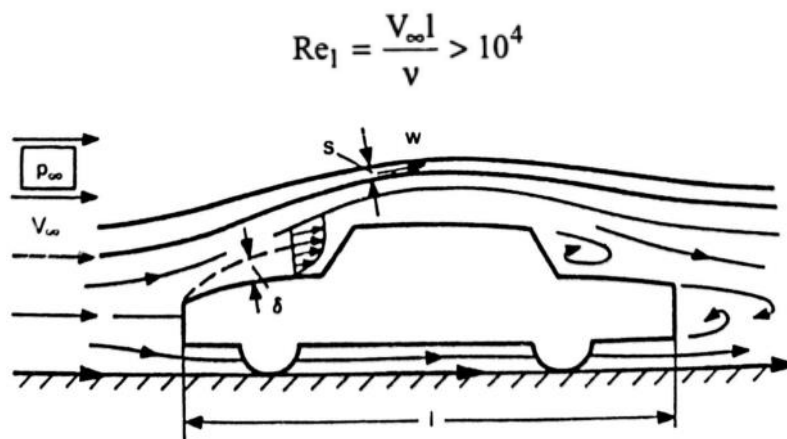


Fig: Flow around a vehicle

The law of mass conservation has to be formulated. The simplest form of his law is for incompressible flow (constant):

$$W \cdot S = \text{Constant}$$

where S denotes the local cross-section of a small stream-tube and W is the local velocity, which is assumed to be constant across S indicates narrow distances between streamlines in regions of high velocity and vice versa.

$$p_t = p + \frac{\rho}{2} w^2 = \text{const}$$

Furthermore the flow obeys Newton's well-known law of momentum conservation: Mass times acceleration is equal to the sum of the acting forces. If this law is applied to an inviscid flow, it turns out that inertia forces and pressure forces are balanced. The integration of the momentum equation along a streamline for incompressible flow leads to

$$p_t = p_\infty + \frac{\rho}{2} V_\infty^2 = \text{const}$$

In inviscid flow, the sum of static pressure and dynamic pressure is constant along a streamline, indicates low pressure in regions of high local velocities and vice versa. Where the flow comes to rest, $w = 0$, a so-called "stagnation point" is formed, al on the nose of a vehicle. The static pressure there will be equal to the total pressure, and this is the highest possible pressure in the flow field.

Applications:

The fundamental equations for inviscid flow may be applied to simple examples related to vehicle aerodynamics and experimental techniques. The two-dimensional flow around a vehicle-shaped body as shown in below figure. This flow is a considerable simplification of a three-dimensional flow around a vehicle, and may be regarded as a qualitative picture of the flow at the longitudinal cross-section of a car. The upper part of the figure indicates the streamlines. Three stagnation points occur: in the nose region, in the cove between hood and windshield (scuttle), and at the trailing edge. The pressure distribution on the contour is drawn schematically as $c_p(x/l)$ in the lower half of the figure

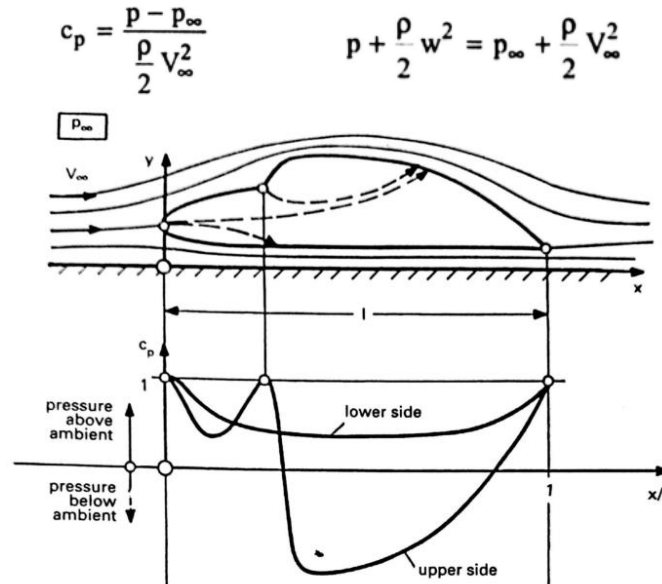


Fig: Flow field and pressure distribution for a vehicle-shaped body in two-dimensional flow

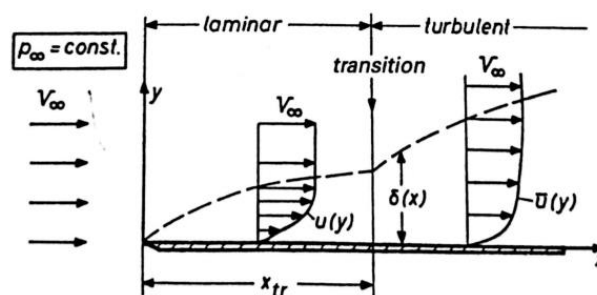
Effects of viscosity

Despite the thinness of the boundary layer at the wall; the viscous flow within it has a strong influence on the development of the whole flow field. The occurrence of drag in two-dimensional incompressible flow can be explained only by these viscous effects.

Laminar and turbulent boundary layer development

The flow in a boundary layer along a thin flat plate is shown in Fig. The corresponding external flow has parallel streamlines and both velocity V_∞ and pressure p_∞ are constant. The viscous flow within the boundary layer fulfills the "no-slip" condition along the wall. In the front part of the plate the boundary layer flow is steady and (almost) parallel to the wall. This state of the flow is called laminar. The thickness of the boundary layer increases downstream according to

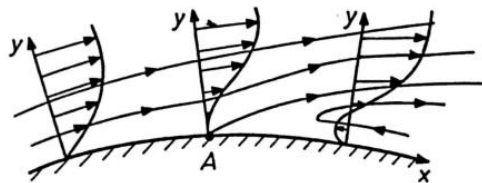
$$\delta \sim \sqrt{\frac{\nu x}{V_\infty}}$$



Separation

Laminar and turbulent boundary layer flow strongly depends on the pressure distribution which is imposed by the external flow. For pressure increase in flow direction the boundary layer flow is retarded. Especially near the wall and even reverse flow may occur. It can be seen that forward and reverse flow a dividing streamline leaves the wall. This phenomenon is called separation. For the separation point A, the condition holds. Turbulent boundary layers can withstand much steeper adverse pressure gradients without separation than laminar boundary layers. This is because the turbulent mixing process leads to an intensive momentum transport from the outer flow towards the flow adjacent to the wall. For a pressure decrease in flow direction there exists no tendency to flow separation.

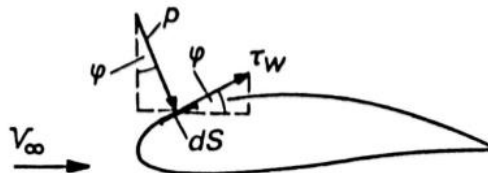
$$\left(\frac{du}{dy} \right)_w = 0$$



Frictional Drag

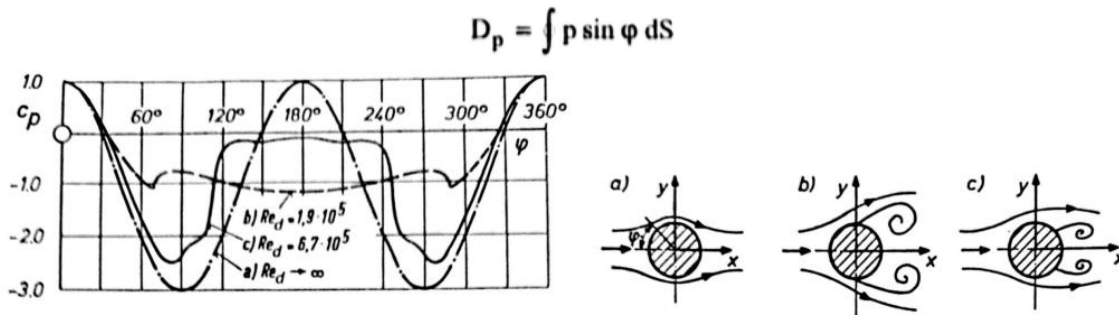
In a viscous fluid a velocity gradient du/dy is present at the wall. Due to molecular friction a shear stress acts everywhere on the surface of the body as indicated in Fig. The integration of the corresponding force components in the free-stream direction according to leads to the so-called friction drag D_f . In the absence of flow separation, this is the main contribution to the total drag of a body in two-dimensional viscous flow. Two examples may illustrate this.

$$D_f = \oint \tau_w \cos \varphi \, dS \quad c_D = \frac{0.91}{(\log Re_l)^{2.58}} \quad (\text{for } Re_l > 10^7)$$



Pressure Drag

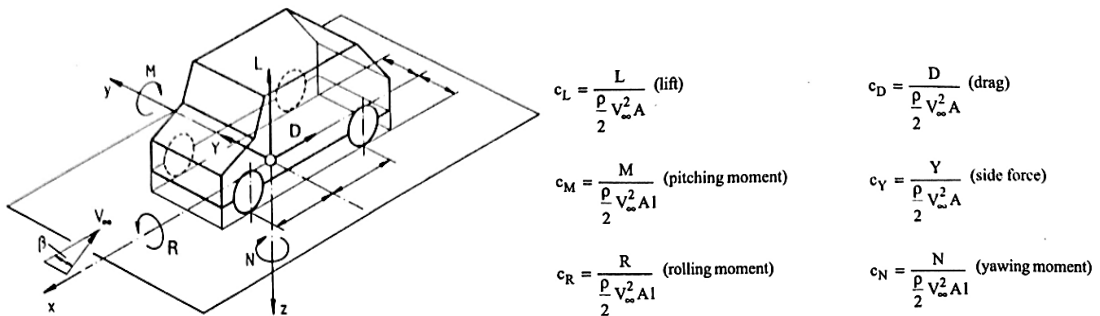
Blunt bodies, such as a circular cylinder, a sphere, or a flat plate normal to the flow, show quite different drag characteristics. On the rear part of such bodies in inviscid flow, extremely steep adverse pressure gradients would occur which lead to flow separation in viscous flow. The pressure distribution is thereby considerably altered when compared to the theoretical case of inviscid flow. The pressure distribution for a circular cylinder. In the front part the pressure distribution is similar to that in inviscid flow, whereas on the rear part the flow separation leads to considerable suction. The pressure distribution is therefore asymmetrical with respect to the y-axis. Integrating the force components in the free-stream direction, resulting from the pressure distribution, gives the so-called "pressure drag" D_p . For blunt bodies the pressure drag is predominant as compared to friction drag resulting from the shear stresses at the wall.



Forces and moments

In symmetrical flow the drag D is accompanied by a lift force L . Furthermore, a pitching moment M with respect to the lateral axis (y -axis) is present. The three components L , D , and M completely determine the vector of the resulting air force. Since the pitching moment reference point is known (generally in vehicle aerodynamics it is located on the surface of the road in the middle of wheelbase and track), the additional forces acting at the front and rear axle resulting from the flow around the vehicle can be easily evaluated.

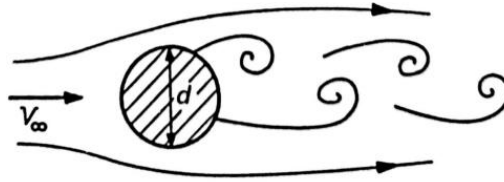
In crosswind condition, an asymmetrical flow field around the vehicle is present. In this case, in addition to the forces and moments mentioned so far, a side force Y is observed. Furthermore, there occurs a rolling moment R with respect to the longitudinal axis (x -axis) and a yawing moment N with respect to the vertical axis (z -axis). Thus six components, L , D , M , and Y , R , N , determine the vector of the total force. For a known position of the reference point the additional forces acting at the four wheels of the vehicle can be evaluated.



Aerodynamic Noise

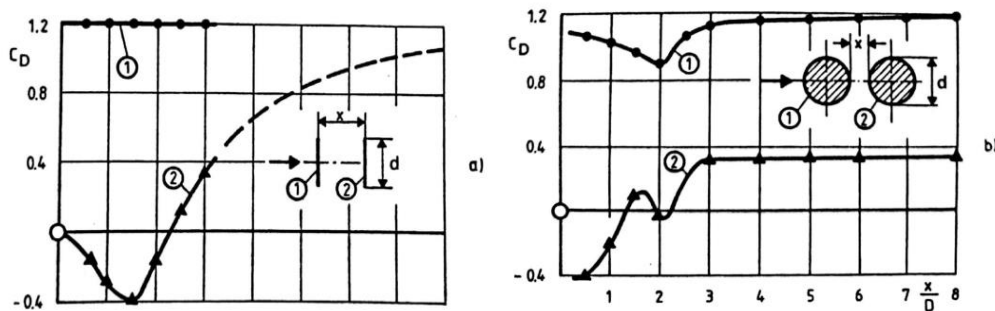
In almost all cases the physical reason is periodic flow separation from certain elements of the surface-gutters, mirrors, and the radio antenna, for instance. Such a periodic flow separation is sketched for a circular cylinder. It is present in the Reynolds number range $60 < Re_d < 5000$. For smaller Reynolds numbers a non-periodic, symmetrical wake occurs, whereas for larger Reynolds numbers a turbulent mixing process without the existence of discrete vortices can be observed.

In the region of periodic flow separation, vortices are shed from both sides of the body in alternating sequence. These vortices move downstream in the wake and they can be observed over a long distance. In a coordinate system moving downstream with the vortices, a regular pattern of these vortices is found, which is called a von Kármán vortex street. Due to periodic vortex shedding, the whole flow field is basically unsteady. At a certain point of the flow field, all flow quantities change with the frequency n of the vortex separation from the body.



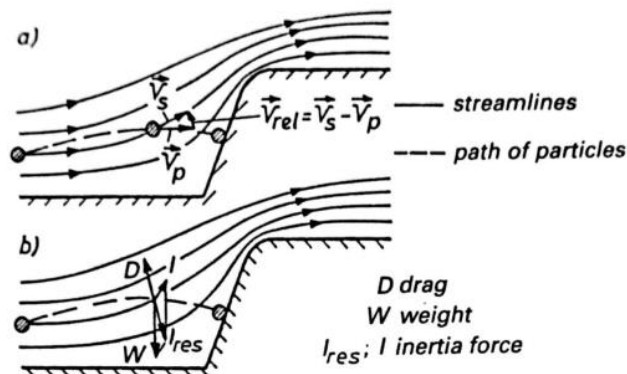
Body to Body Interference

Rarely vehicles are on the road alone. They pass each other or they meet; they follow each other in short distances, be it on the highway or on a racing track. The flow field of each vehicle is then influenced by the fields of the others: the flow fields interfere with each other. Furthermore, vehicles are made up from more than one body. The outside mirrors are located in the flow field of the main body. Car and caravan, cab and trailer of a tractor-trailer truck are very close to each other. The drag D_{1+2} of a configuration consisting of two bodies 1 and 2 are not necessarily the sum of the drag of the single bodies measured in undisturbed flow. The difference, the so-called interference drag.



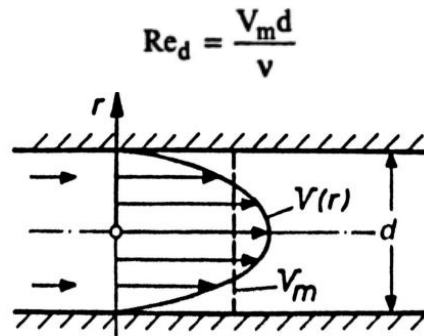
Transport of solids

The flow around a vehicle may contain different inhomogeneities such as raindrops, mud particles, and insects. The behavior of these particles in the flow field of the vehicle is very important for the everyday use of the vehicle. The motion of particles in a flow field, the density of which is different from that of the fluid. The flight paths of the particles and the streamlines are different. For an arbitrarily located point of the flow field the local flow velocity \vec{V}_s is tangential to the streamline and the local particle velocity \vec{V}_p is tangential to the flight path. Thus the flow around the particle is governed by the relative velocity and the drag force D acts on the particle in the direction of this relative velocity. For asymmetrical particle shapes a lift force also may be present, but this is not taken into account for the present considerations. The flight path and the velocity of the particle on it have to adjust in such a way that the resulting inertia force compensates for the drag of the particle, as indicated in Fig. This inertia force contains the gravitational acceleration as well as all other accelerations resulting from the changes in magnitude and direction of the velocity vector of the particle.

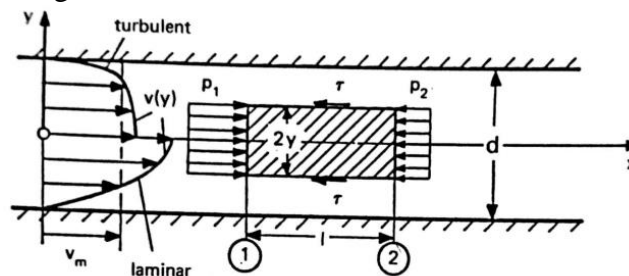


b) Internal flow:

Internal flow is a flow which is surrounded by walls. All streamlines are parallel to the pipe axis. In general, internal flows cannot be divided into an inviscid flow far away from the walls and a viscous boundary-layer flow close to the walls. The effects of viscosity are found everywhere in the flow field. The development of an internal viscous flow is again characterized by the Reynolds number.



Internal flow cannot be split up into an inviscid outa' flow and a viscous boundary layer flow close to the wall. In general, the viscous effects extend over the whole cross-section. Therefore, in the equations of motion, the viscous forces have to be taken into account from the beginning.



The velocity distribution $V(y)$ is the same for all cross-sections $x = \text{const}$. No acceleration is present in the flow and therefore no inertia forces occur. The pressure is constant over the cross-section and, due to the friction forces, a pressure difference $P_1 - P_2 > 0$ between the two sections 1 and 2 must exist to move the fluid against the friction drag through the pipe. This means that the friction effects cause a pressure decrease in flow direction which is called pressure loss due to friction. If this pressure loss is taken into account, Bernoulli's equation,

$$P_1 + \frac{\rho}{2} V_{m1}^2 = P_2 + \frac{\rho}{2} V_{m2}^2 + \Delta p$$

In this equation the internal flow is regarded as a one-dimensional problem. The pressure p and the mean velocity V_m are constant over the cross-section S , and all quantities depend only on the coordinate x in the flow direction are valid only for flows in which no or only negligibly small variations of the geodetic height occur. If such variations are taken into account, terms resulting from hydrostatics have to be added on each side

$$P_1 + \frac{\rho}{2} V_{m1}^2 + \rho g h_1 = P_2 + \frac{\rho}{2} V_{m2}^2 + \rho g h_2 + \Delta p$$

Applications

Laminar and Turbulent Pipe Flow

At a certain distance downstream of the entrance of a pipe the velocity distribution over the cross-section ceases to change. This state is called the fully developed pipe flow

$$P_1 - P_2 = \Delta p$$

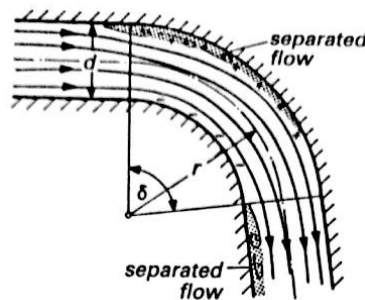
The flow through a pipe is an internal flow problem without any flow separation. The resistance is due to pure friction drag. By analogy to the flow along a flat plate, the frictional resistance depends strongly on the Reynolds number. In the frictional resistance is also shown for rough pipes. As in the case of a flat plate, surface roughness further increases the drag and the frictional resistance becomes independent of the Reynolds number. This is because flow separations occur on the roughness elements. Therefore a rough surface behaves like the sum of a large number of bluff bodies.

The flow through pipes having non-circular cross-sections can be related to an equivalent pipe flow with circular cross-section. For given dimensions of the non-circular pipe (cross-sectional area S , Circumferential length c) the diameter of the equivalent circular pipe is given by

$$d_{eq} = \frac{4S}{c}$$

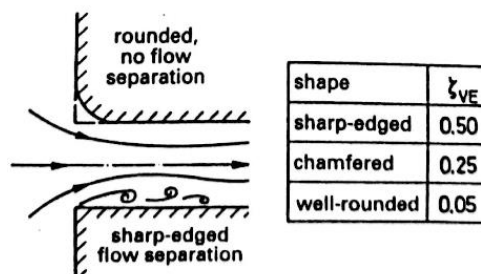
Curved Pipes

Flow separations may occur also in pipes. The deflection of the flow by the walls is induced by a pressure gradient perpendicular to the streamlines. In a curved pipe, the pressure at the outer radius is higher and at the inner radius is lower than the pressure in the flow upstream and downstream. Therefore a danger of flow separation caused by pressure increase in the direction of flow-is present at the outer radius close to the entrance and at the inner radius near the exit of the bend. These effects increase with decreasing curvature radius and with increasing angle S . Due to the flow separations, loss coefficients occur that are almost independent of Reynolds number.



Inlets

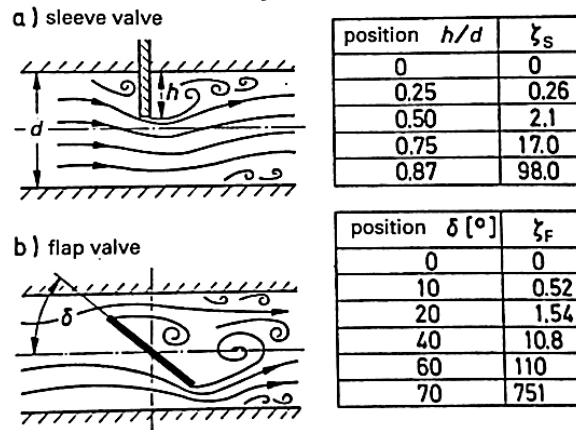
The flow through an inlet may also cause total pressure losses. Especially for sharp-edged inlets, flow separation occurs, and the corresponding values for the loss coefficient ζ_{VE} according to arc high. The values indicate that, to achieve small loss coefficients, inlets have to be well-rounded rather than sharp-edged.



Local Contraction

Local reductions of cross-sectional area - for instance in sleeve valves, nap valves etc.-are used to control the flow rate in pipes, in the control of heating and cooling systems. In local contractions, high velocities and low pressures are present. On the rear part of the element, which produces the contraction, the flow separates. Downstream of the smallest

cross-section the pressure increases at the walls, and the flow may separate here, too. The corresponding loss coefficients are extremely high especially for nearly closed position of the valve.

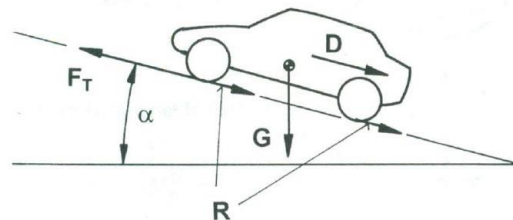


Resistance of motion

According to Newton's second law of motion, the tractive force F_T required at the interface between the tires of the driven wheels and the road is

$$F_T = D + R + m \frac{dV}{dt} + mg \sin \alpha$$

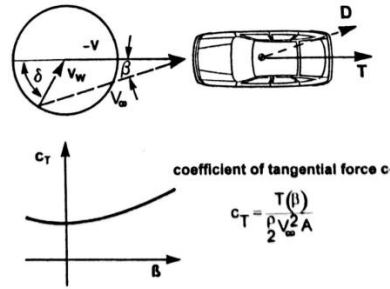
where D is the aerodynamic drag, R is the tire rolling resistance, m the vehicle's mass, V the road speed, g the acceleration of gravity, and α the inclination angle of the road. The last two terms on the right side of are also called resistances; accordingly, $m \frac{dV}{dt}$ is called acceleration resistance and $mg \sin \theta$ is climbing resistance.



Aerodynamic drag depends on the size of a vehicle (which is characterized by its frontal area A), the drag coefficient C_D (which is a measure of the flow quality around the vehicle), and the square of the road speed V . Hence, aerodynamic drag D can be expressed as:

$$D = \frac{\rho}{2} V^2 C_D A$$

A wind is blowing; its speed V_w and direction δ vary randomly. The vector sum of (negative) road speed V and wind speed V_w yields the resulting wind speed V_∞ which approaches a vehicle with a yawing angle. In this more, general case the aerodynamic force to be overcome is no longer drag (which, by definition, is the force in the direction of the resulting oncoming wind) but the tangential force T (which is in the direction of the vehicle's longitudinal axis and thus in the direction of its forward motion). In the U.S. this tangential force is called drag.

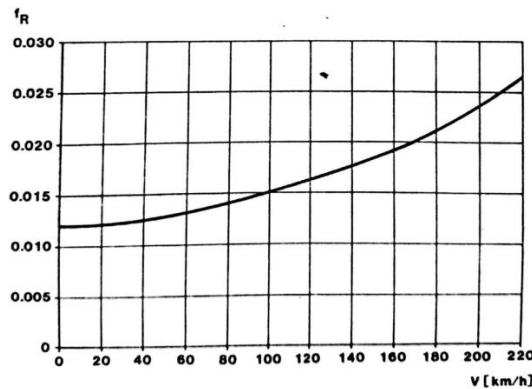


Tire Rolling Resistance

The rolling resistance R of a vehicle depends on its mass m and a coefficient of rolling resistance f_R

$$R = f_R G$$

where $G = mg$ is the force the vehicle exerts on the ground due to its mass m . The coefficient of rolling resistance f_R is a function of the following variables: tire construction and size; tire pressure; axle geometry, i.e., caster and camber; road speed; and whether the wheels are driven or towed. The f_R must be determined by experiment. Most frequently, f_R is measured on a drum, with the tire either rolling on its inner or its outer surface, which is not the same as rolling on a flat street. Consequently, f_R data from drum and road differ. Sometimes, for purposes of research, rolling resistance is measured on the road.



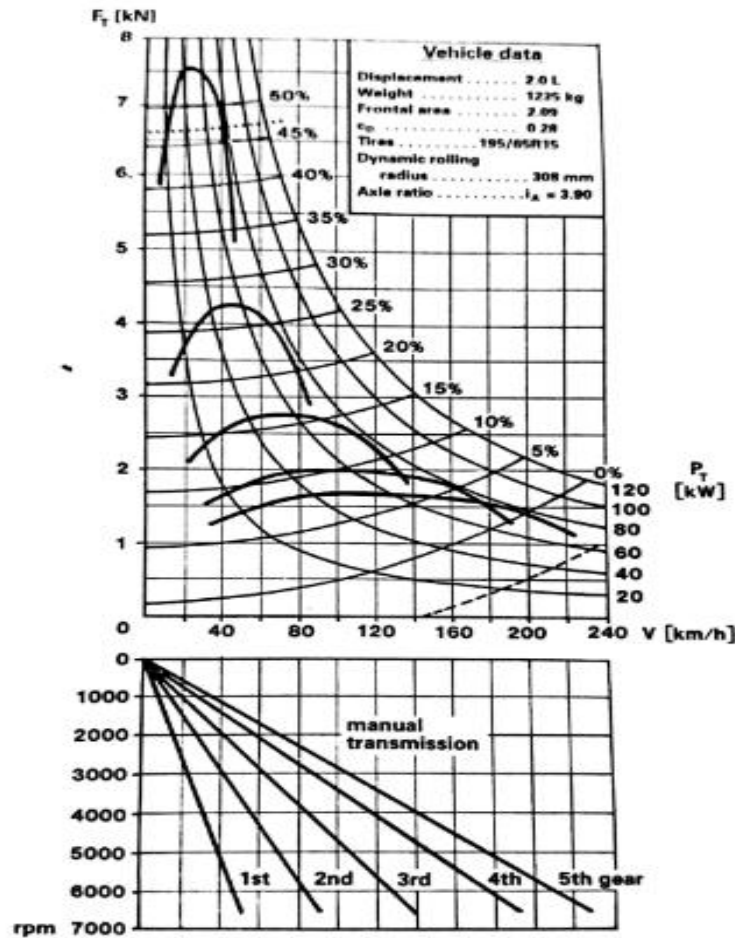
Climbing Resistance

Generally, climbing resistance is not taken into account in fuel consumption assessments, neither for constant-speed driving nor for specific driving schedules. The reason for this is that it is difficult-if not impossible -to define a representative geodetic (altitude) profile.

Performance

Traction Diagram

The performance of a car can be described with a so-called traction-force diagram. A typical example for a European middle-class car. Tractive force F_r is plotted versus road speed V . Hence, lines of constant tractive power are hyperbolas. The road-load curves-in principle second-order parabolas-are drawn for various grades. The thick lines are the WOT (full load) engine curves in all five gears. For any point on a road-load curve the "surplus" tractive force MT available in any gear for either acceleration or hill climbing is the vertical distance to the WOT engine curve for that gear.



Maximum speed

Today, when assessing the operating characteristics of a car, maximum speed has become less important relative to fuel economy. However, this "officially" drawn conclusion is not in accordance with what the customer really wants in all countries. In Europe, motor magazines still quote maximum speed; particularly for the sporty versions of cars it is still a very strong selling point. However, as a self-imposed constraint, auto manufacturers in Germany limit the top speed of their cars to 250 km/h. Maximum speed can be approximated from tractive force F_T and maximum installed engine power $P_{b, \text{nom}}$. Generally, the tractive power

$$P_T = F_T V$$

At the maximum-speed point, this becomes

$$V_{\max} = \frac{P_{T, V \max}}{F_{T, V \max}}$$

Fuel Consumption

The fuel consumption B [L/100 km] of a vehicle is computed by integrating its instantaneous volume fuel rate b [L/s] over a time period T [s], and dividing this integral by the distance traveled in that time period:

$$B = \frac{\int_0^T b dt}{\int_0^T V dt}$$

where V [km/h] is the instantaneous road speed of the vehicle (for consideration of dimensions different from SI units). The ride on a road (and also the various official driving schedules) can be divided into three different modes of vehicle operation:

1. Powered driving, where $FT > 0$.
2. Braking, where $FT < 0$.
3. Idle, where $V = 0$.

1. Powered driving ($FT > 0$): The instantaneous volume rate of fuel consumption b follows from the engine power $P_{b,T}$ needed to produce the instantaneous tractive force required to follow the driving schedule, and from the related specific fuel consumption b_0 (also known as bsfc, brake specific fuel consumption, in g/kWh); i.e.,

$$\dot{b} \rho_{fuel} = b_e P_{b,T}$$

2. Braking ($FT < 0$): When the instantaneous deceleration required by a driving schedule is sufficiently large, the retarding forces generated on a vehicle by aerodynamic drag and tire rolling resistance must be supplemented by negative tractive forces at the wheels. As engine throttle setting is progressively reduced for a deceleration, engine power can eventually become so small that the tractive force generated at the driving wheels becomes zero. With further throttle reduction the engine power is no longer sufficient to drive the powertrain at the rotative speed consistent with vehicle speed. The shortfall is made up by the extraction of kinetic energy from the vehicle's motion. The corresponding incremental torque supplied to the powertrain (engine, vehicle accessories, drivetrain losses) generates a reactive negative torque (braking) on the driving wheels. As throttle setting is reduced further the powertrain braking increases, and reaches a maximum when the throttle is closed (i.e., when the driver's foot is removed from the gas pedal).

If the axle ratio (final drive) is kept constant at $i = 3.27$, which was the correct value for the vehicle in its initial state with a drag coefficient of $c_D = 0.35$ (solid line), the broken line and the dotted line show the road load curves for $c_D = 0.30$ and 0.25 , respectively. Two effects are evident:

1. With decreasing drag the road-load power is reduced, and the road-load curve running through the bsfc map is shifted toward operating points with higher specific fuel consumption.

2. At the same time, the engine top speed exceeds the engine's nominal top speed.

Strategy for low fuel Consumption

The challenge for a vehicle engineer is to achieve good fuel economy without asking buyers to sacrifice performance, safety, and comfort; buyers would never accept that. Rather, it is his task to improve fuel economy while at least maintaining the state of the art in all three areas. Consequently, a reduction in engine power—which a lower aerodynamic drag per se would allow—is acceptable only if it can be accompanied by an appropriate reduction in vehicle mass. Hence, "lowest possible fuel consumption" must be seen in a context where vehicle properties are well balanced.

To achieve, fuel consumption for any specific vehicle the following sequence can be followed:

1. Reduce air drag
2. Reducing engine power to the extent that the increase in top speed (which follows from No. 1) measure will be offset. If the vehicle's mass remains unchanged, this measure will worsen performance.
3. Reduce the vehicle mass as much as necessary to recover the loss of performance due to No.2

Engine cooling system:

The most important internal flow fields are the air flow through the radiator and engine compartment, and the heater or ventilation flow through the passenger compartment. Some types of vehicles—such as racing cars—have separate flow ducts for the oil cooler, brake cooling, and the combustion air for the engine. The engine cooling system has the task of removing a heat flux Q , which is of approximately the same magnitude as the useful engine power P : $Q \sim P$

The requirements for cooling air have increased considerably. Since a larger cooling air flow is required for water cooling than for air cooling, these requirements must be related to the type of cooling:

1. Engine power has increased continuously over the years, making necessary greater volumes of cooling air.
2. Following the demands of styling and aerodynamics, the front end of cars has become flatter over the years. The openings available for entry of the cooling air have become smaller as a result. Moreover, the earlier large coherent inlet area has been broken up into individual sub-areas.
3. As a result of compact design, less space is available in the engine compartment for the radiator and cooling air duct.
4. In the interests of safety the body has continuously been reinforced at the front end ('hard edge'), so that the flow is impeded by wide bumpers and cross-members.

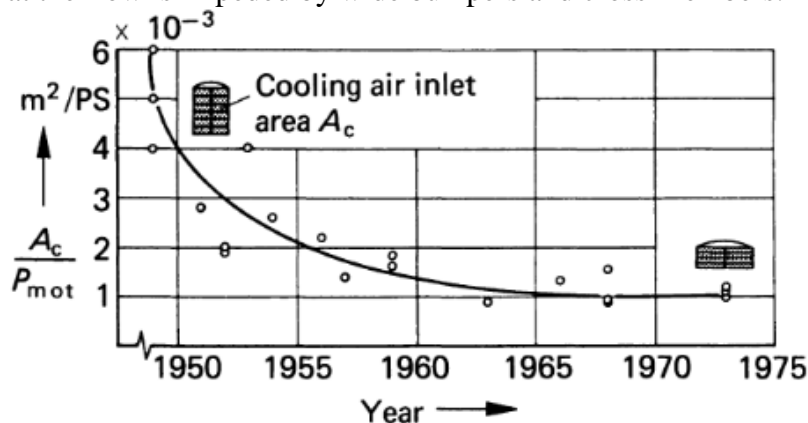


Figure: Cooling air inlet area in relation to installed engine power

Air flow through the passenger compartment:

The air flowing through the passenger compartment must perform three groups of tasks:

1. Sufficient ventilation must be assured. All contaminants in the form of gases, vapours and dust must be expelled from the passenger compartment. Simultaneously, this provides for replacement of the oxygen consumed through breathing.
2. A comfortable internal climate must be produced and assured for a wide range of variation in the external conditions. For winter operation a high-performance heater must be provided. In summer comfort must
3. Be ensured by the circulation of fresh air. In extremely hot countries this alone is not sufficient and the air must be cooled with an air conditioner.

The internal flow must pass along the windows so that mist evaporates (demisting) and ice, which can form on both sides of the windows, melts (deicing).

UNIT I INTRODUCTION TO AUTOMOTIVE AERODYNAMICS



SATHYABAMA

**INSTITUTE OF SCIENCE AND TECHNOLOGY
(DEEMED TO BE UNIVERSITY)**

Accredited "A" Grade by NAAC | 12B Status by UGC | Approved by AICTE

www.sathyabama.ac.in

**SCHOOL OF MECHANICAL ENGINEERING
DEPARTMENT OF AUTOMOBILE ENGINEERING**

SAU1601 AUTOMOTIVE AERODYNAMICS

UNIT II AERODYNAMIC DRAG OF CARS

UNIT II AERODYNAMIC DRAG OF CARS

Cars as a bluff body, flow field around car, drag force, types of drag force, analysis of aerodynamic drag, drag coefficient of cars, strategies for aerodynamic development, low drag profiles.

Car as a bluff body

It is true that the mass of published experimental data is now so great that, with the aid of this information, it is possible to *estimate* drag from the geometrical particularities of any specific configuration. This estimate may be based on either the experience and intuition of the estimator or on a formalized process which will be described in detail in Section 4.5.6. However, as in the past, experiment remains the only means of obtaining reliable quantitative data for drag. Definitive aerodynamic information, not only on drag, is indispensable for rational vehicle development since it is part of the combination of objectives that have to be carefully balanced against one another in order to properly position a vehicle in the marketplace.

The reason it is so difficult to solve the problem of car drag becomes evident when, according to their drag, cars are classified against other bluff bodies. The result is shown in Fig. 4.1 in which, for the purpose of the present comparison, the effect of ground proximity is ignored.

Despite being bluff, the body of revolution (with comparable dimensions to a car, $d/l = h/l$) has almost exclusively friction drag: $c_D = 0.05$. In its purest form, friction drag occurs in the case of a flat plate aligned with an oncoming flow. Theoretical study of friction drag has progressed considerably. With reference to H. SCHLICHTING [4.1] and to Section 2.3.3, its origin can be characterized briefly as follows.

The viscosity of the air is effective only in a thin layer adjacent to walls. This layer is known as the *boundary layer*. Based on experimentally determined universal laws for turbulent shear stress on a wall, the development of a boundary layer, at least in two-dimensional cases and in the case of a body of revolution, can be computed even for configurations in which the static pressure along the wall is not constant. In particular, the point of flow separation can be identified. With this information, the shape of a body of revolution can be "optimized" with regard to its drag. For a slender body of given solidity d/l and volume, the shape that provides minimum drag can be computed in advance fairly well. Moreover, boundary layer theory can be used to convert measurements obtained from a model in

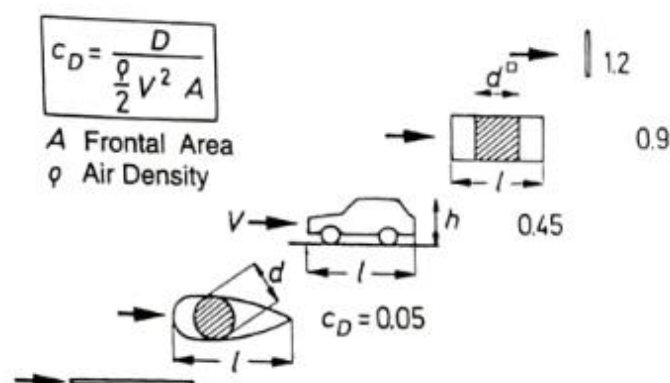


Fig. Drag of car compared with other bluff bodies

Flow field around a car

Generally, the airflow around a moving car is asymmetrical with respect to its longitudinal axis because absolute windlessness is only rarely encountered. The driving speed V and natural wind speed combine to produce a relative flow speed u at a yawing angle p . For the sake of simplicity, symmetrical flow is considered first. The influence of side wind (a natural wind that is not aligned with the direction of vehicle travel) on drag and its effects on directional stability.

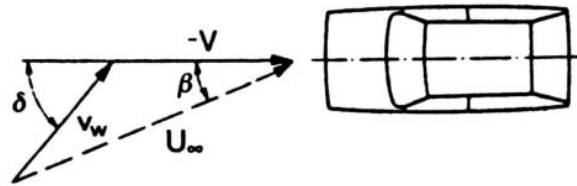
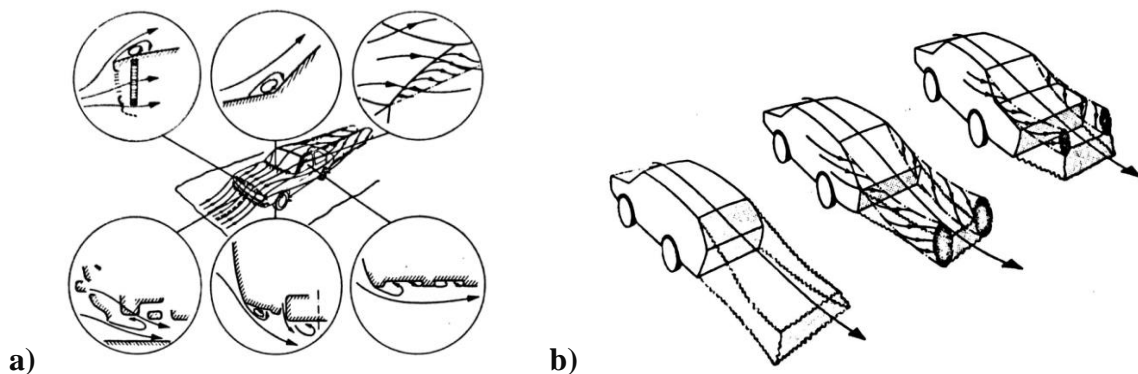


Fig. Road speed V and wind speed v_w combine to produce the relative flow U_∞ .

The main reason for this progress is that flows observations are no long confined to the surface of a car body but include the entire surrounding space. First, flow can separate on edges running perpendicular to the local direction of flow. Vortices roll up, their axes normally being parallel to the separation line. Most of their kinetic energy is dissipated by turbulent mixing. Separation also occurs at a truncated rear surface, leading to a wake which includes a zone of recirculation frequently called dead water.



Air flow around car on front end

Three types of rear end of car

The streamlines are drawn according to observed flow pictures and represent the average of a highly turbulent flow. In all three cases two contrarotating vortices are visible, being typical for the flow inside the dead water behind the base of a bluff body. The lower, counterclockwise vortex can transport dirt thrown up by the wheels onto the rear surface.

The second type of separation is three-dimensional by nature. At edges around which air flows at an angle, the airstream forms cone-shaped stream wise vortices similar to those observed on aircraft wings, especially delta wings with low aspect ratio.

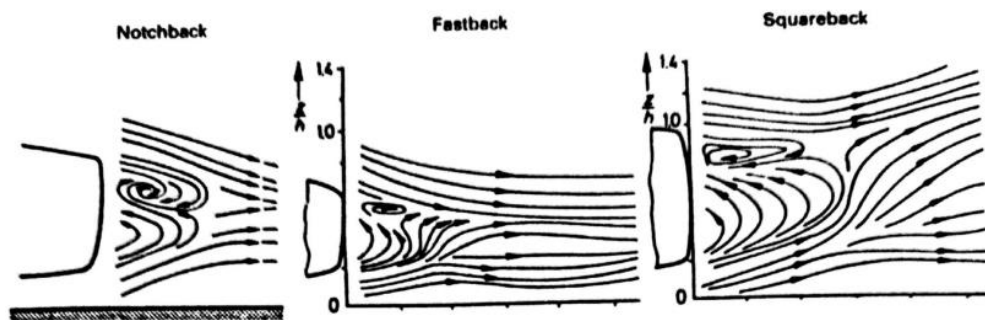


Fig. Vortices in the dead water behind cars of different shape

These "free" vortices have considerable effect on their environment. The vortices on the A-pillars stress the side windows. They also influence water flow in this area and cause wind noise. At roof level, the A-pillar vortices are "bent" rearward. Evidence of their existence can be clearly seen in the surface flow patterns of rainwater, the surface patterns of dirt deposition or by snow from the roof of a car. They continue downstream far behind a car. However, in the flow field behind a car they can be definitely identified only with wake measurements.

A second and generally much more powerful pair of trailing vortices is formed on the slanted back of a car. They rotate in opposite directions so that a downwash is induced between them which, in turn, influence the formation of the dead water at the rear. The induced downwash "pulls" the air flowing over the roof downward. The separation line is fixed at the lower end of the slanted surface, and the dead water is closed within a short distance. However, if the separation is artificially generated at the end of the roof by a deflector vane (left photo), no such pair of free vortices is formed. The dead water starts to form at the trailing edge of the roof and stretches far behind the car.



Fig. Long, Open and Short, Closed wakes for square back and fastback flow

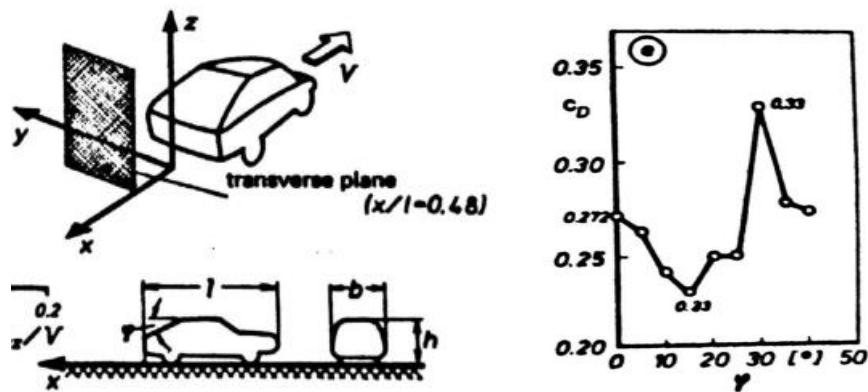


Fig. Drag co-efficient of a fastback, as a function of slant angle ϕ

The dead water is large, and a pair of weak outward-turning stream wise vortices is detectable. With increasing slant angle ϕ a pair of inward-turning vortices appears whose strength increases with slant angle. However, exceed a critical value in the region of 30° , these vortices break up (“burnt”) in a manner similar to what has been observed for slender delta wings and the flow pattern return, to that of a square back.

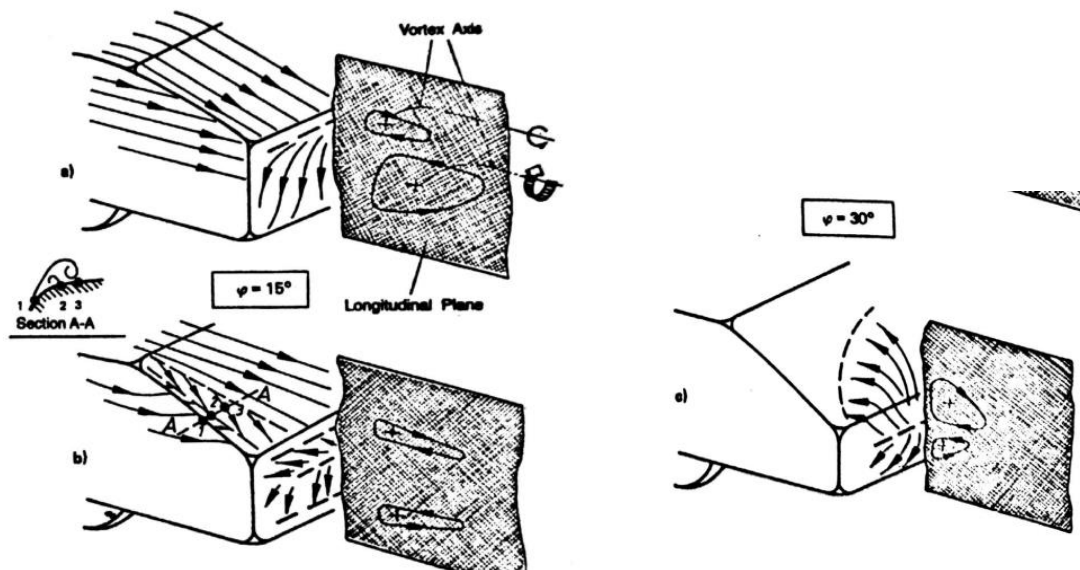


Fig. Air flow patterns on a fastback with different slant angles ϕ

In contrast, the flow inside the radiator cooling-air duct and its effect on drag are well understood. While computation of this flow was formerly based on a one-dimensional model transferred from aeronautics. It is now treated completely three-dimensionally, and including temperature effects.

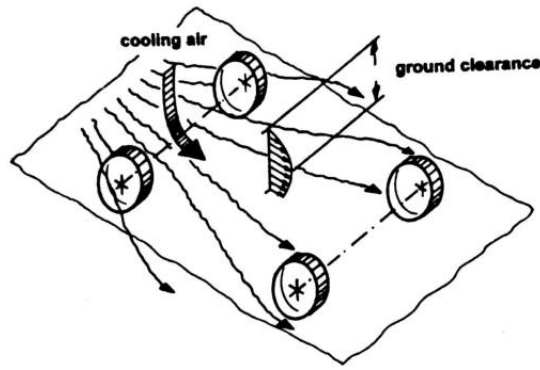


Fig. Outward – spreading flow underneath a car.

Analysis of Drag

a) Possible Approaches

The objective of analyzing aerodynamic drag is to establish a relationship between cause and effect. As already emphasized, this task is made extremely difficult by the interaction of the individual flow fields around a vehicle. Drag can be considered from three different points of view. We can:

- Examine the physical mechanisms generating drag.
- Allocate fractions of the drag to local origins.
- Investigate the effect of drag on the surrounding flow field.

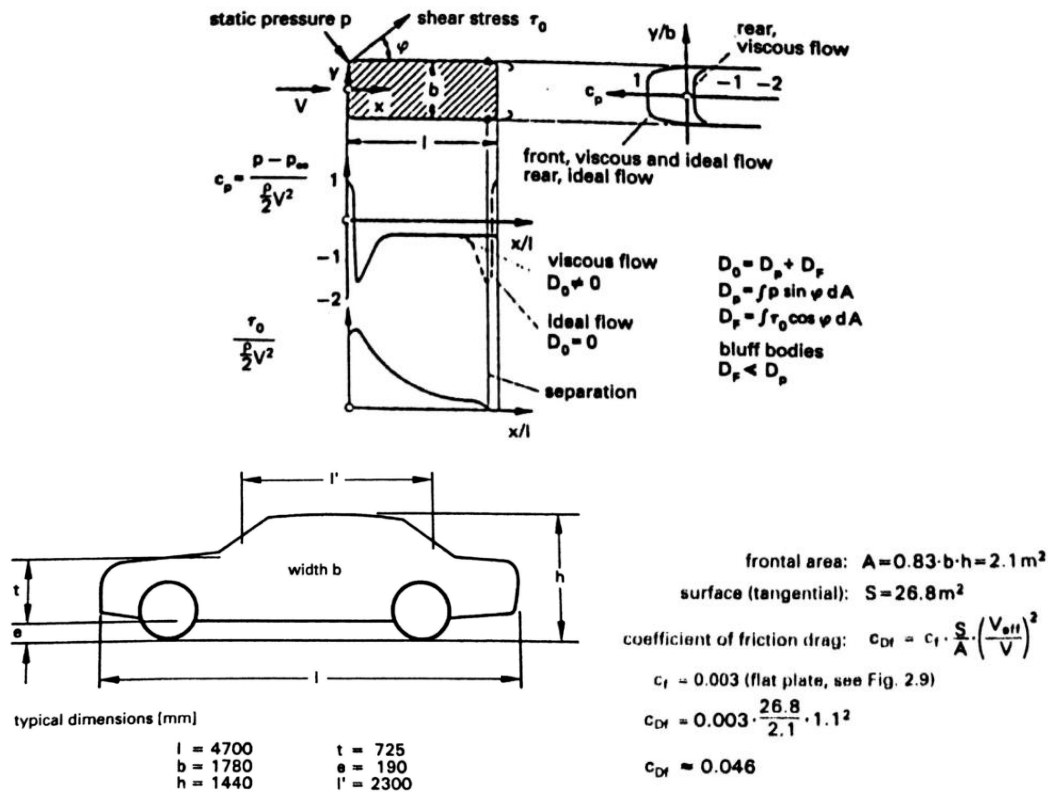
b) Physical Mechanism

The physical cause of drag can best be understood by comparing the actual airflow around a car, i.e., the flow of a viscous fluid, with the ideal now, i.e., that of a frictionless medium. Drag, the aerodynamic resistance to motion, can be explained by the difference between these two forms of flow, because in friction-free flow, drag is always equal to zero ("d' Alembert's paradox"). The friction-free result, due to its obvious contradiction to reality, discredited fluid dynamic theory in the eyes of practitioners for a long time.

The energy loss within a boundary layer (which is due to friction) causes the flow to separate from its adjoining surface if it is opposed by too steep a pressure gradient. In cars, this is always the case at the rear, even if not at other locations. Pressure recovery downstream of a separation is much weaker (if not zero) than would be the case with attached flow.

If the pressures on the front and rear of a vehicle are plotted versus its width. It becomes evident that the pressures over the front end are almost identical for frictionless and viscous flow if, as supposed here, there is no flow separation. At the rear, on the other hand, there are considerable differences. These are the differences that make the pressure integral

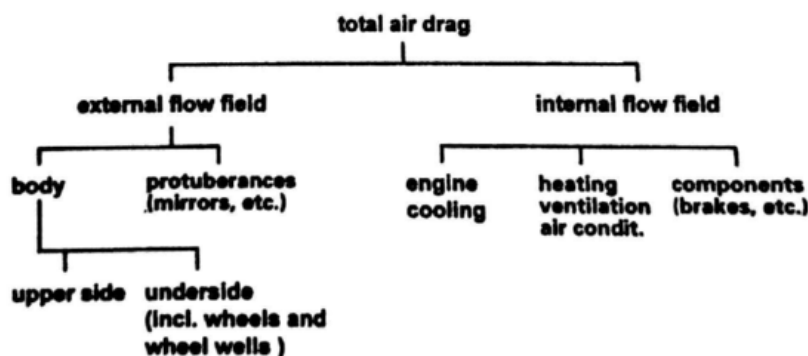
different from zero and create pressure drag - not the stagnation pressure itself at the front of the car.



c) Local Origins:

An approximate subdivision of drag according to its regions of generation is provided. This classification is the basis of all following considerations on drag and will be further detailed. However, for an actual car a classification of this type is rather difficult to make for two reasons:

- The first is the same as in the previous section: pressures and shear stresses are not known with the resolution needed.
- The second is the interference effects between the components.



For a generic car body, performed such segmentation into local drag contributions. For this smooth body without attachments, four geometric zones can be distinguished:

- The front end.
- The rear slant.
- The base, i.e., vertical panel at the rear.
- The side panels, roof and underbody

Their individual contribution to overall drag for various slant angle. The drag of the front end, c_k is very small. Front drag and frictional drag, c_F are unaffected by variation of the rear geometry. With increase slant angle there is a change in the distribution of drag around the body. The strength of the vortices shed from both sides of the slant increases with slant angle and so does the negative pressure induced by them on the slant. The slants fraction of the projected rear surface area increases at the same time.

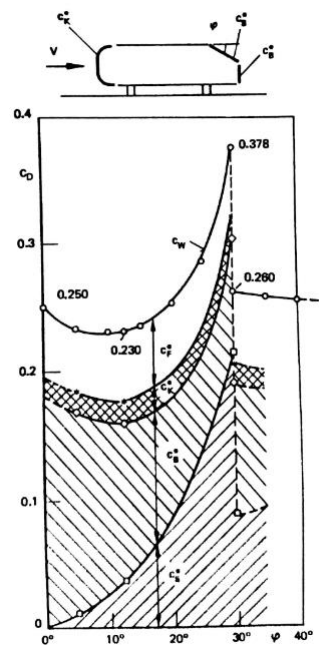
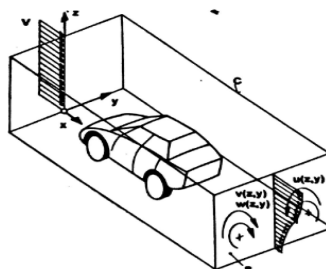


Fig: Influence of slant angle ϕ on overall drag and the percentage of total drag generated at the individual “zones” of a generic vehicle model

d) Effects of the environment:

Drag computed turns out to be greater than the drag measured with a balance in a wind tunnel if the tunnel is equipped with a stationary ground floor; the momentum loss within the boundary layer along this floor will be accounted.



e) Drag and Lift

The airflow around a vehicle usually causes lift. If no special precautions are taken, this lift is generally positive, i.e., directed upward. The result is that the downward force on the tires is reduced as a function of speed. The unfavorable effects of this lift on handling characteristics. Also, the "price" of lift (whether it is positive or negative) is usually drag, and this relationship is analyzed. Race-car tuning is dominated by the interaction of lift and drag.

Accordingly, with reference to airfoil theory, the overall drag c_D should be composed of a profile drag and an induced drag:

$$c_D = c_{D0} + c_{Di}$$

Induced drag:

$$c_{Di} = k \frac{c_L^2}{A}$$

Cars are bodies with a low aspect ratio A ,

$$A = \frac{b^2}{A_{plan}}$$

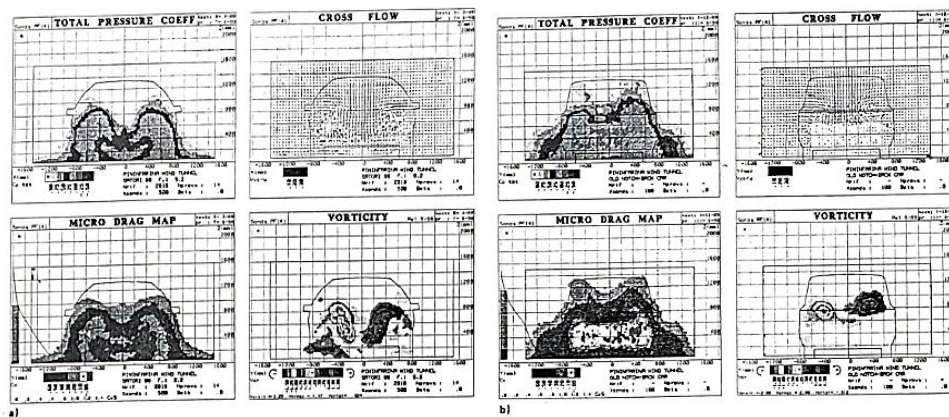


Fig. Total pressure, cross-flow velocity, micro drag, and vorticity in z, y – plane at $x = m$ behind vehicle

Drag Fractions and Their Local Origins

The drag components is made according to the pragmatism with which an aerodynamicist performs his work in a wind tunnel, and the majority of examples go back to actual car development projects. The aerodynamicist tracks down "weak points" in the flow around a car. Measuring drag (and all other components of resultant air Force) by means of a balance is the typical way of validating the success of a specific measure. However, the balance does not tell anything about the physical process "on site," and simple visualization means such as a smoke probe give not more than a very coarse idea of the flow pattern. The

result of the "before/after" comparison is interpreted as the contribution to drag of the specific detail under investigation.

Front End

The front end of a car can be roughly approximated as a square block. The streamlines around this block are shown schematically in Fig. 4.21; for further simplification the cooling air intake is assumed to be closed. A stagnation point is formed on theoretical front face. Because of the close proximity of the road, the air tends to flow over and around a vehicle rather than under it, streamlines near the end are therefore directed upward. The flow is significantly deflected at the intersections between the front face and the hood and fenders.

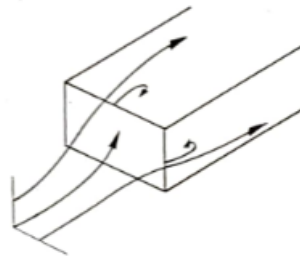


Fig. *The square block as a simplified substitute model for the front end of the car*

Without special measures, this flow pattern will cause separation, with the result that the pressure distributions near the edges of the forebody will deviate from those for ideal flow. The suction peaks at the leading edge of the hood and the fenders are very much less pronounced than for ideal, separation-free flow for a longitudinal cross-section. The streamwise pressure force on the front end is therefore greater than in ideal flow, and a drag component is generated.

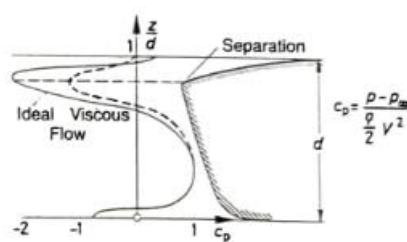


Fig. *Schematic pressure distribution in the longitudinal cross-section of a front-end structure with separated (real) and attached flow*

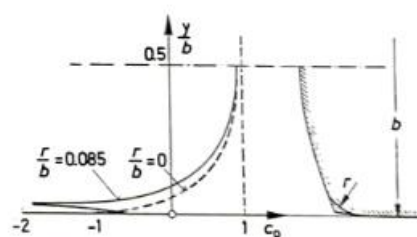


Fig. *Influence of body contour on pressure distribution*

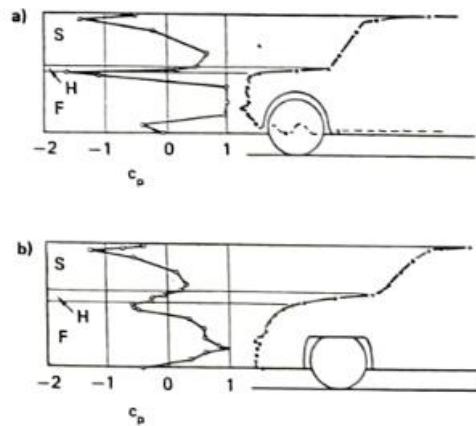


Fig. *Pressure distribution in longitudinal cross-section, a) for sharp cornered and b) for a rounded front-end structure*

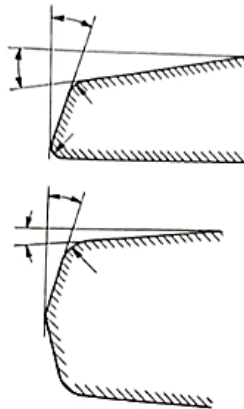


Fig. *The essential geometric parameters used to describe the shape of a car front end without bumper and spoiler.*

The essential geometric parameters used to describe the shape of a car front end without bumper and spoiler: harmonized empirically, taking into account, of course, the front bumper and the cooling air inlet, which are not shown here. Systematic results are now known for some of the parameters identified namely the edge radii, the slope of the hood, and the slope of the front-end face. In the case of the edge radius, well-known key data can be found in the literature and are summarized, based on is at first reduced Separation rapidly.

Then, longer occurs, radius after of a passing leading edge a certain value, is increased, and the real flow comes close to the ideal. Drag remains drag of the relevant body constant ("saturation"). When applied this observation means that only minor rounding of the leading edges is required to prevent flow separation, thereby minimizing the forebody's contribution to drag When transferring the numerical values to the problem under

consideration here (i.e., the fore body of a car), it should be remembered that they apply to right-angled boxes, whereas the deflections on a real car are less sharp. The precise radius that can stand in a flow without separation must be determined by experiment, and taken into account its dependence on Reynolds number. The second geometric parameter that has been studied in detail is the inclination angle of the hood.

The effect of hood inclination on drag is also subject to a saturation effect; there is no further decrease in drag after even only moderate inclination.

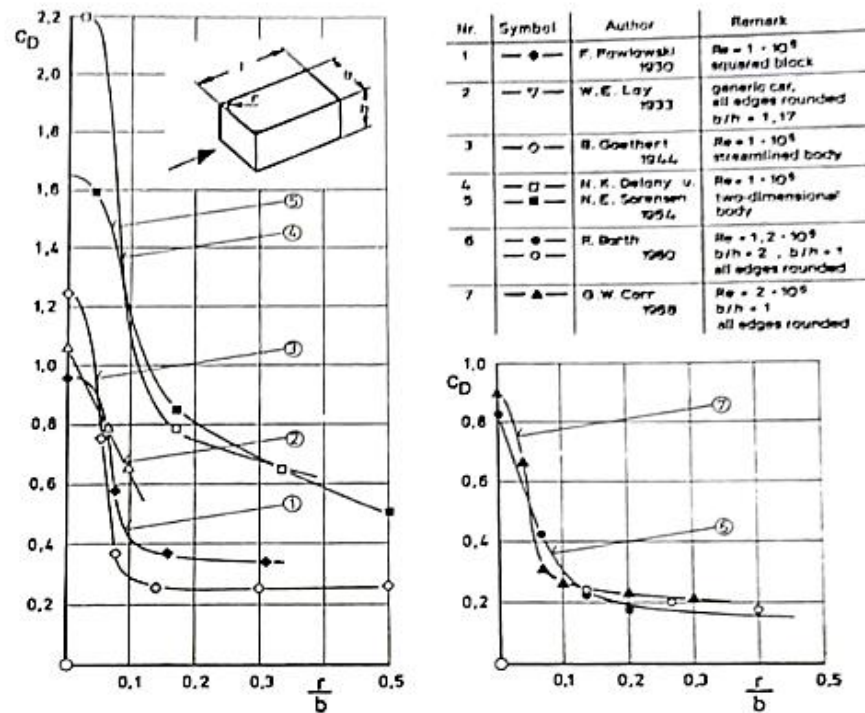


Fig. Influence of edge radius on the drag of squared blocks

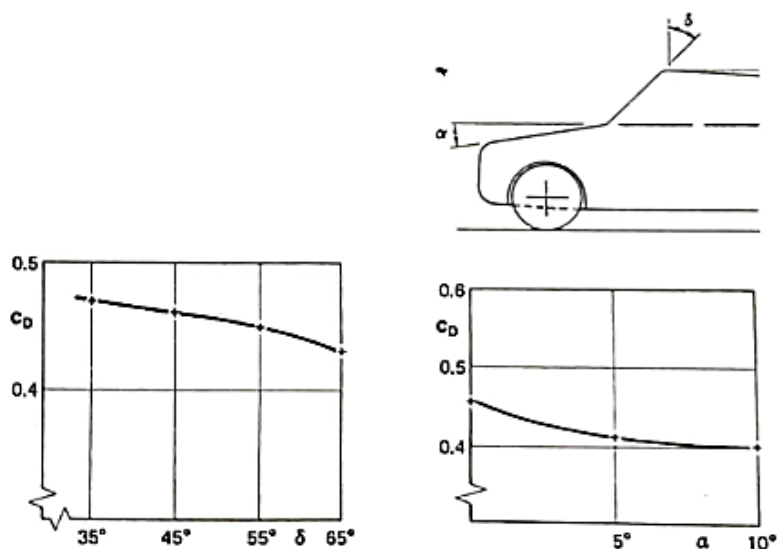


Fig. Reduction of drag with hood inclination angle α and windshield inclination angle δ

The third parameter examined separately is the inclination angle of the front face. The fact that this effect is so slight here is probably due to the large front-corner radii used with this model.

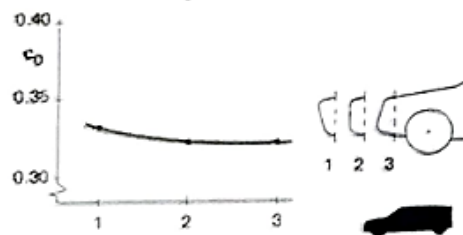


Fig. Influence of front-end inclination on drag, after A. GILHAUS

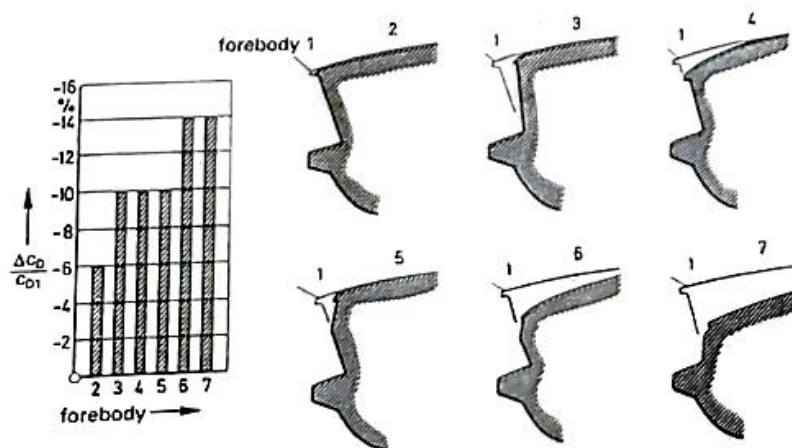


Fig. Formal variants for a front end structure and their c_D

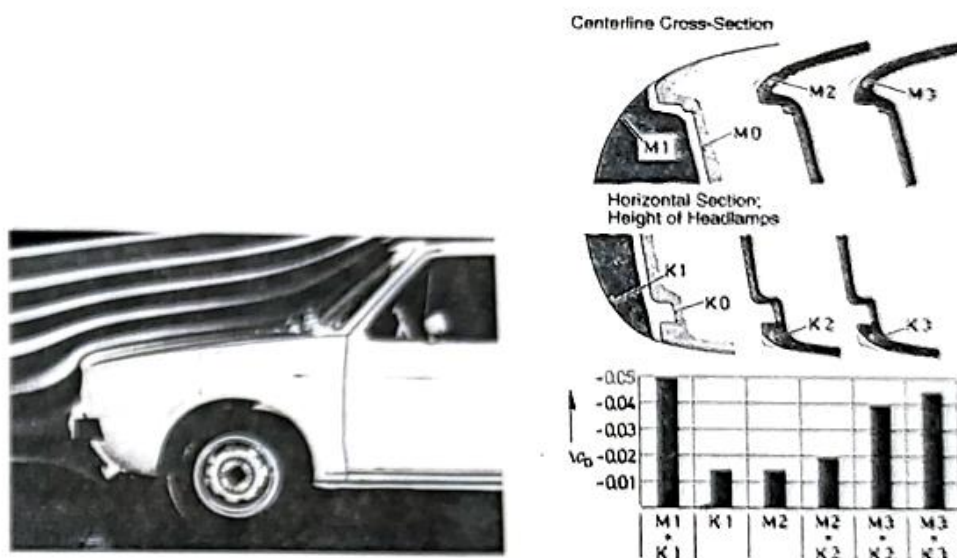


Fig. Example for optimization of front end design

A forebody as long as there is no flow separation. Also, as a general rule it can be concluded that the lower the stagnation point the better. The flow around an edge can also be

improved by chamfering the edge instead of rounding it. The same drag reduction as for the optimum nose can be obtained. A flow separation that originally occurred at the sharp edge was entirely eliminated by a chamfer, as proved by the photographed smoke streaks shown. The fact that it is also possible to proceed improvement toward low in drag by less demonstrated spectacular with the means demonstrated. The improvement in the drag demonstrated with the optimum nose has here been fully achieved by coordinating the hood radius and grille position.

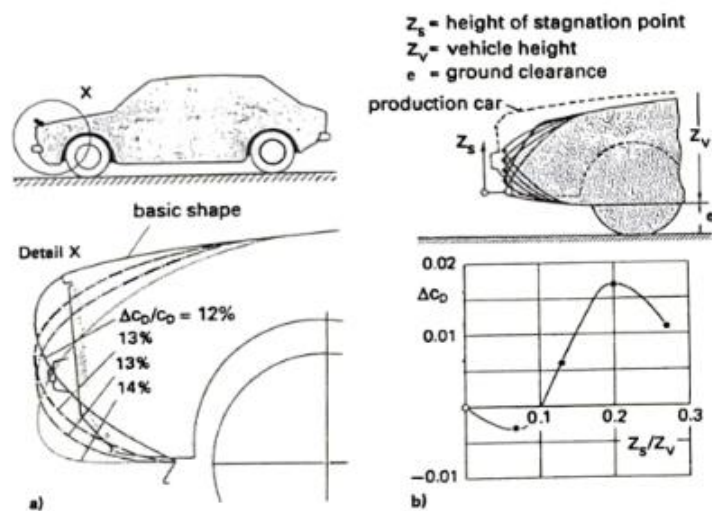


Fig. variation of drag co efficient with the position of stagnation point

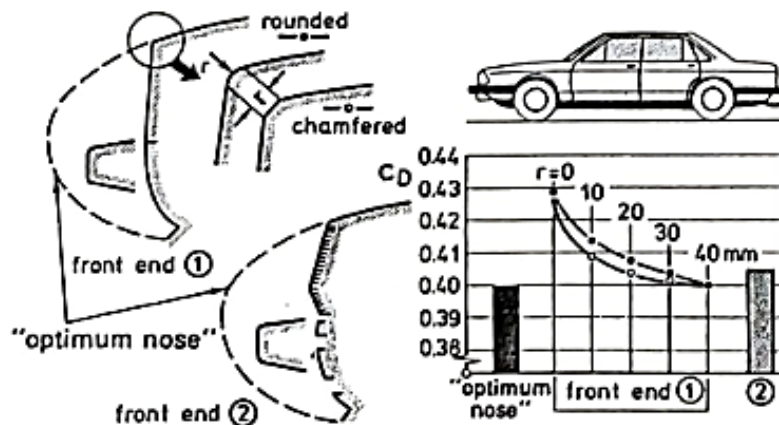


Fig. Reduction in drag by rounding or chamfering the front edge

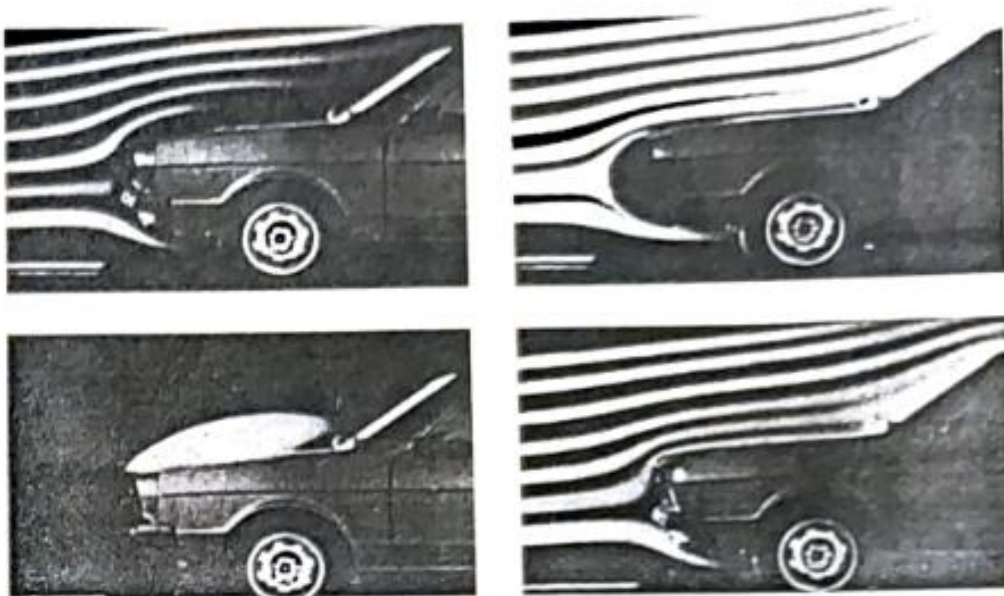
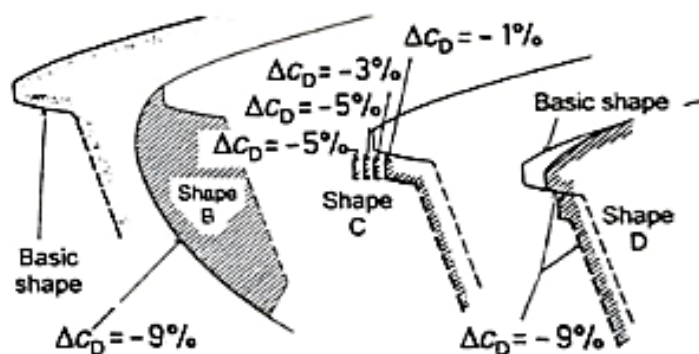


Fig. Flow around the front end of the Volkswagen Passat.



Drag reduction by fine-tuning the hood radius and grille design.

Fig.

Windshield and A-Pillar

A schematic of the flow around a windshield is shown. Separation is likely to occur at three different locations:

- At the base of the windshield, in the concave space formed by its junction with the hood.
- At the top of the windshield, at the junction with the roof.
- At the A-pillars.

The size of the separation bubble at the base of the windshield is determined by the inclination angle δ of the windshield, and more precisely by the angle ϵ that the windshield makes with the hood. This has been investigated by A.J. SCIBOR-RYLSKI [4.37] with the aid of a quasi-two-dimensional model (planar windshield); results are reproduced in Fig. 4.37. Points of separation S and reattachment R are plotted versus the inclination angle γ of the windshield. However, these results should not be considered to indicate anything more than a trend. Even smoke photographs on standard production vehicles with comparatively steep windshields (see Fig. 1.2) reveal no separation at this location. The reason is that, as a rule, the junction does not have a sharp corner but is rounded, and the windshield is curved; both of these features reduce the tendency for flow separation.

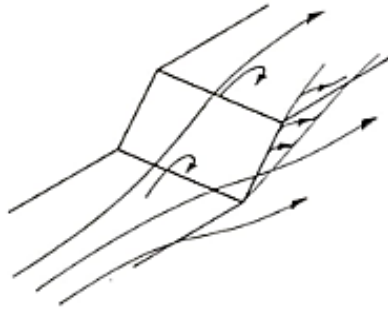


Fig. 1. Highly simplified model of airflow around the windshield.

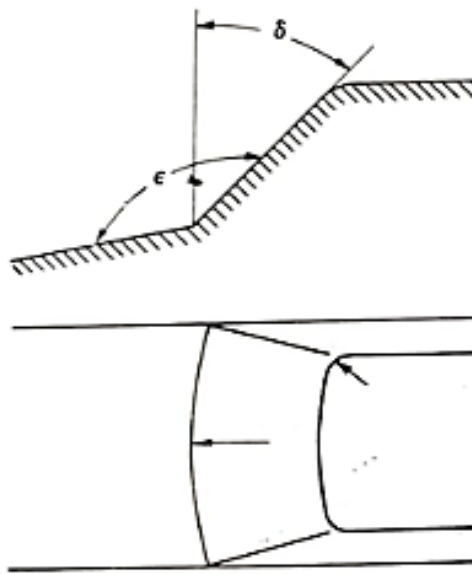


Fig. 2. The main parameters for designing the windshield

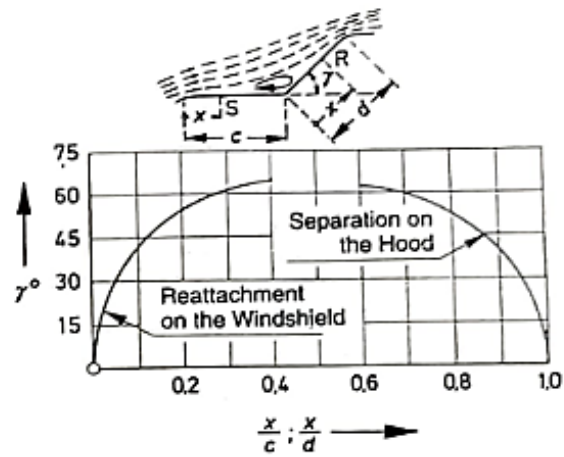


Fig. Flow separation point A and reattachment point S as a function of windshield inclination

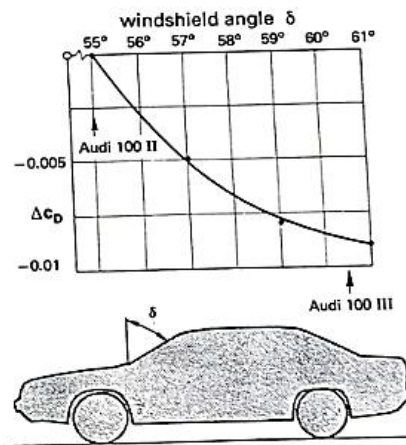


Fig. Influence of windshield inclination δ on drag, after R. BUCHHEIM,

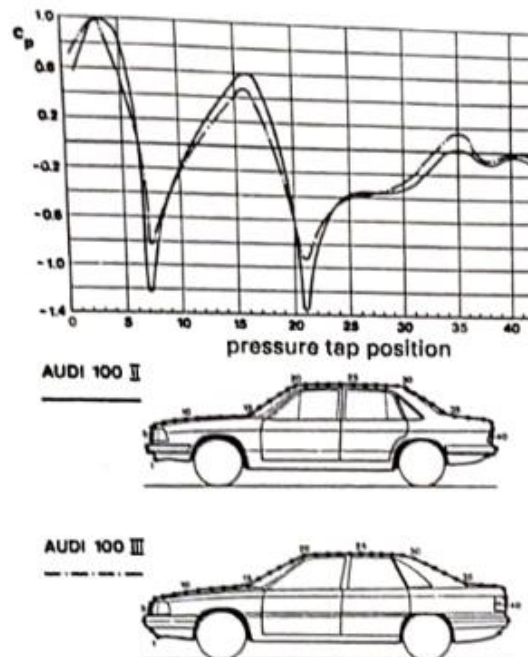


Fig. Reduction of pressure peaks in the further development of Audi 100

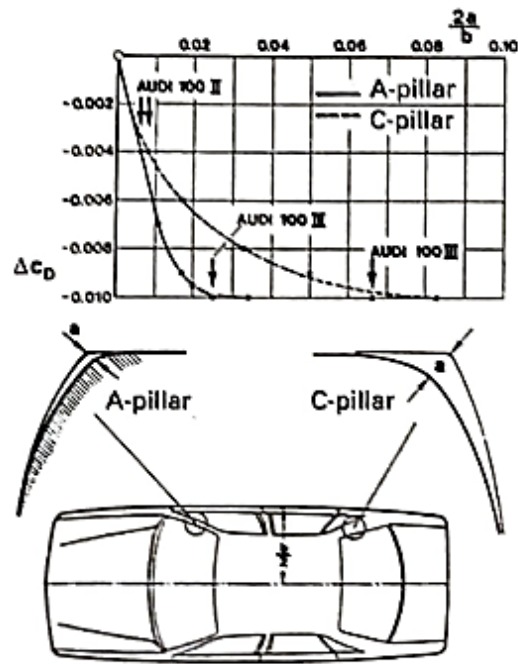


Fig. Drag reduction by rounding the A- and C-pillars of the Audi 100 III.

Roof

The drag coefficient can be produced by arching the roof in the longitudinal direction; however, if the curvature is too great, c_p again can increase. The favourable effect of arching depends on maintaining sufficiently large bend radii at the junctions between windshield and roof and between roof and rear window, so that the negative pressure peaks at these locations are no large and pressure gradients are small.

However, the design of the roof arch must ensure that the frontal area of a car remains constant; if not, the absolute drag ($c_D \cdot A$) can increase despite a reduction in drag coefficient c_D , as shown in the upper graph of Fig. 4.41. Since a driver's upward viewing angles must not be reduced, the windshield and rear window must be incorporated into the longitudinal arching; as a result, windows get spherical and thus more expensive.

The airflow on the roof runs parallel to the direction of travel; there is no flow around the sides of the roof. A drip molding along the roof rail therefore does not disturb the flow and does not increase either drag or wind noise. The wool-tuft photograph shown in Fig. 6.1 serves as a proof.

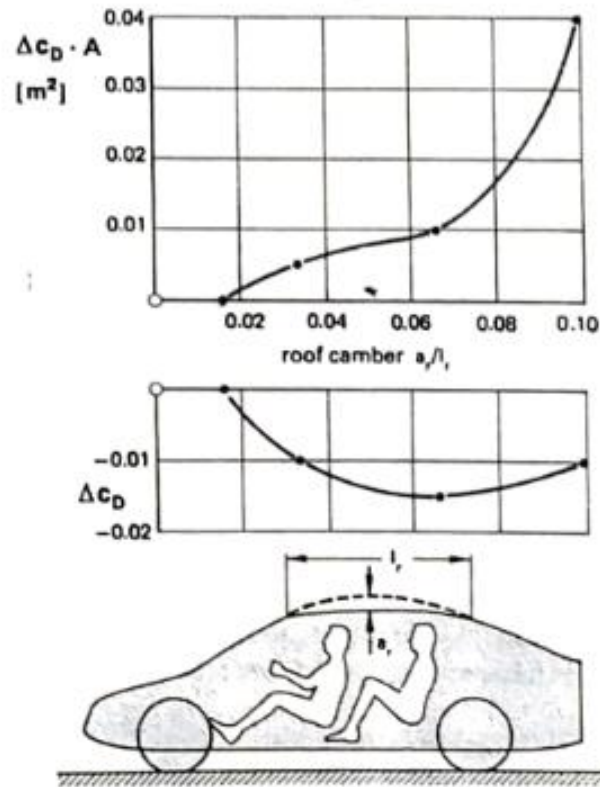


Fig. *Effect of roof camber on drag coefficient c_D and absolute drag.*

Rear End

Geometry and Flow Separation

Three types of rear end are common for cars: squareback, fastback, and notchback; in highly simplified form they are sketched. The main parameters for each shape are outlined, only those dominant for each type are shown. For example, "boat-tailing," which is here drawn only for the squareback, can also apply to the other back variants.

The flow separates at the rear of a car because the body is truncated. Two types of separation occur, characterized by the terms "quasi-two-dimensional" and "three-dimensional." Depending on the rear geometry, these two types of separation can interact. Both forms of separation are governed by specific parameters. For quasi-two-dimensional separation, this parameter is boat-tailing, which is defined formation of three-dimensional vortices is determined by the angles by the at the roof, sides, angles of the rear and under panel. The end the two separation types on their governing shape parameters will first be discussed separately. Their interaction will then be considered when describing results from specific car development programs.

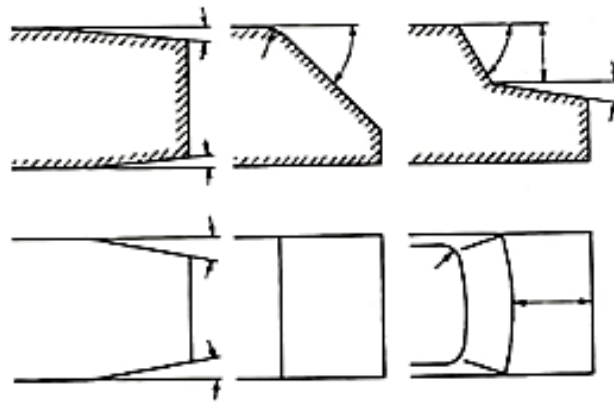


Fig. *The three traditional types of car back and their essential geometric parameters.*

Boat tailing

An aim of shape development is to make the static pressure at the end of a vehicle's body, the so-called *base pressure*, as high as possible, and the base itself, where this base pressure acts, as small as possible. This requires drawing in (tapering) the rear, a technique called "boat-tailing"; in-depth studies of this subject have been undertaken by D.J. MAULI [4.39] and W.A. MAIR [4.40,4.41]. Fig. 4.43 shows the extent to which the drag of a *body of revolution* can be reduced by tapering. The optimal tapering angle of 22° given in this diagram should be taken only as indicative; the specific optimal angle depends on the upstream history of the flow. Extending the rear end encounters a saturation effect; with increasing length the positive effect on drag becomes progressively weaker. If the rear end is properly truncated, which is called "bob-tailing," very little drag-reduction potential is lost. This finding confirms the idea of W. KAMM.

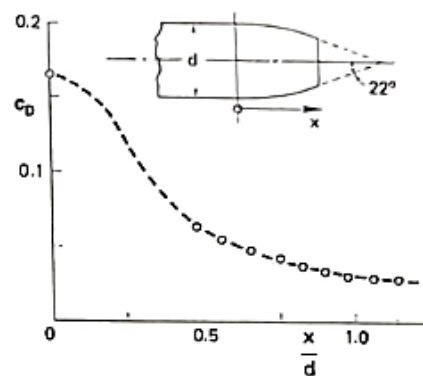


Fig. *Drag reduction of a body of revolution by boat-tailing, after W.A. MAIR*

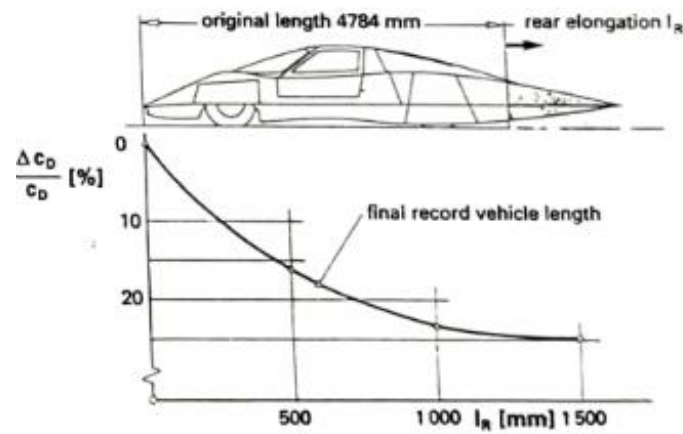


Fig. 4 Boat-tailing applied to record vehicle C111 III from Daimler-Benz.

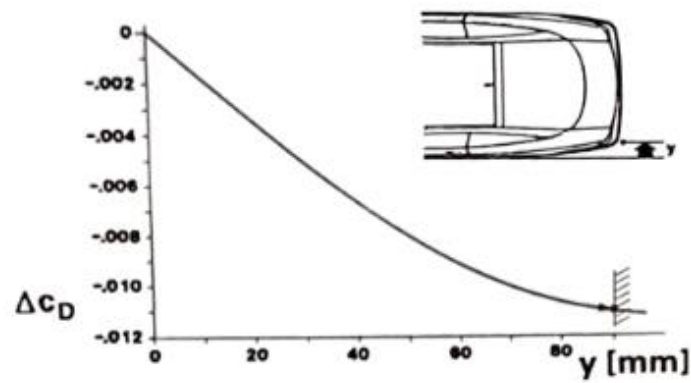


Fig. 5 Boat-tailing applied to the Opel Calibra Coupe, after H.-J. EMMEL.

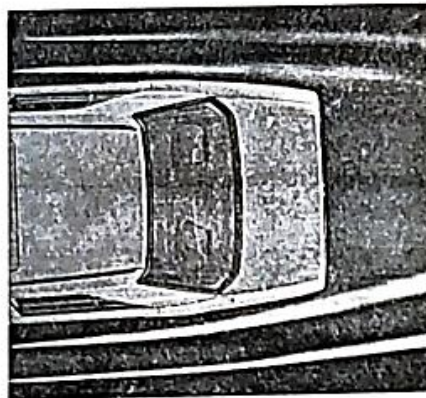


Fig. 6 Wisps of smoke follow the boat-tailed contour of the rear of the Mercedes-Benz 190.

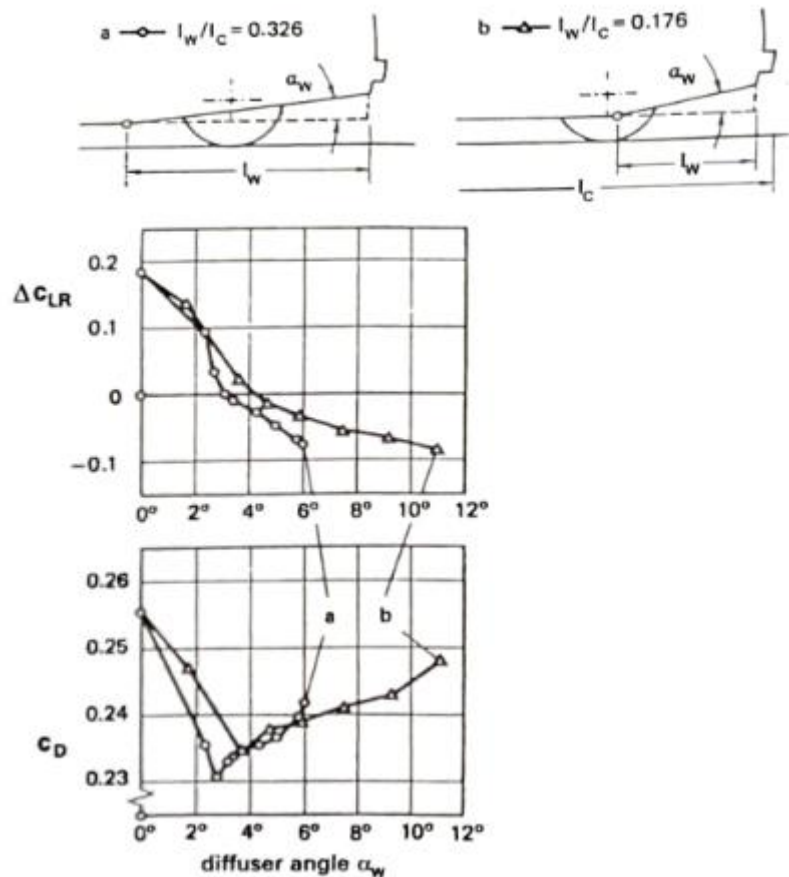


Fig. Reducing drag and lift on the rear axle

Fast back

As outlined in Section 4.2, the formation of vortices on the slanted upper-rear surface of a vehicle is determined by its angle of inclination ϕ . This relationship has been studied in considerable depth both on simple bodies and on complete vehicles. The main results for a body of cylindrical cross-section in free flow, i.e., out of ground effect, are given in Figs. 4.49 and 4.50. The force measurements of T. MOREL [4.46] and P. BEARMAN [4.47] coincide in indicating that drag and lift at first rise steeply with increasing slant angle ϕ . At a critical angle of roughly $\phi = 50^\circ$, both forces suddenly drop. The fact that these investigators measured different values for this critical angle may be due to a slight difference in angle of attack.

Flow observations and pressure-distribution measurements provide a conclusive explanation for the characteristic curves of these forces. Already at $\phi = 20^\circ$, the pressure coefficients in section YY (see Fig. 4.50) show negative pressure peaks on the slant close to its edges. These pressure peaks are induced by side vortices that roll up from the cutting edge in the same way as on the leading edges of a delta wing (see Fig. 2.13). With increasing slant angle ϕ , the negative pressure peaks increase in proportion to the increasing strength of the vortices. Beyond the critical slant angle, these vortices break up ("burst"); this observation matches the observations on delta wings discussed in Section 2.3.3.4. A dead water is then formed, and the pressure on the slanted rear surface is almost constant.

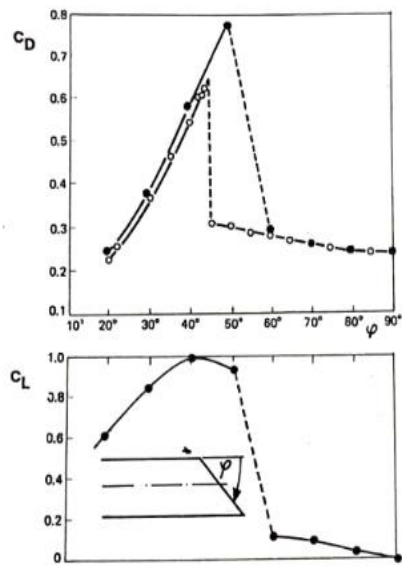


Fig. Effect of slant angle φ on the drag and lift of a free-flying body of revolution.
 —○— Measurement by T. MOREL [4.46]
 —●— Measurement by A.D. STUART and A.T. JONES, see [4.47]

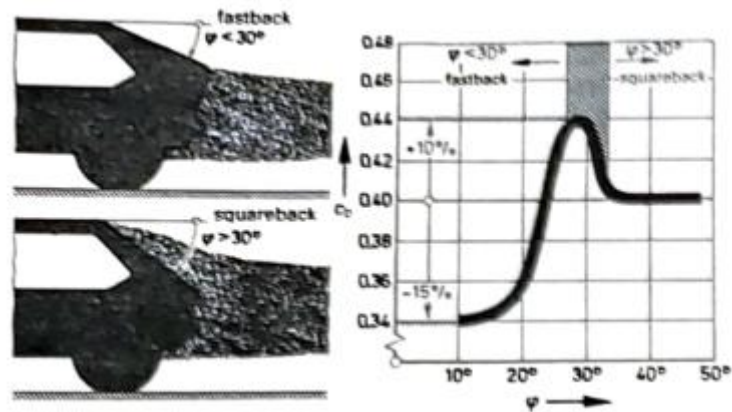


Fig. Influence of slant angle and drag co efficient and flow regime in rear end of car

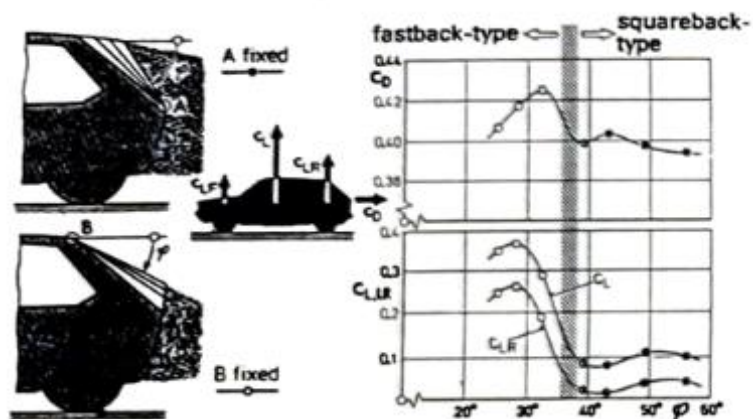


Fig. Influence of slant angle on drag and lift co efficient on c_D and c_L

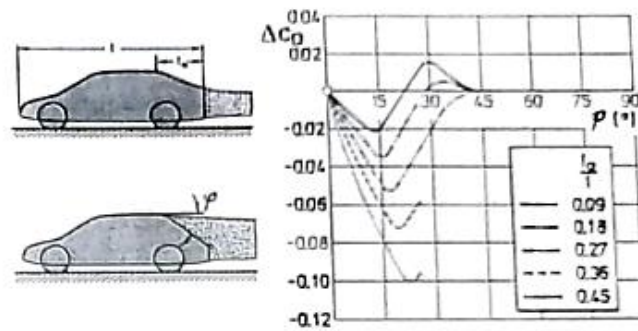
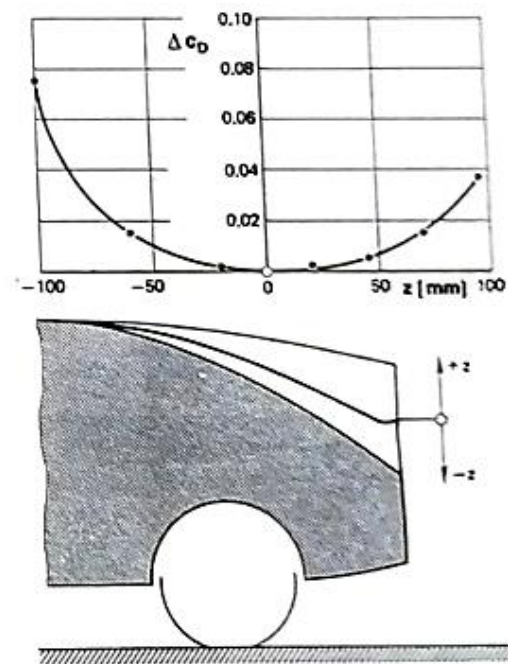


Fig. Influence of slant angle φ and rear length l_0 on drag, after R. BUCHHEIM.



Effect of rear-end height z on drag coefficient c_D for a car with rounded rear, after R. BUCHHEIM, et al. [4.52].
Fig.

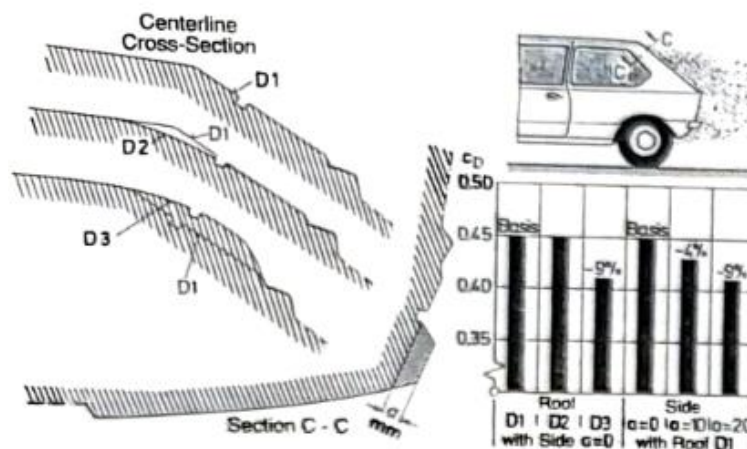


Fig. Effect on drag of minor details at the roof end and side parts

Notchback

The most simple model for a notchback is the two-dimensional backward-facing step. The relevant flow pattern is sketched in Fig 4.62(a). So far, only 90° steps (and wedges) have been investigated. The flow separates at the sharp corner S and forms a clockwise-rotating vortex. The separation streamline, which divides the recirculating flow (dead water) from the outer flow, reattaches at point R. The length x_R at which the flow reattaches is three to five step-heights, the exact value depending on the thickness of the (turbulent) boundary layer ahead of the step (see P. DILGEN [4.53]). H.-D. PAPENFUS [4.54] (see also [4.2] and [4.5]) arrived at a universal pressure distribution inside the dead water behind bluff bodies (see Fig. 4.62(b)). This is used to put together so-called "zonal models" as described in Section 15.7.

However, the length of the trunk in passenger cars is only about twice the step-height (and the angle at location S is greater than 90°). If for specific configurations the flow nevertheless reattaches on the trunk, the reason can be traced to the side vortices. As with a fastback, two trailing vortices are shed at the C-pillars (see Fig. 4.61(a)) and induce a downwash over the rear part of the vehicle, "pulling" the flow over the roof down to the trunk. The sloping rear window of a notchback, like the slope of a fastback, can be compared to a rectangular wing. Its aspect ratio $\Lambda = b^2/A_R$ of 3 to 4 (A_R being the area of the rear window) is greater than that of a fastback, which is roughly 1.5. With the same inclination angle φ , the induced downwash in the longitudinal center section of the notchback is therefore weaker, and the effect of the side vortices on the flow over the rear of a car is less marked. Depending on the

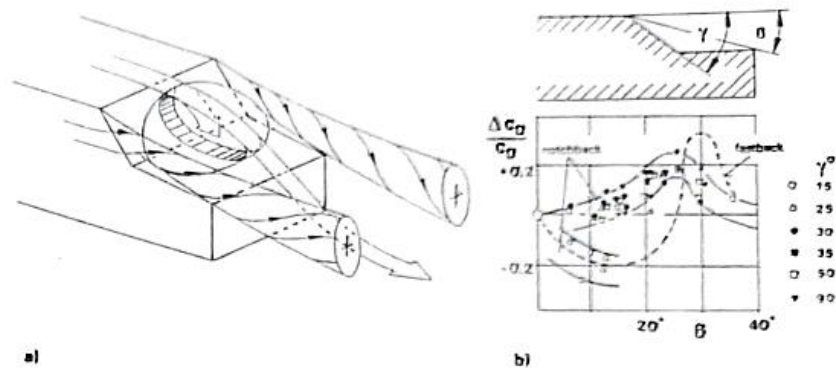


Fig. Flow field and drag of a notchback: a) Flow pattern, b) Drag coefficient c_D vs angle

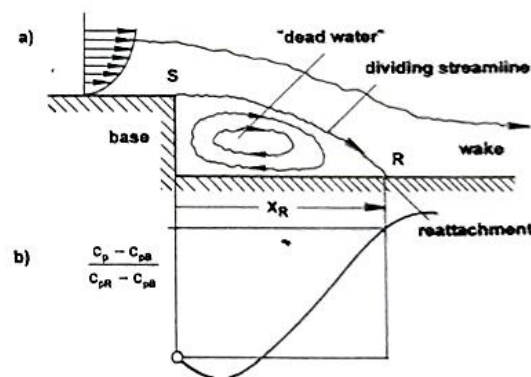


Fig. Flow field on a backward-facing step (notch): a) flow pattern, schematic, b) universal pressure distribution, after H.-D. PAPENFUS [4.54].

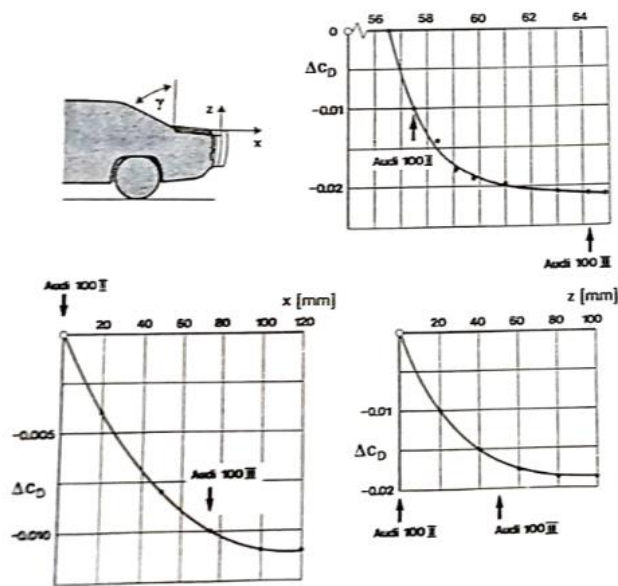


Fig. *Tuning three parameters of the rear end for Audi 100 III*

Plane view and side panels

The starting shape for the plan view of a car is a rectangle. However, a considerable improvement in the flow around a car is achieved by bulging out the sides and thereby tapering the front and rear fenders. The angle between the nose and fenders is thereby made more obtuse, and the junction with the boat-tail is smoother. This measure reduces drag, as does arching of the roof, but only if the c_D value is reduced faster than the frontal area is increased. It is the product $c_D \cdot A$ that counts, not c_D alone. In the Audi 100 III, side flaring was a success, as shown in Fig. 4.66 (after [4.38]). However, the example in Fig. 4.67 shows that success does not always occur. In the Volkswagen research car "Auto 2000,"

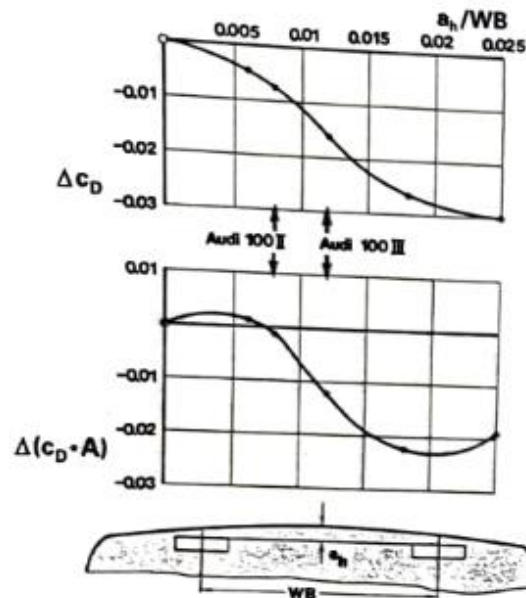


Fig. *Effect of plan view camber on drag of a notchback car*

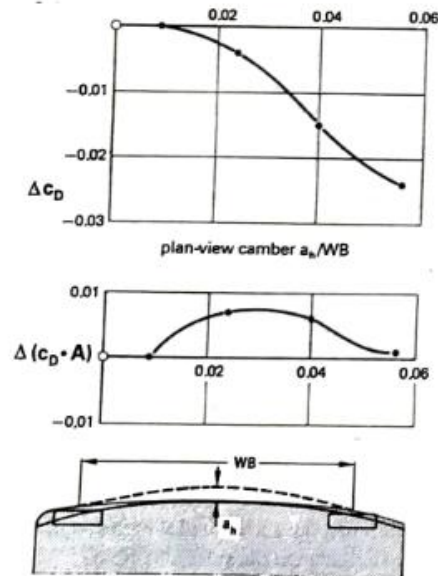


Fig. *Effect of plan view camber on drag of a fastback car*

The drag-increasing effect of rails and recesses placed *across* the line of flow is known from aircraft technology (see S. HOERNER [4.57] and K. WIEGHARDT [4.58]). These findings have since been exploited in car construction. However, it can be seen from Fig. 4.68 that it is not essential to set windows perfectly flush with the bodywork. A recess depth of 5 mm is permissible without any adverse effect on drag, although stricter requirements may be necessary for acoustic reasons, i.e., wind noise. Fig. 4.68 emphasizes that the effect of flush mounting is greatest for front windows, and is progressively weaker the farther back windows are located.

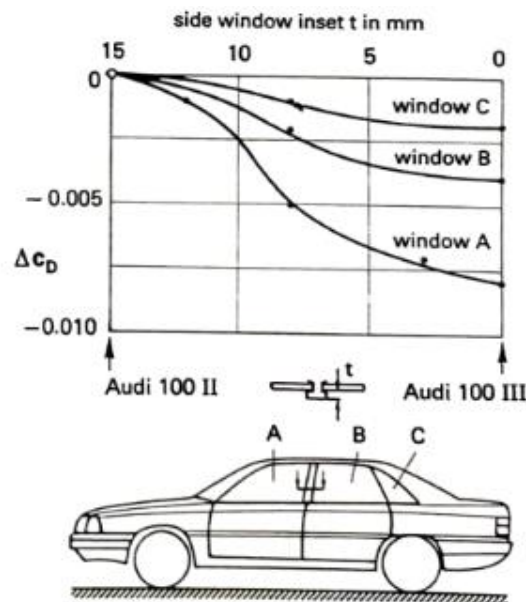


Fig. *Effect of side-window recess on drag, after R. BUCHHEIM,*

Underbody

The underside of most vehicles still resembles a very rough surface. The extent to which drag is increased relative to that of vehicles with a smooth underside can be determined using Fig. 2.9. The fact that a smooth underbody reduces a car's drag significantly has been repeatedly emphasized, but so has the fact that this change would be complex and possibly even disadvantageous. Unless carefully adjusted, trim panels could prevent adequate cooling of the brakes, oil sump, and exhaust system. R. BUCHHEIM, *et al.* [4.38] have smoothed an underbody in stages; the results are given in Fig. 4.69. They total to $\Delta c_D = -0.045$, which comes close to an earlier finding by G.W. CARR [4.59]. However, as already mentioned when discussing Fig. 4.12, considering the flow underneath a car as a flow along a very rough flat plate is too far-reaching a simplification. A more detailed examination of this flow field is needed.

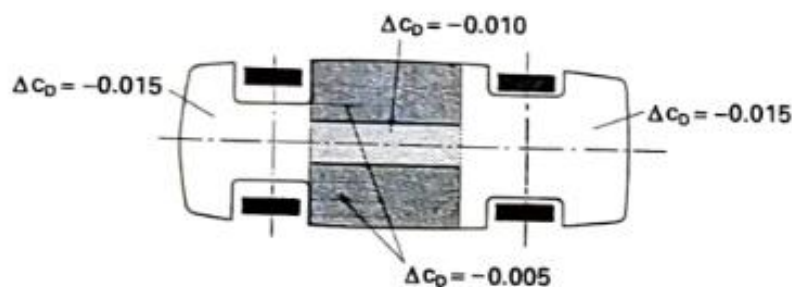


Fig. Drag reduction by section by section smoothing the underbody

Wheels and wheel housing

The contribution of wheels to the drag coefficient of a car is very high; with streamlined cars it can account for as much as 50% of the total drag. As mentioned in Section 1.2.3, this fact was already discovered by W. KLEMPERER in the early 1920s when he was performing model measurements for P. JARAY. Test results on the Pininfarina CNR research car carried out in the mid-1970s, but reported much later (1983) by A. COGOTTI [4.60], are summarized in Fig. 4.70 and confirm this fact. After a long period

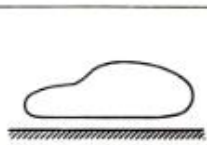
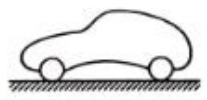
	c_D	c_L	A in m^2 M 1:2
	0.073	-0.044	0.407
	0.157	-0.009	0.462

Fig. Increase in the drag and lift of a low-drag vehicle body by adding the wheels, data from A. COGOTTI [4.60].

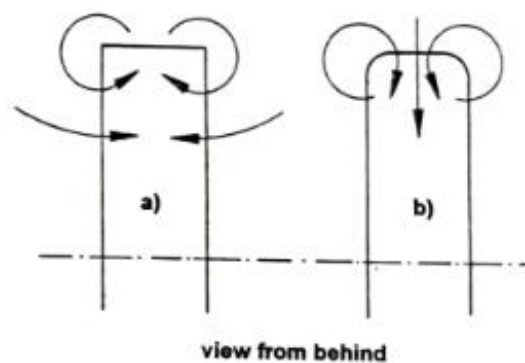
of being considered impossible, the first steps toward improving the aerodynamic properties of car wheels now seems possible.

The cause of the disproportionate contribution of the wheels to overall drag has three main reasons:

1. Wheels are not streamlined.
2. The local flow approaches them under yaw.
3. They rotate within wheel housings.

All three effects interact strongly. But in order to understand their nature, they will be discussed separately.

1. The non-streamlined character of a wheel becomes evident when it is considered as a circular cylinder, off ground and not rotating. For passenger cars the width w of this cylinder is small compared to its diameter d , while for monoposto (single-seat) racing cars the ratio w/d is about one (or even more). For $w/d \rightarrow \infty$, the flow around the cylinder (off ground) is well known and described in Section 2.3.3.4. Flow separates at the rear, resulting in a dead-water region of low pressure and a subsequent wake; the drag is almost entirely pressure drag. At both sides of a cylinder of *finite* width w , two pairs of vortices roll up, one pair at the top and the other at the bottom. Two cases must be distinguished: If the edges ("shoulders") of the cylinder are sharp the flow around the cylinder separates on both *forward* sides and vortices are shed from the sharp "yawed" edges which roll up *outward* (see Fig. 4.71(a)). If the "shoulders" are well-rounded—as is the case for tires—flow passes the forward facing part of the round shoulders without separation. It remains attached on both sides and separates at the rear. Two vortex pairs (upper and lower) are shed from the round shoulders and turn *inward* (see Fig. 4.71(b)).



Vortex formation at the rear of a stationary wheel off ground, as seen from behind:
a) sharp-edged "shoulders," b) rounded shoulders, drawn according to

E. MERCKER and H. BERNEBURG [4.61].

Fig.

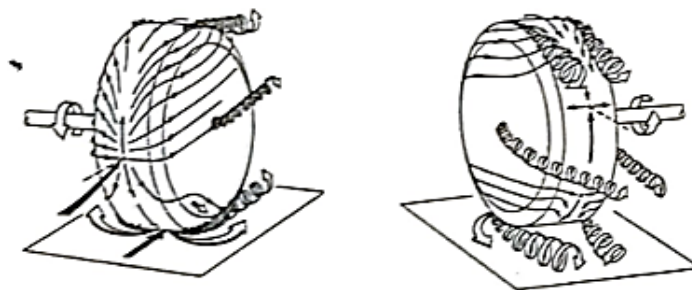


Fig. Flow pattern of a wheel rolling on the ground



SATHYABAMA

**INSTITUTE OF SCIENCE AND TECHNOLOGY
(DEEMED TO BE UNIVERSITY)**

Accredited "A" Grade by NAAC | 12B Status by UGC | Approved by AICTE

www.sathyabama.ac.in

**SCHOOL OF MECHANICAL ENGINEERING
DEPARTMENT OF AUTOMOBILE ENGINEERING**

SAU1601 AUTOMOTIVE AERODYNAMICS

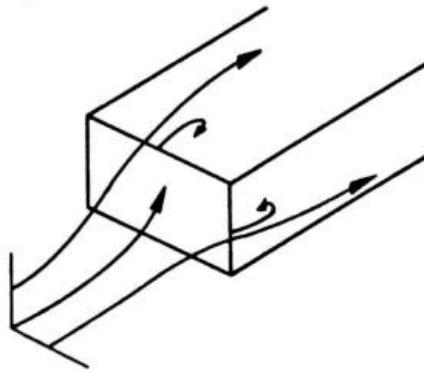
UNIT III SHAPE OPTIMIZATION OF CARS

UNIT III SHAPE OPTIMIZATION OF CARS

Front end modification, front and rear wind shield angle, boat tailing, hatch back, fast back and square back, dust flow patterns at the rear, effects of gap configuration, effect of fasteners.

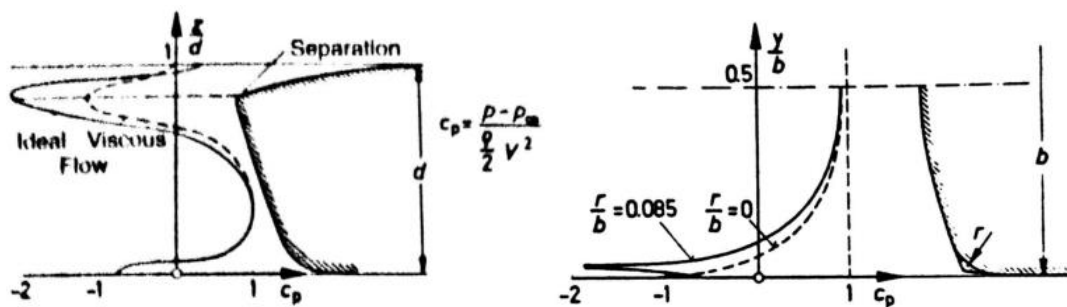
Front End Modification

The front end of a car can be roughly approximated as a square block. The cooling air intake is assumed to be closed. A stagnation point is formed on the vertical front face. Because of the close proximity of the road, the air tends to flow over and around a vehicle rather than under it; the streamlines near the front end are therefore directed upward. The flow is significantly deflected at the intersections between the front face and the hood and fenders.



Without special measures, this flow pattern will cause separation, with the result that the pressure distributions near the edges of the fore body will deviate from those for ideal flow. The suction peaks at the leading edge of the hood and the fenders are very much less pronounced than for ideal, separation-free flow for a longitudinal cross-section. The stream wise pressure force on the front end is therefore greater than in ideal flow, and a drag component is generated. A corresponding difference is found in the horizontal cross-section. The extent to which the pressure distribution is influenced by geometry may be concluded. However, it should be emphasized that illustration like these does not reveal anything about the drag of the front end because the difference from inviscid flow is not evident.

Flow separations on the fore body are avoided in practice by various deviations from the initial right-angled shape. In longitudinal section, the essential parameters are the slope of the hood. The slope of the front-end face and the radii of the transitions to the hood and underbody. In elevation, sweepback, taper and another radius can be added. These individual parameters are



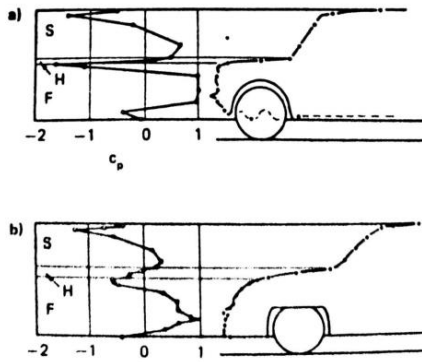


Fig. Pressure distribution in longitudinal cross-section

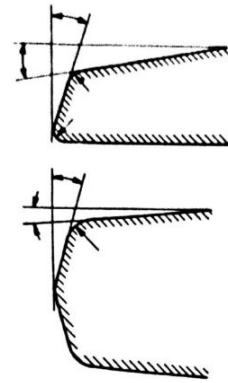
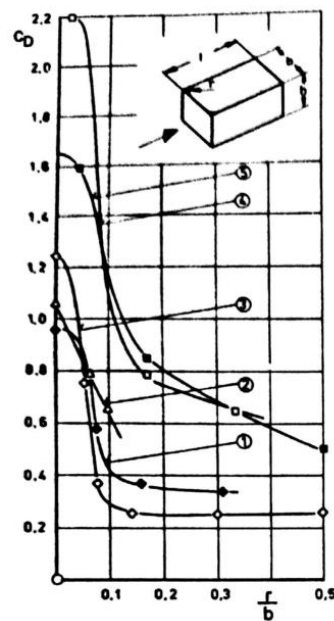


Fig. Essential geometric parameters



Nr	Symbol	Author	Remark
1	—●—	F. Pawlowski 1930	$Re = 1 \cdot 10^5$ squared block
2	—▽—	W. E. Lay 1933	generic car, all edges rounded $b/h = 1,17$
3	—○—	S. Gaster 1944	$Re = 1 \cdot 10^5$ streamlined body
4	—□—	H. R. Delany u 1954	$Re = 1 \cdot 10^5$
5	—■—	H. E. Sørensen 1954	two dimensional body
6	—●— —○—	R. Barth 1960	$Re = 1,2 \cdot 10^6$ $b/h = 2$, $b/h = 1$ all edges rounded
7	—▲—	G. W. Carr 1968	$Re = 2 \cdot 10^5$ $b/h = 1$ all edges rounded

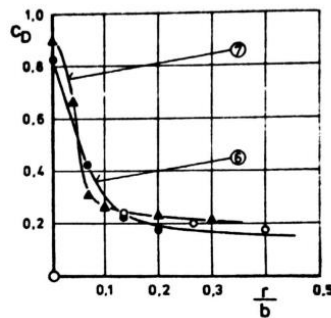


Fig. Influence of edge radius on drag on square blocks.

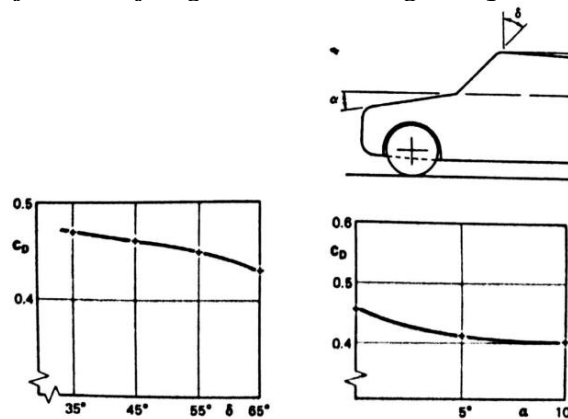


Fig. Reduction of drag with hood inclination α and wind shield inclination δ

The third parameter examined separately is the inclination angle of the front face. Its effect on drag is shown in the fig. based on the work. The fact that this effect is so slight here is probably due to large front corner radii used with this model.

These parameters cannot always be individually varied and so several may be changed at the same time. The specific aim was not to optimize front shape but to demonstrate its possible variations. The initial shape, designated forebody 1 is compared to

different variants. With minor changes in the geometry, the flow around the front end could be considerably improved, and drag significantly reduced.

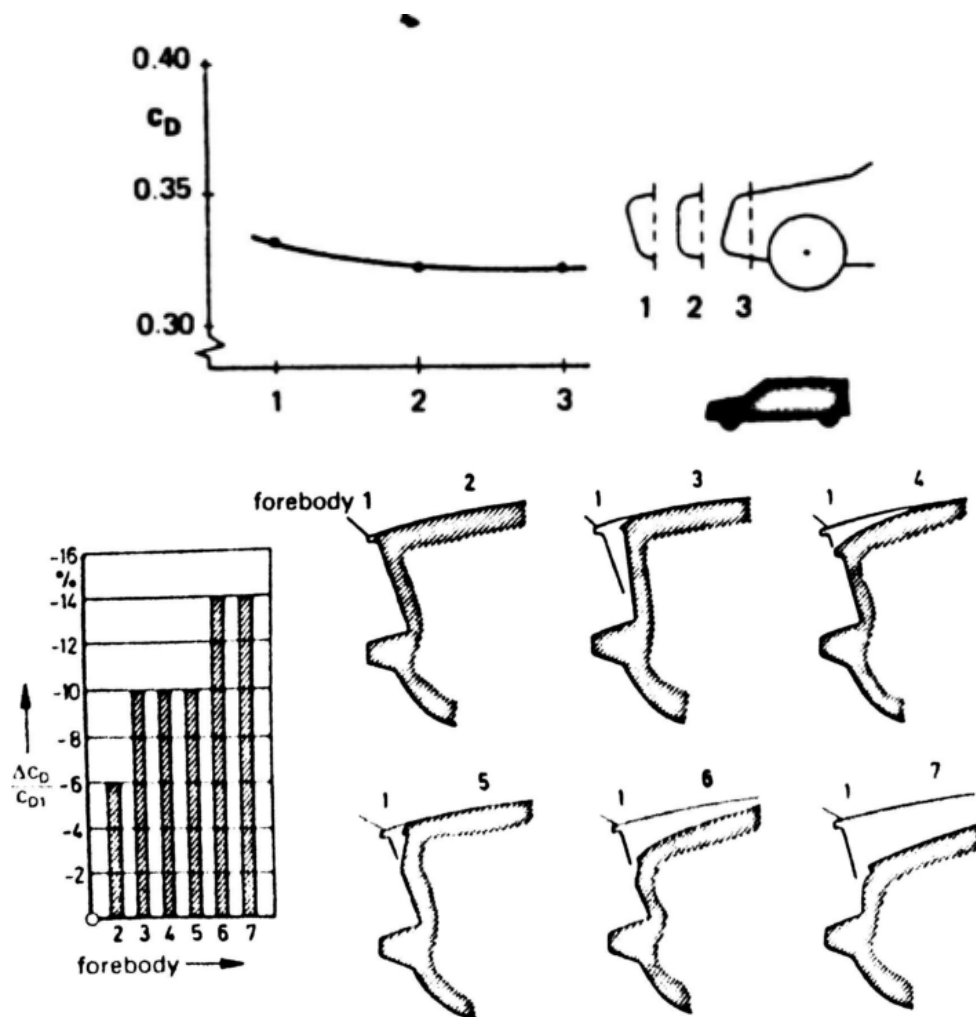


Fig. Formal variants at the front end and drag values.

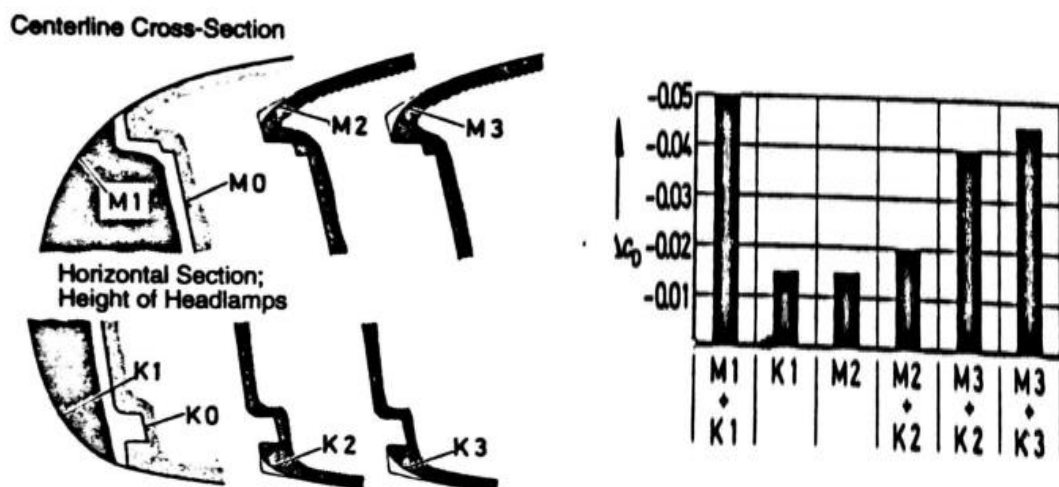


Fig. Optimization of front end structure

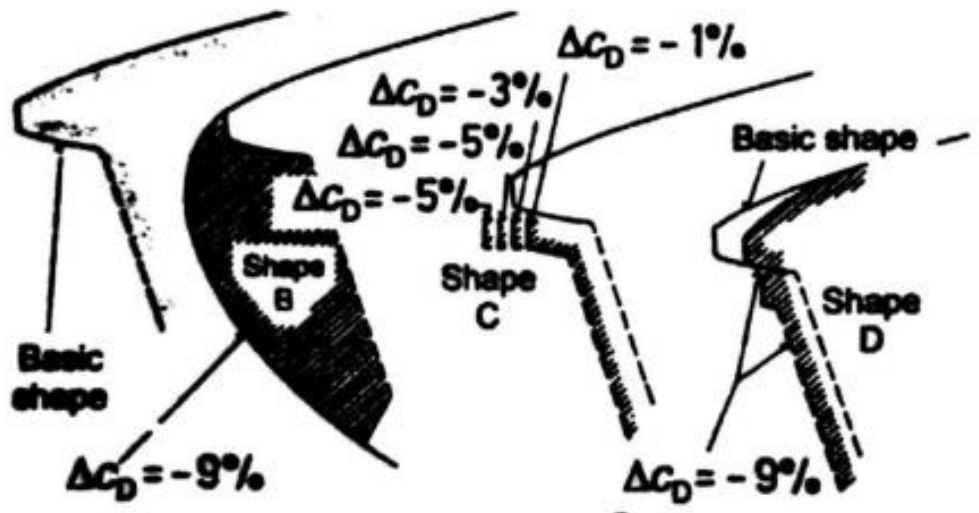


Fig. Drag reduction by fine tuning hood radius and grill design

Front Spoilers

Three positive effects can be achieved with a properly designed front underbody spoiler:

1. Reduced Drag.
2. Reduced lift on the front axle.
3. Increased volumetric flow of cooling air.

Their relative emphasis can be set differently, depending on the particular objectives. Whereas drag was originally the focus of attention, interest very rapidly shifted to lift, in particular for fast cars. An increase in cooling airflow was originally mainly a side effect. It has since been deliberately sought for cars with more powerful engines. The negative side effects of a front spoiler should not be overlooked, but can be offset by special precautions. The spoiler's shielding of the underbody impairs the cooling of the oil sump, and particularly the brakes. However, special air ducting with suitably located openings in the spoiler can help overcome this problem.

There are three variants of front spoiler design. As an add-on part, usually made of plastic, it provides the greatest freedom in terms of geometry, position and height, but additional cost is incurred. The two other versions have a more or less neutral effect on cost, in these, versions; the spoiler is integrated either into the front-end panel or into the bumper.

The drag-reducing effect of a front spoiler is based on the fact that it diminishes the air speed under a vehicle thus attenuating the contribution of the underbody airflow to overall drag. This contribution is normally high due to the "roughness" and the non-streamlined nature of the underbody surface. However, the spoiler itself experiences drag and so careful design is required to achieve positive net effect,

The drag D_{B+S} of the underbody and spoiler combinations:

$$D_{B+S} = D_B + D_S$$

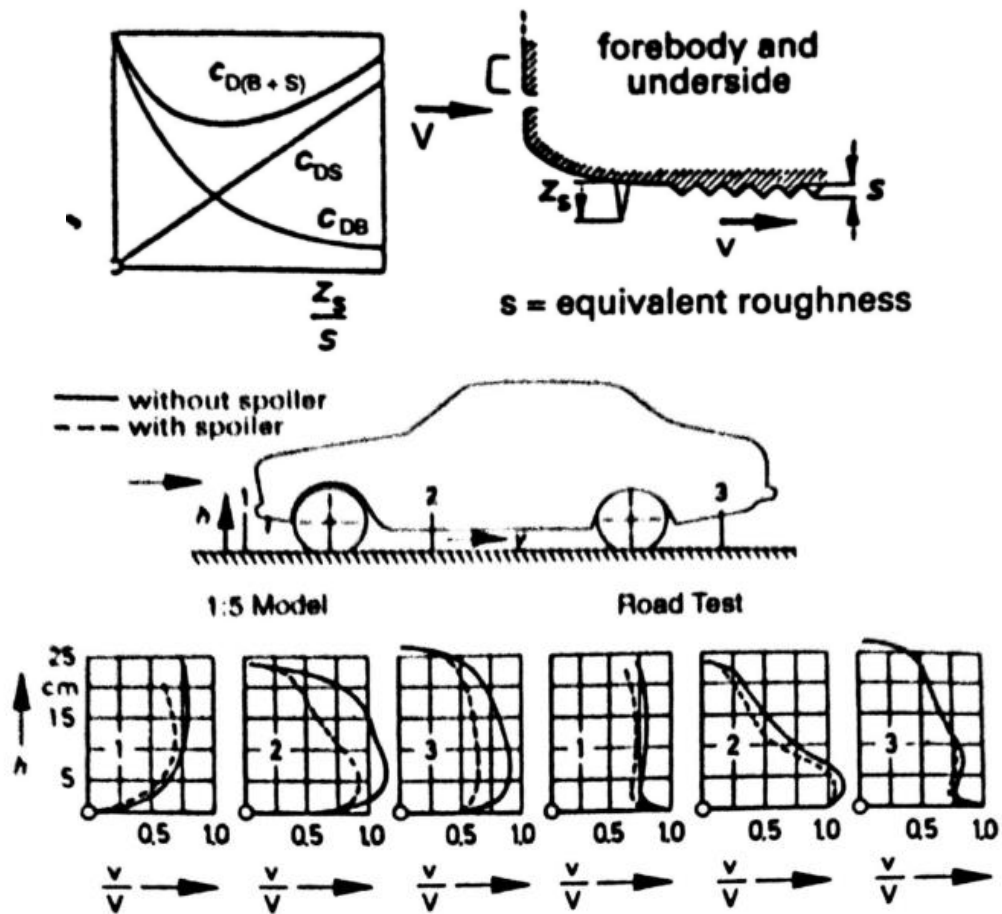


Fig: Velocity distribution a car with and without front spoiler

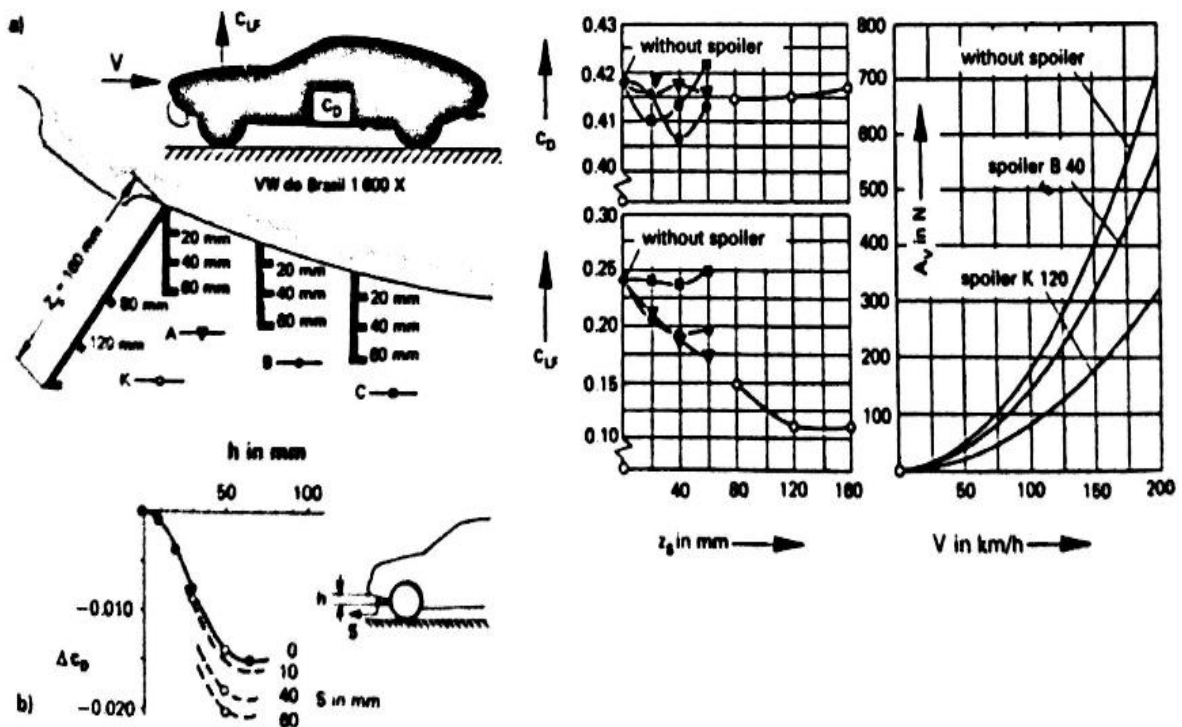


Fig. Front spoiler optimization with minimizing drag

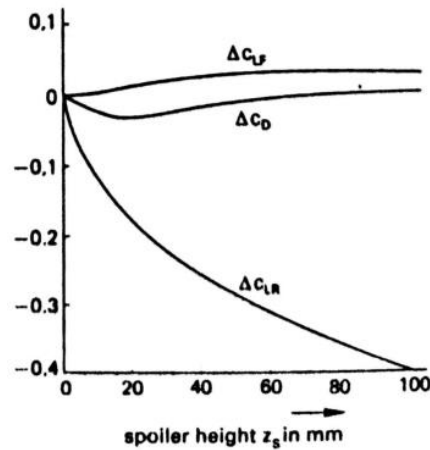


Fig. Influence of Height of rear Spoilers

	A in ft ²	c_D	$c_D \cdot A$	c_{DCar}
Car without Trailer	24.6	0.53	13.0	$\left. \begin{array}{l} (= 1.9) \\ = 1.6 \end{array} \right\}$
Car in front of Trailer	24.6	0.30	7.4	
Trailer without Car	54.2	0.62	33.6	
Trailer behind Car	54.2	0.59	32.0	



Fig. Drag of trailer and towing vehicle

	car towing trailer	car model	C_{D1} $C_{D(1+2)}$	$A \cdot C_{D1}$ $A \cdot C_{D(1+2)}$
trailer, "old" generation		Opel Rekord C	0.452	0.87 m ²
		Opel Rekord C Caravan	0.435	0.84 m ²
		UNI-CAR	0.240	0.48 m ²
		Opel Rekord C	0.754	4.10 m ²
		Opel Rekord C Caravan	0.864	4.63 m ²
		UNI-CAR	0.743	3.98 m ²
		Opel Rekord C	0.605	3.24 m ²
		Opel Rekord C Caravan	0.562	3.01 m ²
		UNI-CAR	0.581	3.11 m ²

Fig. Drag of Trailer Combinations

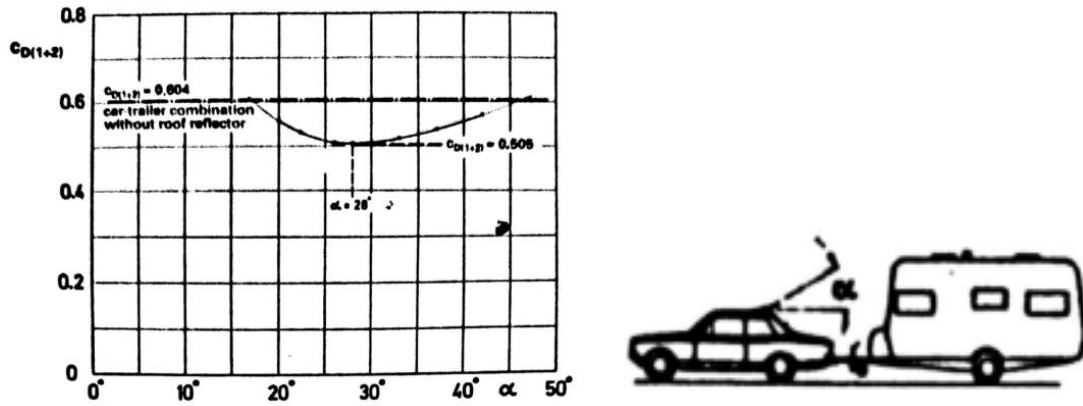
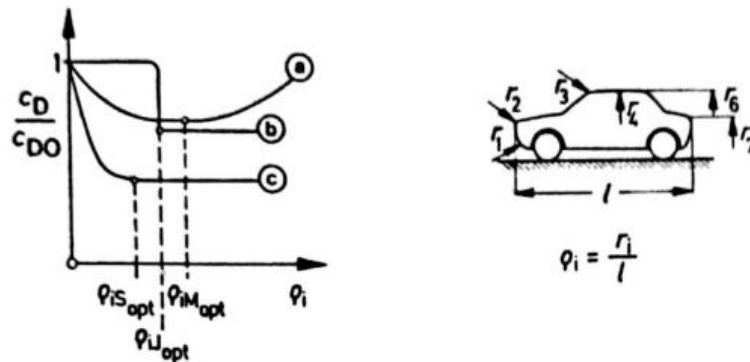


Fig. Optimum position of roof deflector

Detail Optimization

The function link drag coefficient c_D to the vectors r , that describe individual shape elements i.e., that define their configuration. These r_i vectors can be radii, heights or lengths, they are referenced to a characteristic dimension. In this case the vehicle length l :



The following three types of function exist:

1. Saturation. A typical curve is found in the case of rounding an edge. The effect on a body's drag of rounding an edge in a cross-flow. Boat-tailing is another example of saturation.
2. Jump. This type occurs when the flow changes suddenly from one form to another, e.g., when changing from a fastback flow regime to a squareback one.
3. Minimum. This pattern always occurs when the drag is made up of two components that are influenced in opposite directions by the relevant shape parameter. A typical example of this function is the height of the front spoiler

One strategy in aerodynamic development is to determine these functions $c_D(\varphi_i)$ for all the parameters expected to have an effect on the drag of a given model. Due to interference between individual details the process has to be iterative, but if the sequence of tests is chosen to correspond with the path of the flow, i.e., from front to rear, the major portion of such interactions is taken into account.

A common feature of all three functions is that they each have a vector P_i beyond which any further change will produce no further significant reduction in drag. This vector P_i as termed "optimum," because it identifies the optimal φ_i value. Functions provide a basis for the practical consideration of proposed body styling measures.

It played an essential part in convincing designers to abandon their traditional aversion to aerodynamics because they found that the optimal parameters often differed only

slightly from the initial values they had chosen for aesthetic reasons. Significant reductions in drag therefore became possible without perceptibly altering the appearance of a car and without violating its styling concept.

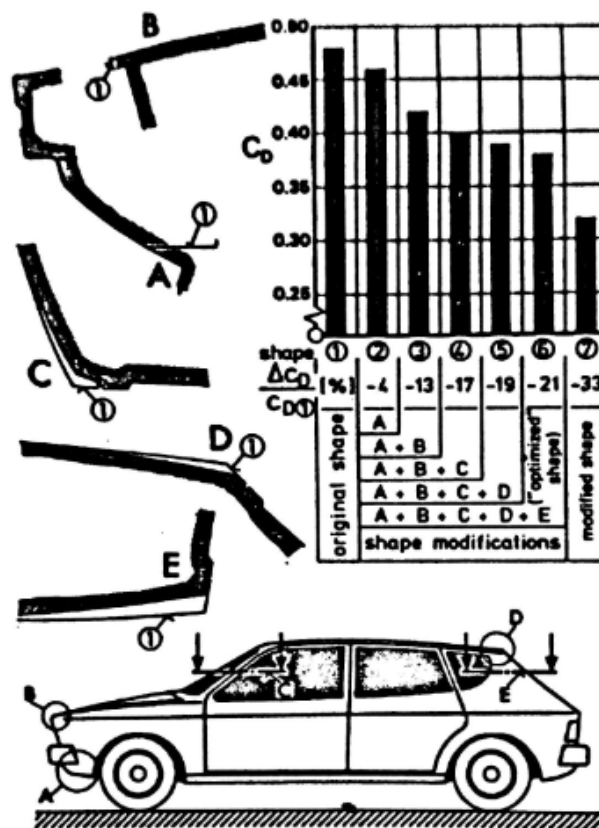


Fig. Detail optimization of a car

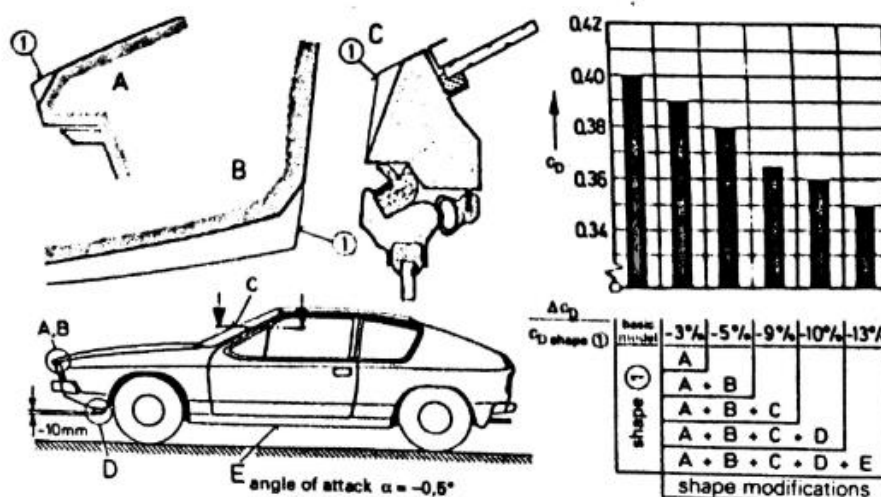
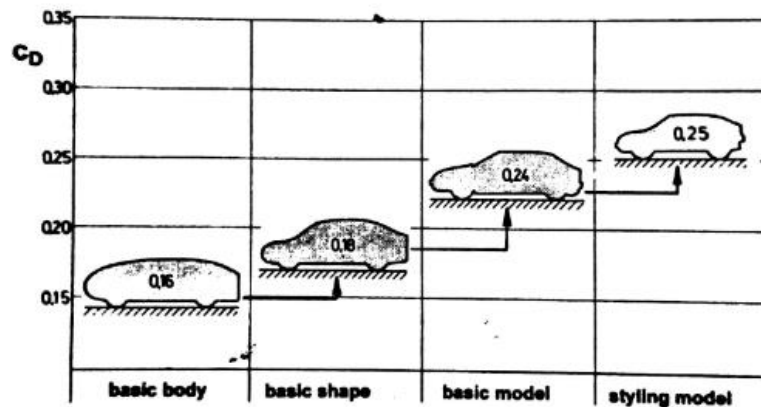
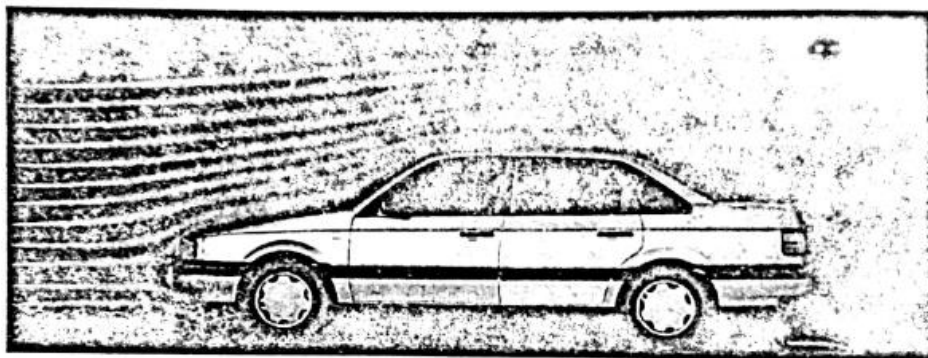
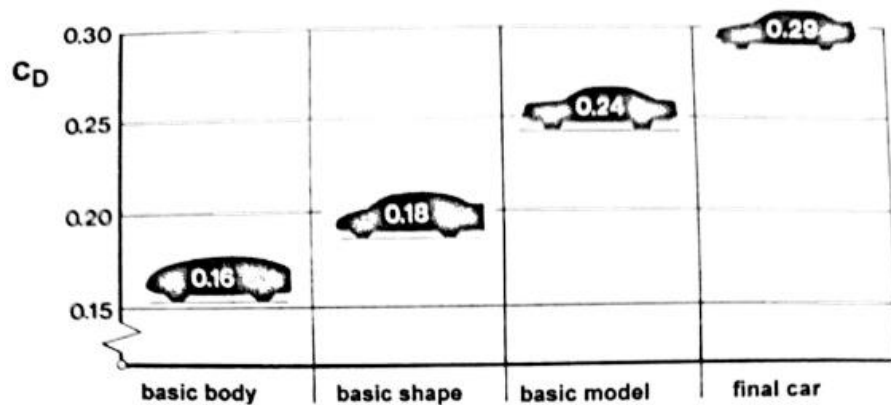


Fig. Detail optimization of coupe.

Shape optimization

In shape optimization, aerodynamic development starts with a shape having very low drag teamed the *basic body*. The only constraint on this basic body is that it must not exceed the main overall dimensions of the projected car, i.e., length, width,

and height, and it must have the car's ground clearance. During the development process this basic body is progressively transformed into a car.



As with detail optimization, shape optimization generates a set of functions that link individual modifications to drag increments. The basic shape that results contains all the essential shape elements of the subsequent car but is still entirely smooth; it has only a slightly higher drag than the body. The fact that in progressing from the basic shape to the basic model a large increase in drag is inevitable demonstrates once again the importance of detail. Depending on how far this basic models deviates from the design concept, the model may undergo a further rise in drag in progressing to the final car, the aesthetically acceptable vehicle.



SATHYABAMA

**INSTITUTE OF SCIENCE AND TECHNOLOGY
(DEEMED TO BE UNIVERSITY)**

Accredited "A" Grade by NAAC | 12B Status by UGC | Approved by AICTE

www.sathyabama.ac.in

**SCHOOL OF MECHANICAL ENGINEERING
DEPARTMENT OF AUTOMOBILE ENGINEERING**

SAU1601 AUTOMOTIVE AERODYNAMICS

UNIT IV VEHICLE HANDLING

UNIT IV VEHICLE HANDLING

The origin of forces and moments on a vehicle, lateral stability problems, methods to calculate forces and moments – vehicle dynamics under side winds, the effects of forces and moments, characteristics of forces and moments, dirt accumulation on the vehicle, wind noise, drag reduction in commercial vehicles.

The effects of aerodynamic forces and moments on the driving stability are most noticeable in side wind gusts. This is especially true when, in passing maneuvers or because of "obstacles" (buildings, trees, bushes, etc.) in the landscape, quick changes in direction and speed of ambient wind occur.

The flow around a vehicle becomes asymmetrical. A lateral force (called side force), a yawing moment, and a rolling moment result, and lift and pitching moment are also changed. This leads to course deviations which must be compensated by the driver's steering corrections. The airflow pattern resulting from the forward motion of the vehicle produces a lift and a pitching moment. This results in changed road loads of the wheels and affects the road-gripping ability of the Tires. The alternating play of these forces and moments on the vehicle influences its directional stability in straight-ahead driving as well as its inherent steering behavior during directional changes.

The term shaping does not only refer to the basic shape of the vehicle, but also includes those aerodynamic effects created by details such as cooling airflow, body gaps, rearview mirrors, tires, spoilers, and roof loads. Finally, along with the aspects of aerodynamics and vehicle dynamics, the driver's steering behavior must be considered.

A new situation arose in road traffic; three important changes contributed to making the effects of aerodynamic forces on the driving behavior noticeable:

- First, improved roads and highways allowed higher speeds.
- Encouraged by aerodynamicists who were striving to reduce the drag force, and by designers who were searching for new, more dynamic styling to replace the carriage-related "monumental" shapes, flowing lines and softly rounded curves became popular. The typical slender fastback designs at the end of the 1930s reduced the aerodynamic drag; however, compared to the conventional square-edged vehicle bodies, these shapes were unfavorable with regard to directional stability. The rear lifts, and under side wind also the yawing moment, greatly increased.
- Finally, quite a number of vehicles with rear engines were introduced to the market at that time. This concept reflected the new styling trend toward "teardrop" shapes. Today, the driving-dynamic disadvantages of vehicles with the center of gravity located way back have become well known.

$$L = c_L(\beta) \frac{\rho}{2} v^2 A$$

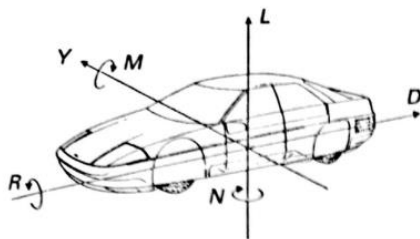


Fig: Forces and Moments in a Vehicle

$$M = c_M(\beta) \frac{\rho}{2} v^2 A l$$

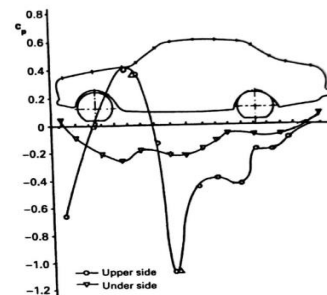


Fig: Origin of lift and pitching moment

In side winds and during passing maneuvers, the flow will be asymmetrical. This, in turn, leads to an asymmetrical pressure distribution for a typical horizontal cross-section. As a result of high local flow speed there is an area of negative pressure on the forward lee-side edge and in the region of the A-pillar, while a slight positive pressure on the windward side is observed. At the rear end there is a zone of slightly lower pressure on the lee side as compared to the windward side. This pressure distribution results in a lateral force and a yawing moment which can be reduced to side forces at the front and rear axle.

The direction of the airflow relative to the vehicle's movement and the direction of the resulting aerodynamic force are not the same. The angle of yaw is smaller than the angle between the x-axis of the car and the resulting aerodynamic force. In strong crosswinds, the lateral force can easily be higher than drag. Similar to lift and pitching moment, side force Y and yawing moment N .

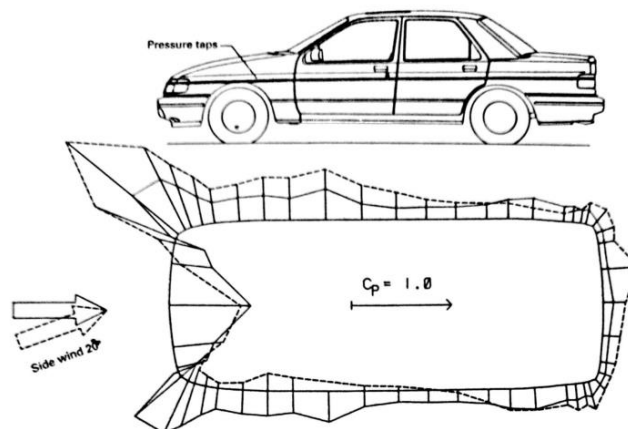


Fig: Pressure distribution in horizontal section, $\beta = 20^\circ$ yawing angle

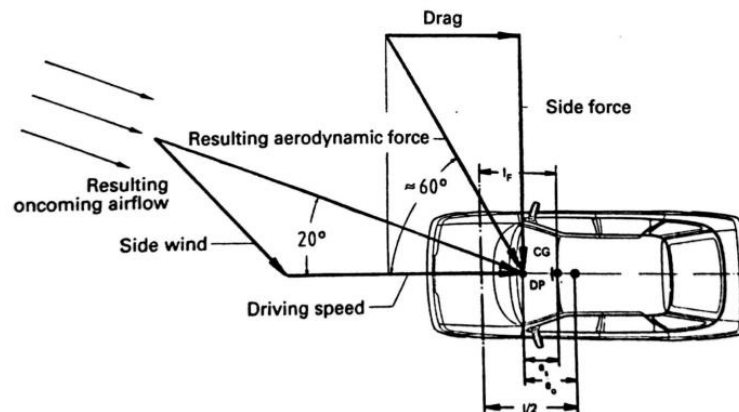


Fig: Resultant Forces and Moments

Aerodynamic Stability

Aerodynamic stability means that a change in the direction of resulting oncoming wind is generating a counteracting yawing moment which tends to turn the vehicle such as to reduce this change. If a yawing moment produced by a side wind tends to increase the disturbance the vehicle is aerodynamically unstable. An attached flow around the front end and the rear end will result in comparatively large yawing moment. If the quotient from the change of the yawing moment to the change of the yawing angle is positive, a vehicle is aerodynamically unstable. A flow separation at the rear will reduce this instability.

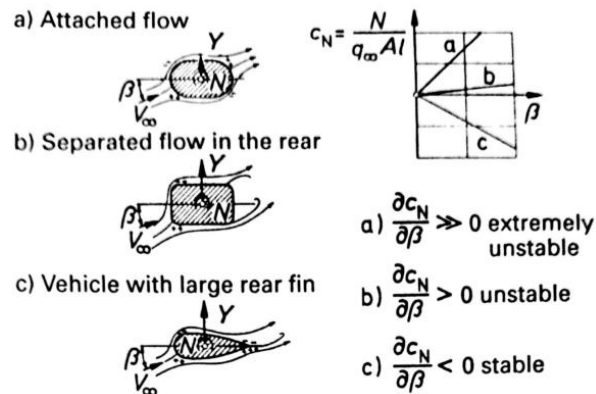


Fig: Aerodynamic Stability in Crosswinds

The effect can be used to attenuate aerodynamic instability without sacrificing fuel economy. The linear increase of yawing moment can be interrupted by controlling the flow separation at a certain yawing angle. The drag then increases significantly, as depicted. However, if the "critical yawing angle" is above the yawing angles occurring under normal driving conditions, this drag increase will hardly affect fuel economy.

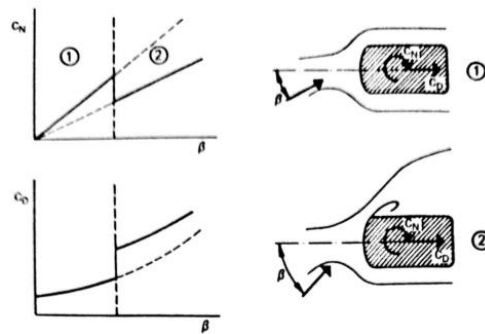


Fig: Reduction of yawing moment

Aerodynamics and Driving Behavior

Vehicles with conventional styling generally have positive lift. At moderate driving speeds and zero yaw, lift and pitch are insignificant. However, at speeds above, say, 150 km/h (94 mph), the wheel loads are clearly influenced by lift. It conveys an impression: at high speeds, the rear axle load of a notchback vehicle can be reduced by 10%. This impairs the directional stability (oversteer) and increases the sensitivity of the steering response to small disturbances. The effect on directional stability can be evaluated by using a stability index. For the sake of simplicity, the actual vehicle is simulated by a single-track model.

$$\dot{\psi} = I_F \cdot F_{SF} - I_R F_{SR} + c_{SP} \frac{Y}{I_Z} \quad A_Y = \frac{F_{SF} + F_{SR} + Y}{m}$$

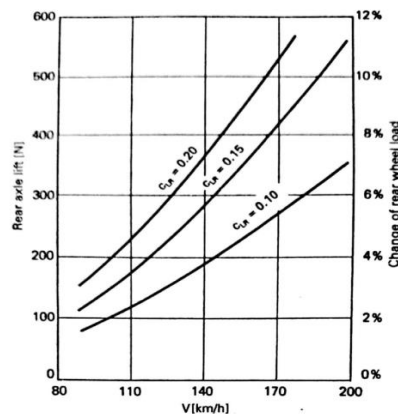


Fig: Change on rear wheel load

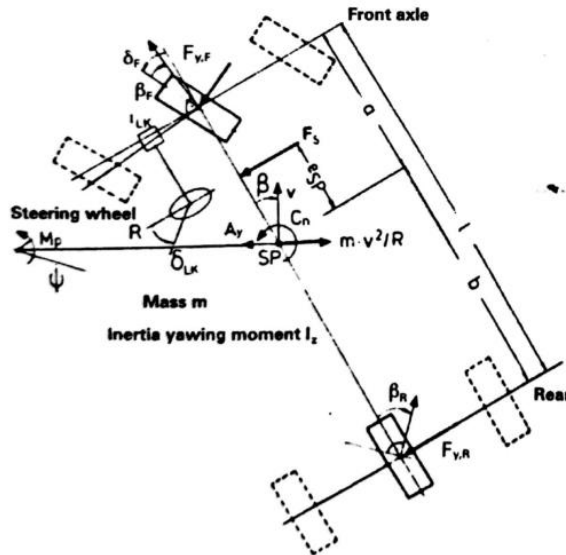


Fig: Single track vehicle course holding model

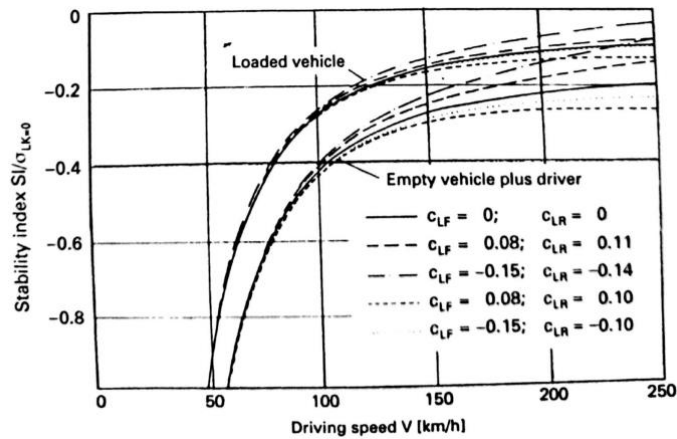
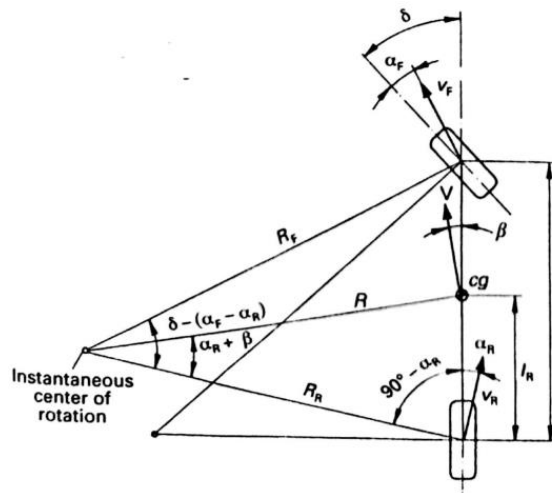


Fig: Stability index versus driving speed, Empty and Loading Condition

Cornering

The cornering behavior is an important criterion in the evaluation of the driving characteristics. Driving a circular course at constant speed is considered first. In a single-track vehicle model, the two wheels of one axle are combined into one wheel in the axle center. The angle between the speed vector V of the center of gravity and the vehicle longitudinal axis is the slip angle β .



An over steering tendency due to high rear lift can be reduced, for example, by a chassis configuration with an increased roll stiffness of the front axle by using lateral stabilizer.

Power On Off Reaction

An important criterion in the evaluation of the non-stationary driving behavior is the power on/off reaction in fast cornering maneuvers. Dangerous driving situations due to load changes often occur, when the radius of the curve decreases along the route ("tightening bend"). In a sudden deceleration, now braking engine reverses the direction of the circumferential forces acting on the drive wheels. The pitching moment shifts the wheel contact forces from the rear to the front axle. The Increased vehicle slip angle leads to a course deviation and, in extreme cases, to an uncontrollable skid.

Driving behavior in cross winds

Crosswinds can lead to an impairment of steady-state straight-ahead driving, or even become dangerous. The resulting phenomenon of crosswind stability must be considered from two points of view. Continuous steering corrections mean a loss of comfort; they require great concentration and thus lead to earlier fatigue of the driver. However, strong wind gusts in combination with wet or icy roads could impair driving safety. Three effects must be considered with regard to crosswind stability: the acting aerodynamic forces and moments, the driver's behaviour, and the vehicle's response.

Natural Wind and Crosswind

The statistical data on wind strength and wind direction normally represent values from measurements which are taken at 10m above the ground. The wind flow near the ground has boundary-layer character. The thickness of this boundary layer depends on the structure of the terrain; the wind speed directly above the road can differs.

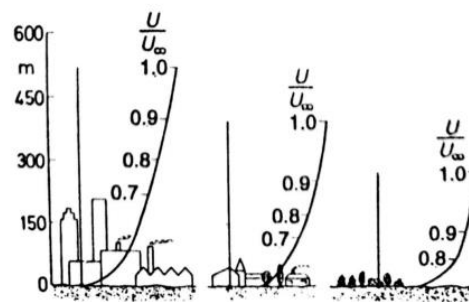
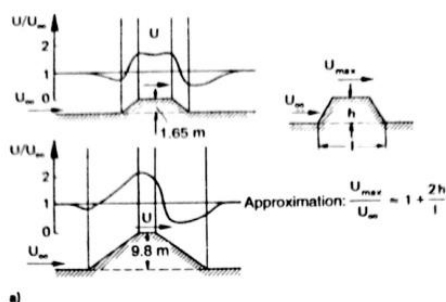
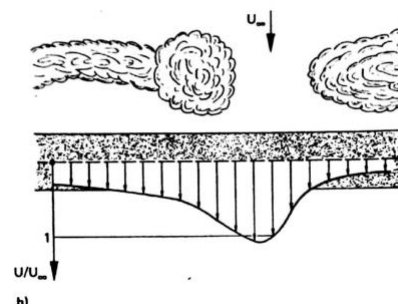


Fig. Natural wind boundary layer over ground with various roughness

There may also occur a local wind speed increase in gaps between bushes or buildings, as shown in Fig. A higher wind speed is also to be expected on bridges, connected with a change of the wind direction. The occurrence of wind (speed and direction) depends on geographical conditions and cannot be generalized. It must be taken into consideration not only when roads are planned but also during the assessment of wind accidents. Suddenly occurring wind gusts can cause difficult driving situations and require high attention from the driver. The gust periods of winds near the ground vary between 7 and 10 seconds.



Increased crosswind velocity



Nozzle effect of a gap

Aerodynamic effects of forces and moments

Lift and pitching moment

The magnitude of lift and the differences between front and rear lift (resulting from the pitching moment), there are decisive factors for directional stability depicts the effect of the basic shape configuration on pitching moment and lift. A high stagnation point at the front enhances front lift. A low line of flow separation and a downward inclination of the streamlines at the rear cause high rear lift. This leads to a small overall lift and a reduced pitching moment.

First to be studied was the effect of rounding off the edges perpendicular to the flow. The individual corners of a sharp-edged generic vehicle model were rounded in the sequence indicated by the numbers in Fig. By progressively rounding the edges, a tendency toward higher lift was observed which can be explained as follows: Rounding off the edges reduces (and with increasing radius finally prevents) flow separation in the affected areas. The flow velocity over the vehicle is increased, the static pressure on its upper surface is reduced, and correspondingly lift goes up.

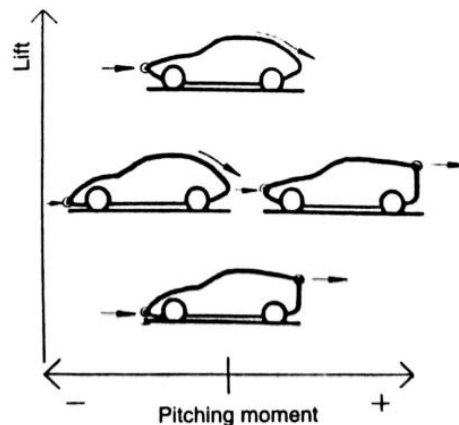


Fig. Influence on stagnation pin point and flow separation height

The flow entering the underbody area was at first accelerated there but, due to the obstruction by the wheels and underbody protuberances was decelerated farther downstream. This created a pressure rise between the road and underside of the vehicle and resulted in increased overall lift, mainly front lift. It measures which create a low stagnation point at the front end direct the flow more upward and reduce the lift. Typical examples are the backward-tilted front panel and low sharp-edged front spoilers. This knowledge has clearly influenced front-end configuration of modern vehicles. Also favorable for low lift are highly tilted windshields. However, within the limited range of today's conventional windshield angles, the differences are marginal.

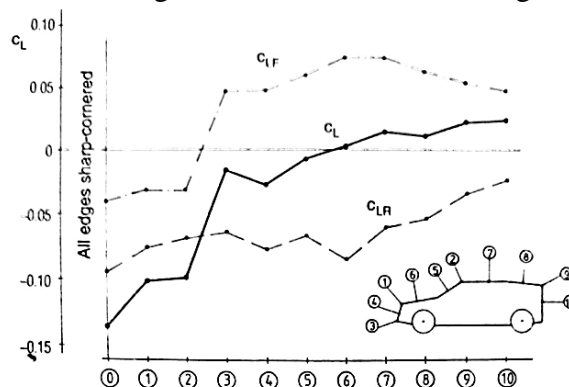


Fig. Impact of rounding edges on lift

Rear lift and overall lift decrease with increasing slant angle and increasing rear flow-separation height. This can be explained in that the streamlines over the rear are curved less downward and directed more in the horizontal line. This result in a higher static pressure over the vehicle and thus less lift.

Side force and Yawing moment

The yawing moment increases approximately linearly up to a yawing angle of $\beta = 20^\circ$, as shown in Fig 5.57(11). The greater yawing angles are not likely to occur at higher vehicle speeds. Therefore, $\beta = 20^\circ$ is a good choice as test condition and it is justified to use the data at this angle as reference values for the comparison of side force and yawing moment characteristics of different vehicles. In the depicted example, the notchback exhibits the highest yawing moment and the squareback the lowest. Since all three models have the same front-end shape so that the side force at the front axle is almost identical, an opposite "sequence" is obtained for the overall side force. Consequently the total side force is lowest for the notchback and highest for the squareback.

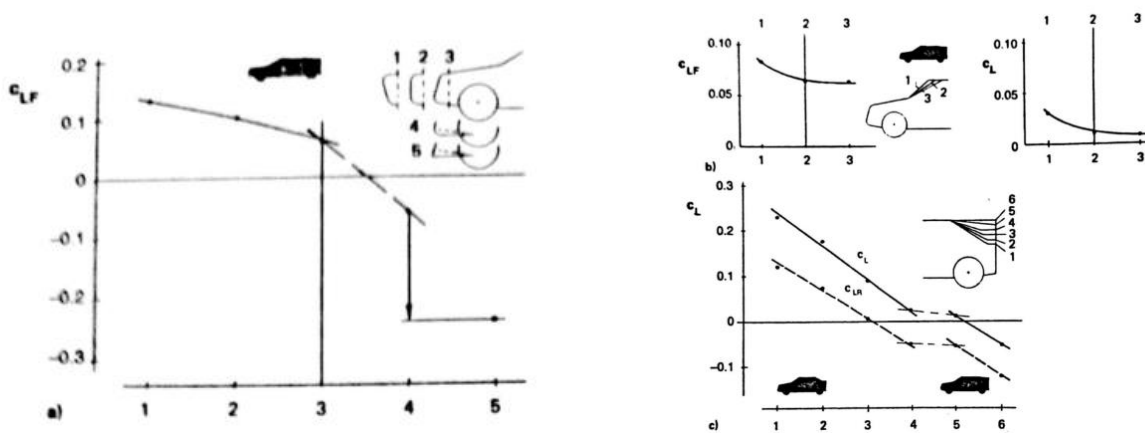


Fig. Impact on front end shape, Wind shield and rear end on lift

The effect of rounding edges on the yawing moment is shown in Fig. The rounding of the edges at the front end-hood (1) and sides (4)-increases the yawing moment and leads to lower pressure on the leeward side of the front end. On the other hand, rounding off the side edges of the front hood (6), as well as the rounding of the A-pillars (5), brings about a reduction of the front side force and yawing moment. In the rear, all lateral rounding's (7, 8, 10) produce a reduction of the side force at the rear axle which corresponds to an increase in yawing moment. In the assessment of these results it must be taken into consideration that the sequence in which the rounding was undertaken affects the magnitude of the individual changes of the aerodynamic forces.

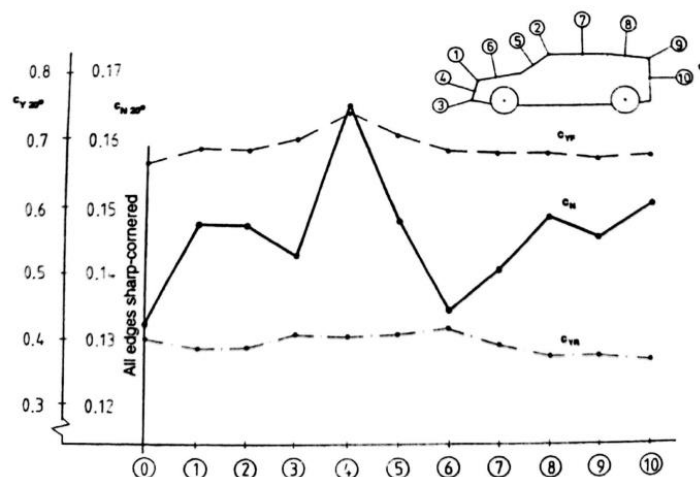


Fig. Effects of rounding edges on side forces and yawing moments

One test result on this model with fully smooth underbody deviates from the experiences on actual passenger cars." The rounding of the lower front-end edge (3), which is favorable on the generic model, creates increased yawing moment, lift, and drag on real vehicles with functional underbody structures, a low front spoiler, on the other hand, produces a reduction of the yawing moment. The characteristics are in good agreement with those observed on actual vehicles. A low-placed cowl (hood-windshield junction) and, to a lesser extent, a greater windshield angle reduce the front side force and, therefore, the yawing moment.

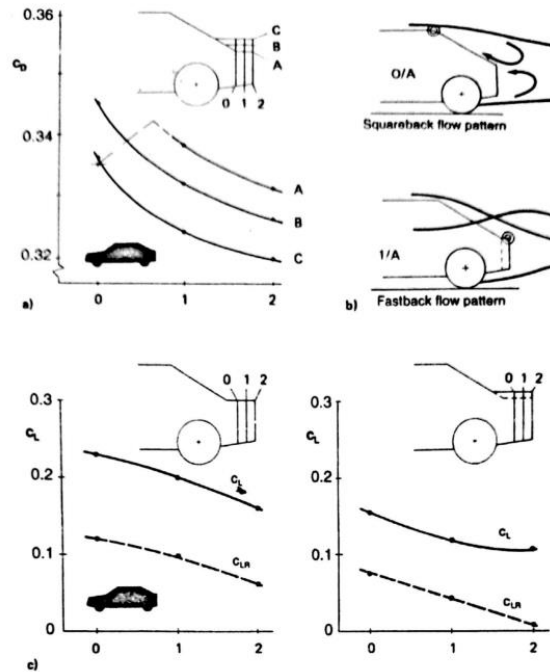


Fig. Drag, lift and wake structures of various rear end

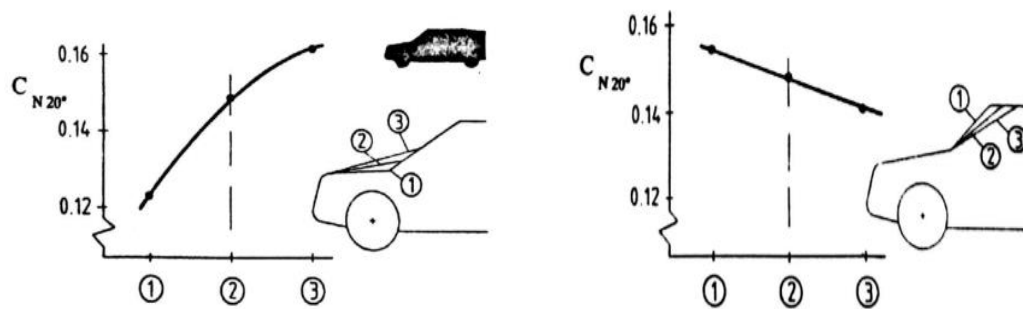


Fig. Impact of cowl height and windshield angle

The lateral projection area in the back will reduce the rear side force and thereby increase the yawing moment. However, this correlation is not valid for well-rounded rear-end configurations. Pronounced plan-view rounding and curvatures in the back impact the yawing moment more than differences in the side projection areas. Minor rounding on the rear pillars can lead to increased yawing moment. This effect is most significant for fastbacks. As the rounding of the D-pillars of fastback shapes reduces the aerodynamic drag, this leads to conflicting goals for the vehicle development.

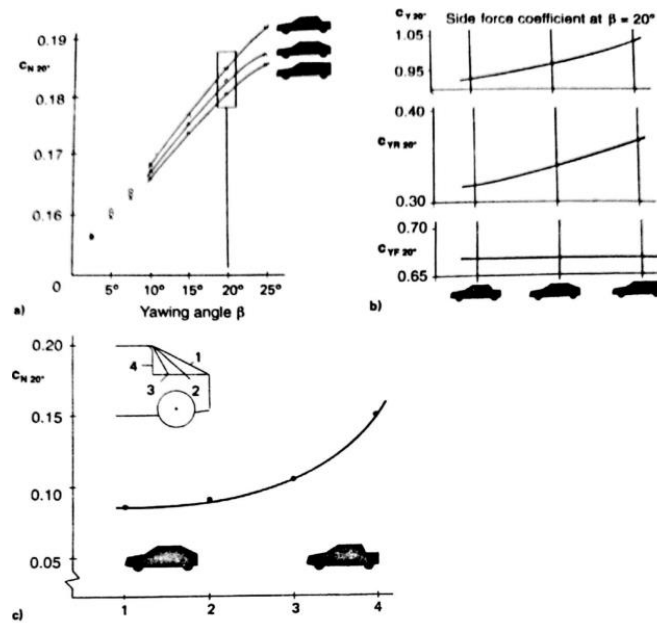


Fig. Yawing moment and side forces of typical car shapes

Rolling Moment

The rolling moment increase with yawing angle β . Again, due to the approximate linearity of the curves in the given range of yawing angles, the figures at a yawing angle $\beta = 20^\circ$ can be used with reasonable accuracy for comparative ratings of various configurations. The squareback exhibits the greatest rolling moment; the notchback the lowest. Regarding yawing moment, an opposite sequence is obtained. The rolling moment increases with the side force.

The rounding of initially sharp edges reduces the rolling moment. The rolling moment increases, however, with the rounding of the lower edge of the vehicle front panel. A sharp edged spoiler produces low pressure below the windward side of the underbody and thus counteracts the rolling moment.

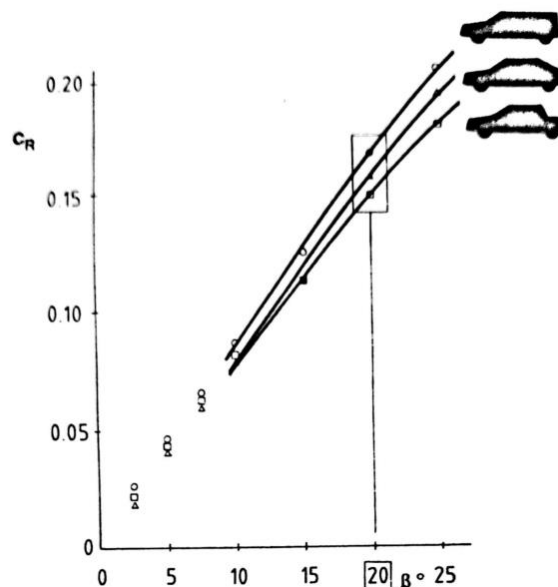


Fig. The rolling moment for three basic shaped cars

- The differences in aerodynamic drag are relatively small for the three designs. The drag increase at yaw is more pronounced for the squareback than for fastback and notchback.

- The squareback produces a considerably lower lift than the notchback and the fastback between 0° and 20° yawing angle. The fastback has the highest lift. With increasing yawing angle, lift increases for all versions. The increase is less pronounced for the fastback, and is the steepest for the squareback. The lift differences are small in the range of higher yawing angles $\beta > 20^\circ$.
- In the entire range of yawing angle, the measured side forces increase almost linearly. Notchback and fastback show similar characteristics. The squareback exhibits a sharper side force increase.
- The yawing moment of fastback and notchback increases almost linearly with yawing angle. In this case, the decrease of the yawing moment of the fastback in the area of large yaw angles ($\beta > 15^\circ$) is attributable to the special comers causing a definite flow separation at the D - pillars.
- The squareback shape is characterized by a relatively moderate yawing moment increase.
- An approximately linear increase of the rolling moment is observed at yawed flow conditions. The squareback leads to a somewhat higher rolling moment than the fastback and the notchback. The characteristic of the curves is similar to that of the side force.
- The pitching moment coefficients of all three rear-end configurations remain negative up to a yawing angle of approximately 20° . This is synonymous to lower lift at the front axle than at the rear axle. The squareback produces the lowest pitch; the absolute values of the fastback are the highest. With increasing yawing angle, the pitching moment for the fastback and notchback decreases. The pitching moment curves for all three configurations get closer and produce somewhat similar values at $\beta = 20^\circ$.

Aerodynamic Effects of the Features of Actual Vehicles

The outer skin and the underbody of actual vehicles exhibit "rough areas," protruding parts, gaps, and openings. Their aerodynamic properties differ from those of the base configurations. A large portion of the aerodynamic research in the industry has concentrated on reducing these differences: weld flanges were moved toward the interior, flush windows were introduced, manufacturing tolerances tightened, and cooling air openings were exactly tuned to the thermal requirements.

Cooling Airflow

The cooling airflow not only affects aerodynamic drag but also lift and pitching moment. The effect is all the more pronounced with increased engine performance and increased cooling air requirement; related drag and lift data are compiled. It is remarkable that the increase of front lift is considerably greater than the increase in drag. As with drag, the increase in lift depends on the volume flow of cooling air: the smaller the flow, the better. This calls for a proper guiding of the cooling airflow from the inlet into the body to the radiator.

The increase of front axle lift due to cooling airflow is remarkable. The change in front lift is an order of magnitude greater than the lift without cooling airflow. Also the rear lift is changed; generally it decreases by half the value of the front lift increase. In other words, the pitching moment changes from positive to negative.

Along with the effect on lift and pitch, the cooling airflow also produces an increase in, Swing moment side force increases at the front and decreases at the rear. The effect, however, is not as pronounced as the change of the lift forces.

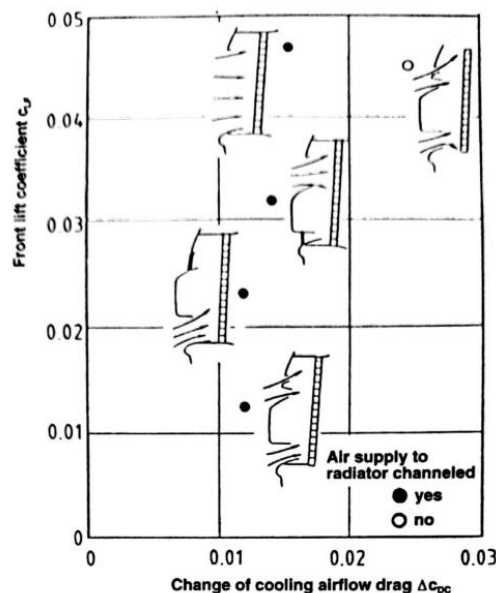


Fig. Influence of position and size of cooling air inlet opening on front lift and drag

Gaps and Openings

All gaps and openings not required for cooling and ventilation are reduced or covered to a degree that they barely have any effect on aerodynamics (wind noise being the only exception). The sealing of joints and openings on the vehicle front end reduces front lift and front side force. Door joints have almost no impact on aerodynamic force and moment.

On fastback vehicles, the sealing of gaps at the sides of the tailgate can increase the yawing moment. This measure may keep the flow at the windward side of the rear pillar and rear window attached a little bit farther downstream, thus causing an extended low-pressure area there which contributes to the yawing moment. In many station wagons and compact cars with inclined rear window, the open gap between the roof and tailgate ensures a stable squareback-type flow separation with low rear lift. Sealing this gap may result in a changeover to a fastback flow configuration with high rear lift and high aerodynamic drag.

Exterior Rear view Mirrors

The exterior mirrors disturb the flow at the A-pillars. Long trailing wakes results which affect the flow at the sides and around the rear end. Along with an increase in drag (approximately 2-5% for today's passenger cars), the flow separation on the A-pillars produces a slight reduction of lift on the front axle on the order of $\Delta c_L = 0.01$. On the rear axle, the change is approximately half as great. With regard to directional stability this is hardly noticeable.

Wheels, Tires, and Underbody

A trend toward wider tires has been observed; they improve tire adhesion on dry roads, are more aesthetic, and thus enhance the customer value of the vehicle.

Aerodynamically speaking, wider tires produce further blocking of the airflow underneath a vehicle. This increases the lift as has been demonstrated with results plotted. How much the lift is increased depends on the configuration of the vehicle front end. The increased lift due to wide tires can be compensated by a spoiler underneath the bumper. It may be advisable to develop special front-end spoilers for sporty models with particularly wide tires. The tire width does not have any noticeable impact on the yawing moment.

Openings in the wheel caps and rims which are useful for brake cooling slightly reduce side force and lift at the front.

Protruding structures and unevenness on the underbody retard the flow underneath a car and increase the static pressure in this region. Increased drag and lift are the result. Smoothing in the front reduces front lift but produces an increased rear lift. Additional covers in the center and rear of the underbody reduce the rear lift and lead to a slightly increased front lift. Cars with a sporty character, in particular, are often equipped with aerodynamic add-on parts. Manufacturers and aftermarket offer a large variety of front spoilers, rear spoilers, and rocker moldings. When properly tuned these parts may reduce drag and contribute to better directional stability.

Directional Stability

The flow around a vehicle not only leads to drag but also causes other aerodynamic forces and moments (as components of the resulting wind force and wind moment) which affect driving stability. At high road speeds, their influence on driving comfort can be felt and, in extreme cases, safety is affected.

The airflow pattern resulting from the forward motion of the vehicle produces a lift and a pitching moment. This results in changed road loads of the wheels and affects the road-gripping ability of the tires. The alternating play of these forces and moments on the vehicle influences its directional stability in straight-ahead driving as well as its inherent steering behavior during directional changes. Through natural ambient wind and passing maneuvers, the flow around a vehicle becomes asymmetrical. A lateral force (called side force), a yawing moment, and a rolling moment result, and lift and pitching moment are also changed. This leads to course deviations which must be compensated by the driver's steering corrections.

The effects of aerodynamic forces and moments on the driving stability are most noticeable in side wind gusts. This is especially true when, in passing maneuvers or because of "obstacles" (buildings, trees, bushes, etc.) in the landscape, quick changes in direction and speed of ambient wind occur. In these cases, the interaction of air forces and inertia forces is decisive for the directional stability. Aerodynamics alone is not sufficient to explain the dynamic behavior of a vehicle; consequently, the relevant driving mechanics must be taken into consideration.

Driving Behavior in Crosswinds

Crosswinds can lead to an impairment of steady-state straight-ahead driving, or even become dangerous. The resulting phenomenon of "crosswind stability" must be considered from two points of view. Continuous steering corrections mean a loss of comfort; they require great concentration and thus lead to earlier fatigue of the driver. However, strong wind gusts in combination with wet or icy roads could impair driving safety. Three effects must be considered with regard to crosswind stability: the acting aerodynamic forces and moments, the driver's behavior, and the vehicle's response.

Natural Wind and Crosswind

The statistical data on wind strength and wind direction normally represent values from measurements which are taken at 10 m above the ground. As reported, among others, by the wind flow near the ground has boundary-layer character. The thickness of this boundary layer depends on the structure of the terrain. Consequently, the wind speed directly above the road can differ greatly from the official data.

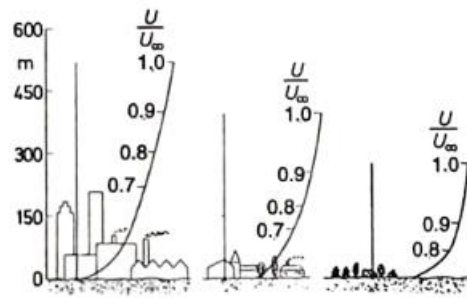


Fig. Natural wind boundary layers

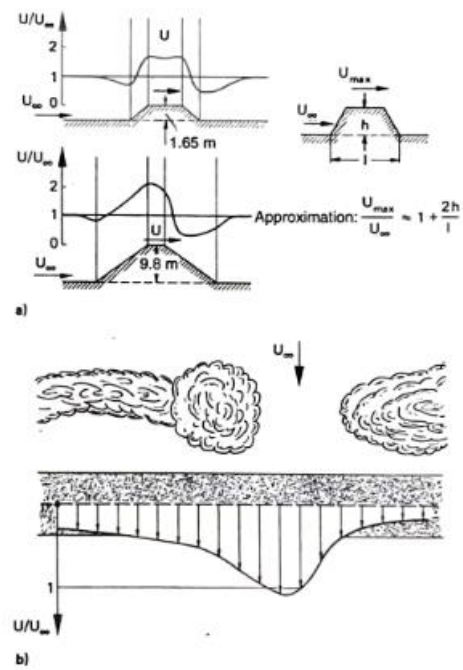


Fig. a) Increased crosswind velocity on top of an embankment; b) nozzle effect of a gap between bushes



SATHYABAMA

**INSTITUTE OF SCIENCE AND TECHNOLOGY
(DEEMED TO BE UNIVERSITY)**

Accredited "A" Grade by NAAC | 12B Status by UGC | Approved by AICTE

www.sathyabama.ac.in

**SCHOOL OF MECHANICAL ENGINEERING
DEPARTMENT OF AUTOMOBILE ENGINEERING**

SAU1601 AUTOMOTIVE AERODYNAMICS

UNIT V WIND TUNNELS FOR AUTOMOTIVE AERODYNAMICS

UNIT V WIND TUNNELS FOR AUTOMOTIVE AERODYNAMICS

Introduction, principle of wind tunnel technology, limitation of simulation, stress with scale models, full scale wind tunnels, measurement techniques, equipment and transducers, road testing methods, numerical methods.

A wind tunnel forms the initial baseline for the interpretation of the interaction between aerodynamic properties and directional stability. Initial estimates can already be derived from it based on practical experience. A distinct correlation exists between the Yawing moment measured in a wind tunnel and the subjective rating of directional stability in a crosswind test; the prerequisite being that the yawing moment is related to the vehicle's center of gravity, the aerodynamic characteristics of a vehicle cannot be determined with reasonable accuracy by numerical methods, all computations predicting vehicle dynamics still are based on wind tunnel results. The same is true for stability tests in a driving simulator. The advantage of wind tunnel tests is that data can be obtained on models (even in reduced scale) in a very early development phase, which allows an estimate of the dynamics of a vehicle concept long before drivable prototypes are available. However, wind tunnel measurements do not perfectly simulate on the road conditions.

In order to achieve a more accurate simulation of realistic flow conditions in a wind tunnel has tuned the profile of the ground-floor boundary layer and created an increased turbulence level by special elements built into the wind tunnel nozzle. Crosswind simulated by these means led to a pronounced increase of side force, yawing moment, and rear lift with yawing angle than with a conventional flat profile of idealized flow.

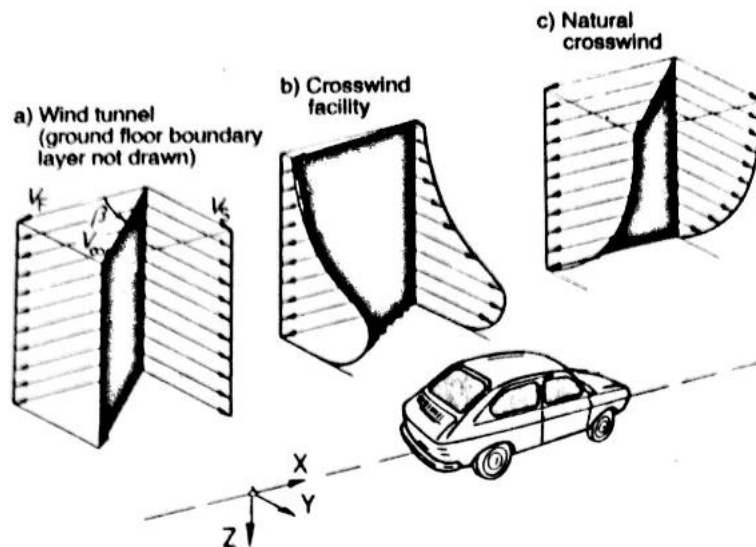


Fig. Comparison of various cross wind profiles

Requirements for a Vehicle Wind Tunnel

Good aerodynamic properties have to be worked into the very first design of a new vehicle, making use of either past experience (or intuition) or computational fluid dynamics (CFD). In a greatly simplified view, aerodynamic development (which is still predominantly experimental) is performed in four phases: It starts with a model, be it small-scale or full-scale, and with the latter often being a hard model. It is continued with a prototype that is ready to drive, is carried further with preproduction vehicles, and is concluded with samples taken from the production line early in volume production.

In the first phase most of the work is done in a wind tunnel. However, experiments can also be carried out in water, either in a water tunnel or a towing tank. Specific problems such as a vehicle's drag when driving through a road tunnel or its response to

crosswind gusts and the wakes of passing vehicles, are studied with models moving through quiescent air and a simulated side wind, respectively. During the second and third phases of development, when drivable prototypes are available, wind tunnel tests are supplemented by road tests. It is on the road that the results of aerodynamic optimization must prove themselves, not in the wind tunnel. Of course, monitoring production vehicles with respect to aerodynamics is performed only in a wind tunnel.

A wind tunnel only simulates the conditions on a road; it does not reproduce them exactly. The variables that influence the flow around a vehicle and its thermal loading: vehicle speed, gusty crosswind, rain, sun load, road dirt, and the grade of the road.

The temperature field above a road is also not always homogeneous. Intense sunlight will heat the surface of the road more than the surrounding air, generating a temperature boundary layer above the road.

Altogether, both fields approaching a vehicle, airflow and temperature, are highly inhomogeneous and non-stationary. The natural wind can be described only by means of statistics and is far too complex to be reproduced in a wind tunnel; the temperature stratification above the road is not reproduced either. Within the limitations mentioned above (homogeneous flow field), the flow of air around a vehicle driving on the road can be simulated in a wind tunnel quite well. However, additional physical factors are involved (e.g., tire rolling resistance, gusty natural wind, engine power, etc.) which are known with only limited certainty.

Adjustments to wind tunnel data for deviations due to limitations of the test setup (lack of simulation) and boundary conditions (interference effects) are made with "corrections". It is mainly unsteady effects that are studied this way: passing or meeting other vehicles, driving through a tunnel, and driving through gusty crosswinds. Furthermore, a towing tank has been used to reveal the differences in underbody flow between a stationary and a moving ground. Towing tests permit the flow field around a car to be reproduced with high accuracy and, when performed in air, not necessarily at the expense of greater effort.

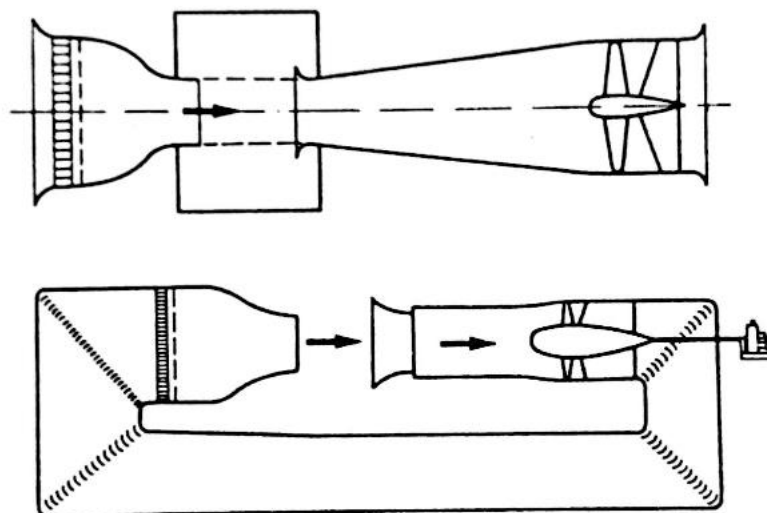


Fig. Wind tunnel with closed return and open return

The same requirements as for forces and moments have to be placed on the quality of flow around a vehicle when flow details are studied. If wind noise is of concern, additional demands regarding the noise level of the tunnel have to be met. The signal-to-noise difference should be at least 10 dB. When soiling is under consideration, the relative motion between vehicle and road and the rotating motion of wheels must be reproduced.

The main advantage of the Wind tunnel is its low power requirement. The gain therefrom is threefold: first, the cost of the drive unit (motor and fan) is comparatively low; second, the operating costs are low; finally, the electric power connection costs are low. The latter are proportional to the electric power installed, and are a considerable part of the fixed costs in the annual budget of large wind tunnels. However, the Gottingen tunnel has disadvantages as well. Due to its length and due to the large settling chamber the costs for the tunnel duct are high. Because many automobile models are made from plasticine (which is susceptible to high temperatures, the tunnel must be equipped with a cooler. To overcome the pressure loss through this cooler requires additional fan power: hence some of the savings from lower drive power are lost. Tunnels with air-temperature control must have a closed circuit, which, in an insulated building, could be of open return.

Properties of the Essential Components

Planning a Test

When planning a test, the user of a wind tunnel should have answers to the following four questions:

1. What kind of wind tunnel is needed (tunnel type, equipment, etc.)?
2. How do the results achieved in a specific tunnel correlate with the road?
3. How many wind tunnel hours are needed?
4. What is the cost of the test campaign?

It depends on the characteristics of the following components of the tunnel:

1. Test section (size, open or closed, kind of road simulation).
2. Nozzle (including the settling chamber).
3. Collector (for tunnels with open test section).
4. Chamber surrounding an open Test section
5. Heat exchanger and full load.

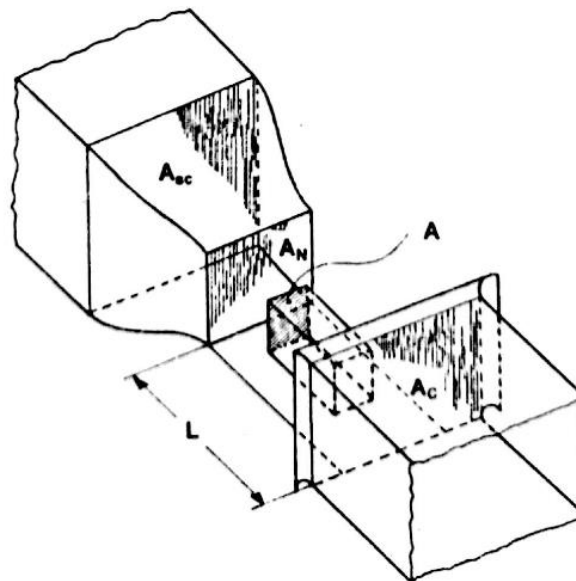


Fig. Test section and its geometric parameters

Test Section

The test section is characterized by two properties: its size and the kind of airstream lateral boundary. The size of the test section is characterized by the cross-section A_N of the nozzle and the length L between the nozzle's exit and the entrance to the collector. Both A_N and L is used in non-dimensional form as follows:

- The blockage ratio $\phi = A/A_N$, where A is the frontal area of the vehicle
- The relative length $A = L/D_N$, where D_N is the equivalent (hydraulic) diameter of the nozzle:

$$D_N = 4A_N/C, \text{ where } C \text{ is the circumference of the nozzle,}$$

With open-jet test sections two further parameters are important:

- The ratio of the cross-sections of collector and nozzle, A_C/A_N .
- The volume of the plenum (and specifically its height and width).

In order to provide kinematic similarity of the flow in a tunnel to that on road, the blockage ratio c_p , which is zero on the road, should be as small as possible. However, cost considerations of a tunnel (construction and operation) demand a blockage ratio as large as "feasible." However, what is feasible in this context is still a matter of discussion.

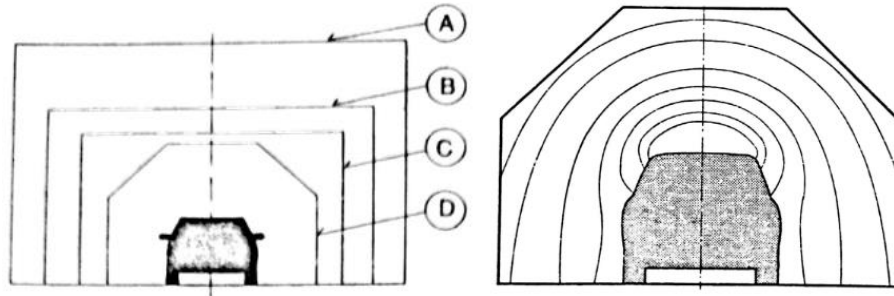


Fig. Various cross sections of test section and matching with isobars

When the first full-scale automotive wind tunnels were built, the blockage ratio was carried over from aeronautics: $c_p = 0.05$. With a frontal area of $A = 2 \text{ m}^2$ typical for cars, this led to a nozzle cross-section of $A_N = 40 \text{ m}^2$. Later, comparative measurements and investigations on test section dimensions and corrections made it clear that a larger blockage ratio could be tolerated; $\phi = 0.10$ seems to be a reasonable limit for cars. Several wind tunnels have been designed with this value, having a cross-section of $A_N = 20 \text{ m}^2$. However, even $c_p = 0.2$ is used: the smallest full-scale wind tunnel has only $A_N = 10 \text{ m}^2$.

Besides the area A_N , the shape of the nozzle's cross-section has been varied. Most frequently the shape of an open-jet's cross-section is rectangular. The ratio of height H to width B is about 0.66. Now and then the corners are rounded off or chamfered. Small, full-scale wind tunnels which are used exclusively for cars have cross-sections other than rectangular.

According to the type of jet boundary, three kinds of test section can be distinguished: open, closed, and slotted walls. The closed test section has been further developed to specific configurations such as streamlined and adaptive walls. The ground floor, which is typical for an automotive wind tunnel, is not a component of the test section. Although physically bound to it. Be it stationary or movable, it is part of the test setup representing the road.

In contrast, in a closed test section the streamlines are constrained by the walls, and so the local speed in the vicinity of a vehicle is increased. In both cases (open and closed test sections) the effect of the jets boundary is the more pronounced the nearer it is to the model, i.e., the larger the blockage ratio ϕ . The motivation for the various types of test-section boundary is to minimize the effect of limited tunnel size, thereby permitting a blockage ratio as large as possible. Frequently, the flow in an empty *open* test section is said to be comparable to an ideal "free jet"; ambient (and therefore constant) pressure is impressed not only on its boundary but also on the entire flow field. A primary advantage that has been assigned to the open-jet test section is a constant static pressure along its axis. Such a property would be advantageous in particular for experiments with bluff bodies because, when measuring the drag of long bodies with large vertical surfaces at the front and the rear, even a small axial pressure gradient in the test section leads to significant error. The second considerable advantage previously attributed to the open test section was a lower absolute value of correction.

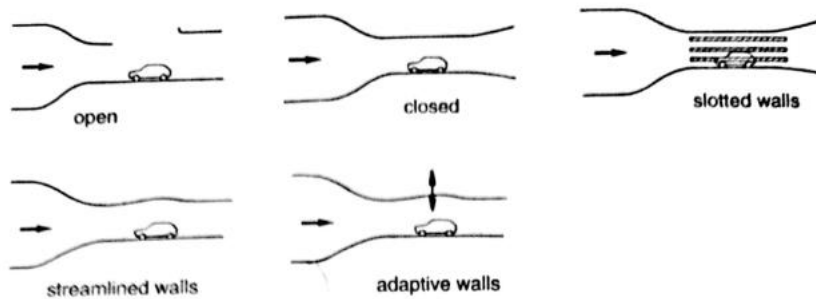
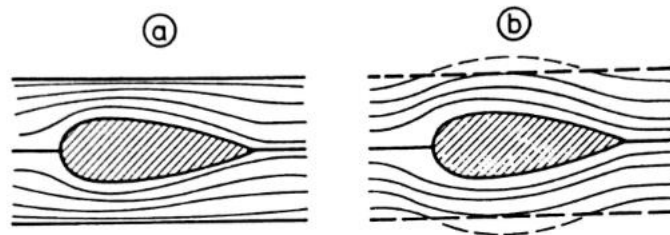
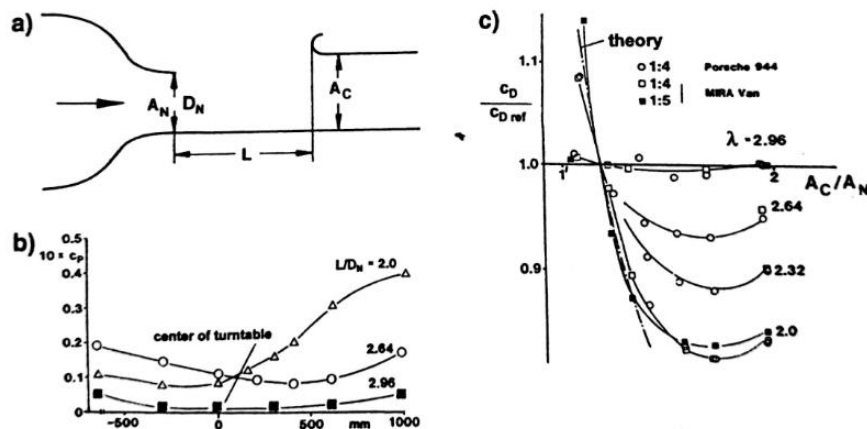


Fig. Test section Boundaries



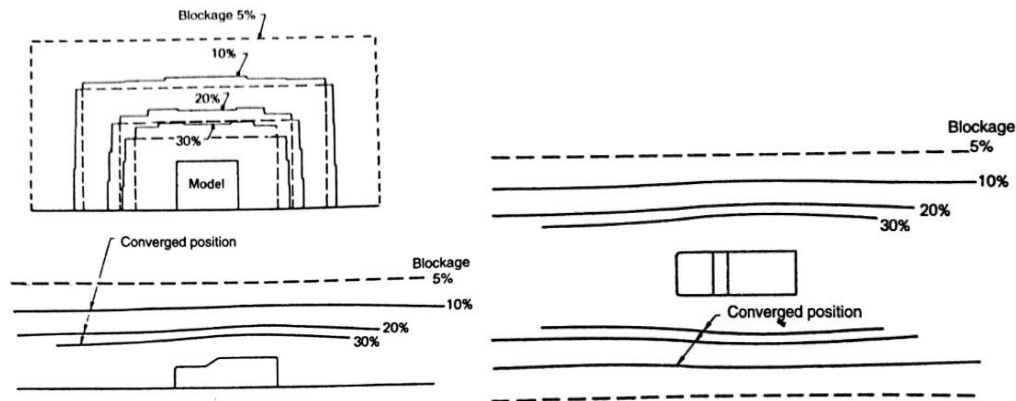
Finally, the third advantage of the open test section is its easy accessibility, which facilitates model installation and the placement probes permit out of flow acoustic measurements, and allows easy. A specific problem may arise when testing race cars in an open test section. Their rear wings produce a high down force (negative lift). The related up wash can be so strong that it bends the airflow behind a car upward and over the collector of the tunnel. Air behind the car is then drawn in from the sides and this may alter the flow pattern at the rear end of the car significantly.



The negative properties of the open test section are the counterparts of the positive properties of the closed. Advantageous for the closed test section is its large usable length. However, boundary layer growth along the walls reduces the effective test-section area, resulting in an increasing velocity and a corresponding decreasing pressure along the axis of the airstream. The related negative pressure gradient can be compensated by slightly increasing the tunnel cross-section in the flow direction. However, this compensation can be correct for only one specific configuration, namely for the empty test section. With a model installed it is merely an approximation. A further advantage of the closed test section is the stability of its flow, i.e., the problem of pumping does not exist.

A disadvantage of the closed test section is its sensitivity to solid and wake blockage; the blockage correction is approximately twice that of a free jet (and is of opposite sign). Furthermore, at a high angle of yaw, the lateral deflection of the airstream may be so strong that the related adverse pressure gradients on the adjacent side walls of the test section may lead to boundary layer separation there. In such a case, a correction for angle of yaw is no longer possible.

The slotted-wall test section is an attempt to combine the advantages of the open and the closed test sections, and, at the same time, eliminate the drawbacks of both. The slots in the walls give ambient pressure access to the flow inside the test section, thus the pressure along the axis is (almost) constant. The solid part of the walls prevents the jet from mixing with the ambient air; the core of the jet therefore remains usable for a greater length. Slotted walls were first used in water tunnels and wind tunnels in marine hydrodynamics to permit research on particularly long bodies at sufficiently large Reynolds numbers.

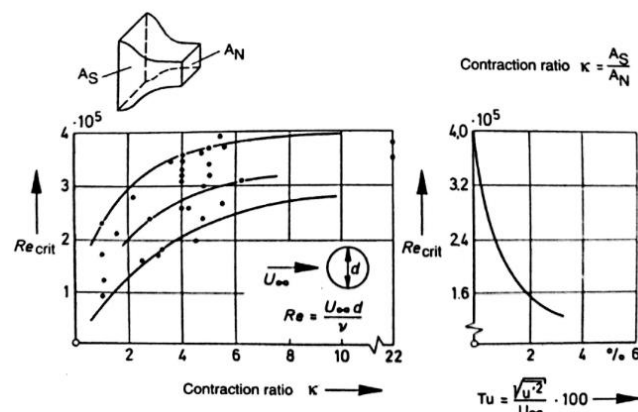


Nozzle

The function of the nozzle is fourfold:

1. It accelerates the flow.
2. It makes the velocity distribution over the cross-section of the flow more uniform.
3. It reduces the turbulence intensity in the stream.
4. It serves to measure the wind speed in the test section.

The quality of the flow in the test section is primarily determined by the design of the nozzle. "Quality of the flow" in this context refers to overall velocity profile, local speed deviations from the average (uniformity), angularity of the flow, and turbulence level. The term "design" represents the geometrical properties of the nozzle, namely its contraction ratio, its length, and its shape (contours of its walls). The contraction ratio is primarily responsible for reducing local velocity deviations from the average, and time wise velocity fluctuations, i.e., turbulence level. Length and wall contours determine the overall shape of the velocity profile at the exit.



When designing a nozzle, two effects have to be considered:

1. To reduce secondary flow in the corners of a rectangular nozzle, the shape of the cross-sections at its entrance and exit should be similar (i.e., for a rectangular

cross-section it should have the same height-to-width ratio at the entrance and the exit).

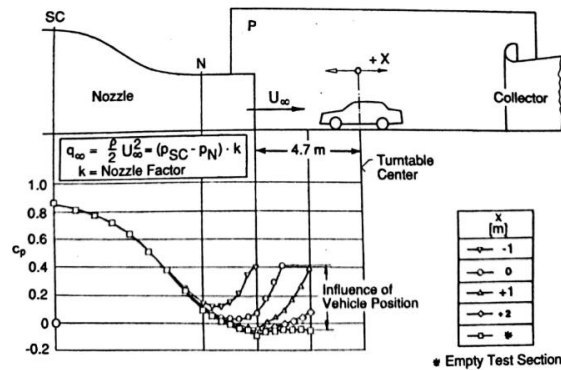
2. The increase in velocity along the axis differs from that along the walls.

While it is monotonic along the axis, the velocity along the walls does not increase monotonically. It goes through a local minimum after the inlet and through a local maximum in front of the exit. Accordingly, there are two regions of adverse pressure gradient, making the wall flow tend to separate. These separations have to be avoided because, first, after reattachment the boundary layer is thicker than without separation and, second, large-scale separation can cause fluctuations in the flow.

If the nozzle is too short the boundary layer at its exit will be thick (because of separation and reattachment); furthermore, the velocity profile may show an overshoot. On the other hand, if the nozzle is too long the boundary layer will also be thick because it will grow along longer walls. But above all, a long nozzle will increase the construction cost of the complete tunnel.

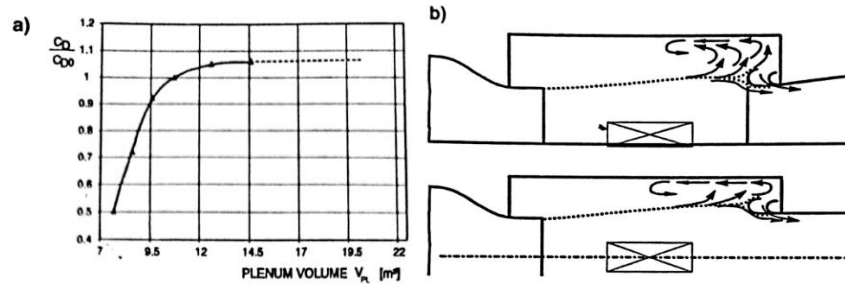
In a wind tunnel with an open test section there are alternatives for the location where the downstream pressure for the pressure difference is measured. The first is the same as for a closed test section. The pressure P_N at a location downstream in the nozzle, close to its exit, is used as the downstream pressure. This method is called the "nozzle method".

Technically, two solutions are available for adjusting wind speed: variable-pitch blades at constant fan speed, and continuously variable fan speed with fixed blades. Today, the latter is used more widely. Variable pitch permits a very quick change of wind speed. However, this advantage is offset by a high noise level at *all* wind speeds, including idle. For test engineers and craftsmen who have to work on a model in a tunnel between two runs while the fan is idling, this is unacceptable.



Plenum

For an open-jet wind tunnel the dimensions of the plenum surrounding the test section have a significant influence on the flow pattern inside the plenum and inside the jet, and thus on the test results from the wind tunnel. Drag is under predicted if the volume of the plenum is less than a specific minimum value. By means of flow visualization has demonstrated that the free jet widens if the walls of the plenum are too close to the jet i.e., if the volume of the plenum is too small. Not only the volume but also the width and height of the plenum have to be properly matched to the jet's dimension; further details are found m.



Limitations of Simulation

Systematic Errors

When a ride on the road is simulated in a test facility (be it a wind tunnel or a derivative thereof like a climatic tunnel or a dynamometer with wind) the realities of the road are approximated by idealizations; these are uniform distribution of velocity and temperature, extremely low turbulence, low noise. However, this kind of idealization is difficult to achieve, mainly for three reasons:

1. On the road a vehicle moves through a space of infinite dimensions ("free air"); in contrast, the dimensions of a wind tunnel's test section are limited and comparatively small.
2. Instead of being quiet, a wind tunnel is extremely noisy if no specific precautions are taken during its design.
3. Generally, the relative motion between vehicle and road is not reproduced; the same is true for rotation of the wheels.

All three kinds of imperfection generate systematic errors and these must be quantitatively known:

- During the design of a wind tunnel in order to decide which of them can be avoided a priori by proper layout and which can be tolerated because test results can be corrected a posteriori.
- In order to select a proper existing test bed with respect to its quality and cost.

Representation of the Road

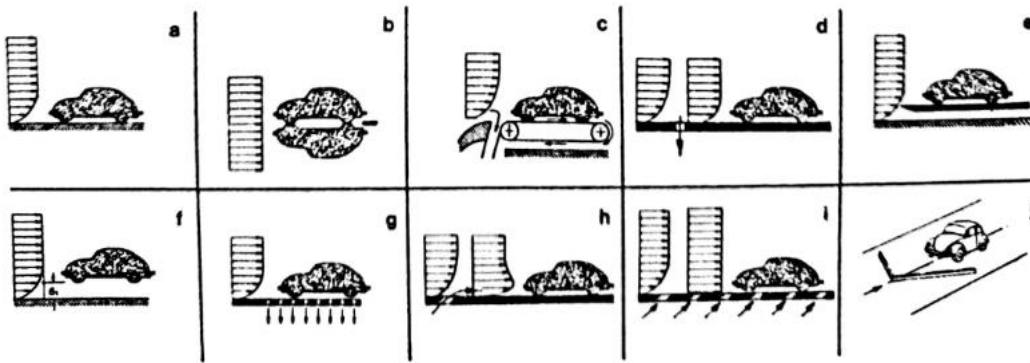
Technically, it is feasible to reproduce both the relative motion between vehicle and road and the rotation of wheels in a wind tunnel. The proper measure is a moving belt spanning the test section's width, and on which the vehicle's wheels roll. However, as will be shown below, the related effort is large. Consequently, simpler techniques for simulating both motions have been developed, or are still under development.

In principle there are two other ways to represent the road:

1. The first is to mechanically decouple the linear (horizontal) motion of the road and the rotational motion of the wheels, but still reproduce both of them. This uses a "narrow" belt for the moving road, and a separate system for rotating the wheels. Although it has limitations (with respect to flow conditions near the wheels) this can still be called a reproduction.
2. The second is made up of several methods which, over the years, have been developed to simulate the road. In most cases, the rotation of the wheels is neglected.

The various techniques for either reproducing or simulating the road are compiled the full wheel load of a car. They developed a wheel suspension that permits the wheel load to be reduced and accurately controlled. A drawback of this procedure is that the aerodynamic resistance due to ventilation of the wheels (in still air), which is part of aerodynamic drag, is included in the rolling resistance suggested how to correctly isolate this drag component. However, this result should not be generalized; the drag

change-in this example a reduction-is the result of three distinct and partly opposing effects:



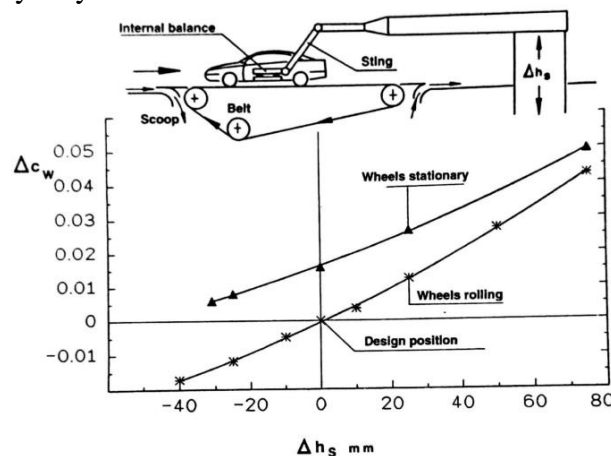
Generally the drag of a body increases when the floor moves.

- The drag of stationary wheels increases when the boundary layer of the ground floor is removed (by a belt, for example).
- The drag of wheels may be reduced when they rotate
- These three effects can well add up to a drag increase when the floor is moving.

Closed Test section

Three types of boundary perturbation

- Solid blockage.
- Wake blockage.
- Horizontal buoyancy.



The effective velocity in the test section is altered (blockage) and axial pressure gradients are generated (horizontal buoyancy).

Solid blockage (SB): With a finite blockage ratio the solid tunnel walls constrain the streamlines of the flow around a test body from diverging as much as they would in free air. Consequently, the local flow-field velocities in the vicinity of the body are greater (relative to the velocity of the oncoming air) than they would be in free air, leading to a higher drag force than in free air.

Wake blockage (WB): The wake of a test body creates a velocity defect in the core of the airstream behind the body. This velocity defect represents a reduction of the effective cross-section remaining open for the flow, inducing an interference velocity, $u_{WB}(x)$. This is corrected for by considering only its value at the model center. The $u_{WB}(x)$ is plotted (schematically) in Fig. 13.49(b), together with the corresponding change in pressure cp_{WB} (again at the ceiling), which is not symmetrical. The overall pressure gradient $\Delta cp_{WB}/\Delta x$ causes a horizontal force called wake buoyancy.

Horizontal buoyancy (HB): The thickness of the boundary layer at the solid walls is growing from the test section inlet to outlet, causing the velocity of the inviscid core to increase along. The test section axis and thus producing a decrease in static pressure. The nose-to-tail decrease in pressure $\Delta C_{DHB}/\Delta x$ generates a drag-type pressure force ΔC_{DHB} on the test body that is not present in free air. In many wind tunnels (but not in all) the horizontal buoyancy force is negligibly small because the pressure gradient in an empty test section is compensated by slightly increasing the cross-section of the test section along its axis. The displacement effect of the boundary layer at the tunnel walls generates an increase in speed for the inviscid core of the test section. This, however, must not be corrected because it is taken into account when the tunnel is calibrated.

The basic mechanism of increased drag due to both wake buoyancy (WB) and horizontal buoyancy (HB) is the same. The non-uniformity of velocity across the tunnel airstream reduces the duct's effective flow area. In both cases the reduction of effective area is greater downstream of a test body than upstream of it, making the downstream pressure less than the upstream value thus generating an extraneous drag-type pressure force on the body that is not present in free air.

Open Test section

For a Long time it was the common perception that an open test section did not need any corrections. A solid-blockage correction (as computed with rules borrowed from aeronautics) was so small that it was generally neglected. Furthermore, it was believed that a buoyancy correction was unnecessary as well because it was tacitly assumed that the airstream of an open test section has no axial pressure gradient, since this is inherent for an ideal free jet. They were able to identify five major perturbations and to compute their effects on the flow using elementary flow models. Their fundamental premise is the same as for the closed test section: The effect of each perturbation-with the exception of the axial pressure gradient of the jet-is to alter the velocity of the oncoming wind these five perturbations are:

1. Jet expansion
2. Jet deflections
3. Nozzle
4. Collector.
5. Pressure gradient

Accordingly, the dynamic pressure is corrected as follows:

If nozzle blockage has been corrected for in advance must be omitted. In the following the physical background of each individual factor will be explained briefly; numerical models for computing them.

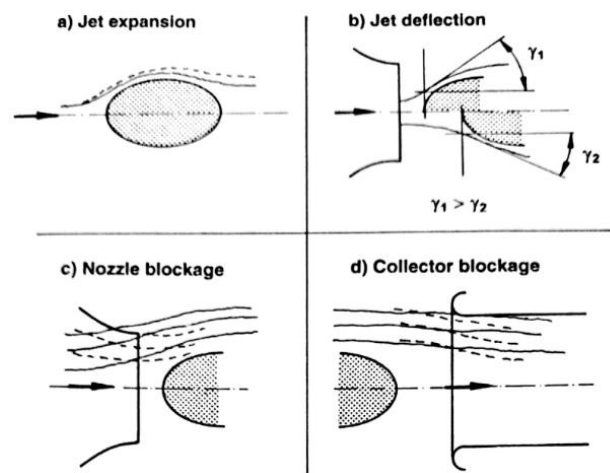
Jet expansion (solid blockage): in an open test section the free boundaries of the jet allow the streamlines around a model to widen more than in free air. With a larger flow area between a model and the jet boundary the local air speed is lower. Consequently the forces acting on the model are smaller. This can be interpreted as the velocity of the oncoming flow being lowered by an amount. The jet expansion factor (solid blockage) can be computed with a model similar to that used for closed test sections. The test object is replaced by a model made from a source-sink configuration. The jet boundaries are generated by reflecting this model at the jet boundaries. However, the boundary conditions are different from the closed test section. Now, at the location of the jet's (free) boundaries the speed and pressure must be the same as without the model. This is achieved by altering the sign of the source-sink arrangement for each new reflected image. Thus the speed on the axis of the original (central) model is lowered by the first-order image, increased a little bit by the second, lowered by an even smaller amount by the third, and so on. The alternating effect of these mirror images is the explanation of why in an open test

section the effect of solid Blockage is small (and of opposite sign) compared to closed test section.

Jet deflections: Because of the short usable length of the airstream in an open jet a model must be placed relatively close to the nozzle exit. To a deflection of the jet that can be interpreted as another expansion, and causes a further decrease in the velocity of the oncoming flow.

Collector blockage: The walls of the collector terminate the lateral spreading of the flow caused by a model and its wake. The flow into the collector is accelerated, and this has an effect as if the speed of the oncoming flow were increased.

Pressure gradient: the static pressure in an open (empty) test section is not exactly constant. In the first part of the test section the pressure gradient is negative, in the middle it can be zero, and it becomes positive farther downstream. The resulting pressure variation along the test section acts on an effective model volume that is 1.75 times larger than its actual volume, and generates a drag-type Horizontal buoyancy force.

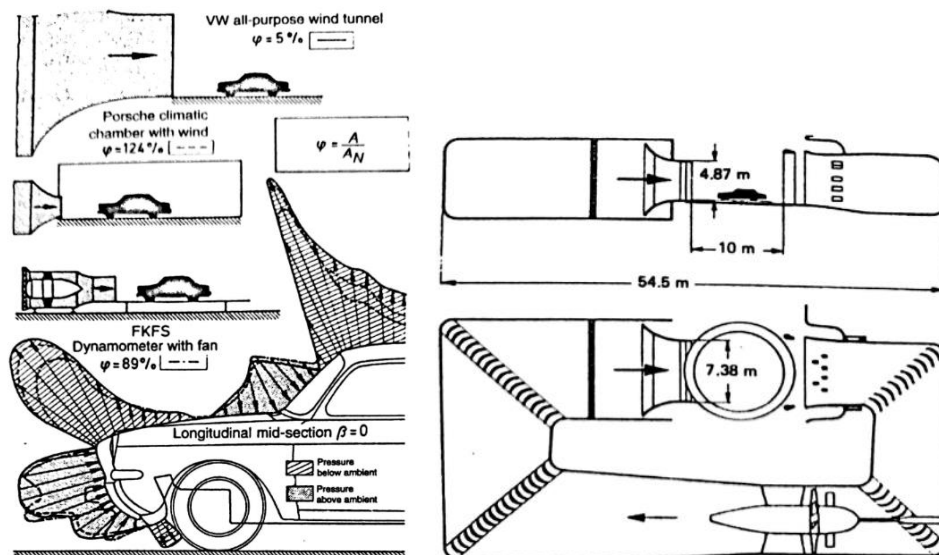


Full-Scale Wind Tunnels

The oldest full-scale wind tunnel dedicated to vehicle aerodynamics is located in Germany. This wind tunnel is distinguished by the exceptionally high blowing velocity of $U_{\max} = 270 \text{ km/h}$ ($= 168 \text{ mph}$). Such high velocity is advantageous for the development of fast vehicles, for instance race cars, even when Reynolds number effects are no longer expected. It allows direct examination of the effects of changing air forces and moments on a vehicle's attitude. Furthermore, the high maximum wind speed together with the large jet cross-section makes the tunnel well suited for experiments with 1:2.5-scale models of heavy commercial vehicles.

The largest automotive wind tunnel ever built was placed in operation by General Motors in 1980 in Warren, Michigan. The dimensions of its test section (closed, with atmospheric vent; cross-section $A_N = 56.2 \text{ m}^2$, length $L = 21.3 \text{ m}$) are adequate for testing even large commercial vehicles in full scale. Its maximum wind speed of $U_i = 250 \text{ km/h}$ (155 mph) is sufficient for tests with race cars. The side walls of the test section have a slight divergence of 0.24 degree to maintain constant static pressure along the axis of the empty test section. The tunnel is equipped with two six-component balances, one in a forward position for reduced-scale concept. The IVK aero-acoustic wind tunnel is now the quietest full-scale wind tunnel ever built. The maximum wind speed of the tunnel was reduced only 7 km/h by the damping measures.

Besides these large full-scale wind tunnels with cross-sections above $A_N - 20 \text{ m}^2$, two small full-scale wind tunnels have been built and one is presently under construction with cross-sections on the order of 10 m^2 .



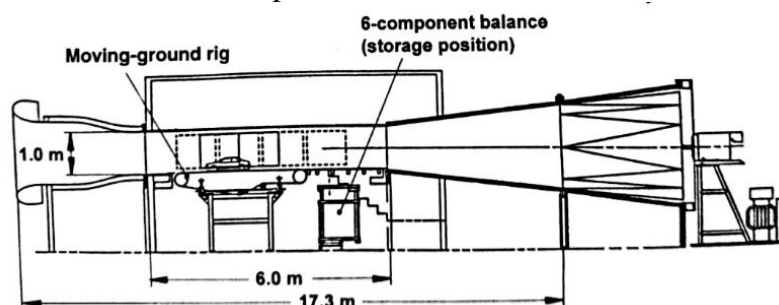
The cross-section of 11.75 m^2 of this tunnel is extremely small (the tunnel had to fit on a particular piece of land). However in a campaign of comparative measurements from different tunnels. The tunnel came out with surprisingly good results. In 1996 the fan-drive system was replaced. In particular, a new fan with 29 blades reduced noise level considerably, especially in the range of flow frequencies. It was designed by L.J. JANSSEN and opened in 1988. With a cross-section of only 10 m^2 it is the smallest full-scale wind tunnel of all. This is the consequence of having to be designed into an existing building. To attenuate fan noise, two dampers were installed: a novel patented one in the short section on the suction side of the fan which, because of its shape, is called a "mushroom-dampener" and a standard baffle-silencer as used in the air-conditioning systems of buildings in the return leg. This tunnel is very silent. The noise quality has been further enhanced by sealing a number of cavities on the outer end of the fan blades.

The sound level of the BMW aero-acoustic tunnel is so low that it permits assessments of subjective speech recognition. The tunnel is equipped with a six-component balance. Measures to reduce wind noise can be assessed with respect to their influence on drag in a single facility. Wheel rotation can be reproduced, and there is room in the frame of the balance for installing a "narrow" moving belt.

Wind tunnel Reduced-Scale Models

There are numerous wind tunnels for testing reduced-scale models, many of them in the academic world where they are only occasionally used for vehicle aerodynamics, and others specifically dedicated to vehicles.

The reduced wind tunnels of Porsche and Chrysler were built as pilot tunnels for the design of full scale tunnel and are now used as development tools during the small-scale-model phase of vehicle development,



There are two advantages for building a pilot tunnel in a comparatively large size. First, Reynolds number in the air path is closer to that of the later full-scale tunnel; thus, results therefrom can be reliably used for the design of the full-scale tunnel. Second, the pilot tunnel can be utilized for testing small-scale models of current scale. Besides the advantage of having such a tunnel at one's disposal this is attractive because, due to the exact geometric similarity between pilot and full-scale tunnel, results obtained with reduced-scale models are more easily transferred to the full-scale tunnel because any required data corrections are identical.

Reduced-scale wind tunnels can be built for very low cost and also the operating cost of such facilities is low, and flexibility is high. Both arguments are major reasons for the renaissance of small-scale testing. Low-turbulence smoke tunnel have been specially developed for flow observations on vehicles and their components. Water tunnels are especially well-suited for flow visualization. Mercedes-Benz employs the water tunnel of the Stuttgart University ($A_N = 1.16 \text{ m}^2$) for flow optimization in the very early phase of product development using 1:5-scale models.

Climatic Tunnels

Climatic tunnels can be classified into three groups according to their size, which is characterized by the jet's cross-section. The cross-sections A_N of the three groups are:

- 10-12 m^2 for cars, light-duty vehicles and, in extreme cases, buses.
- 6 m^2 for cars.
- 4 m^2 for cars.

The air paths of all three of these climatic tunnels come very close to that of typical aerodynamic wind tunnels. Their equipment-dynamometer, control of air temperature and humidity, sun load-makes them suitable for all kinds of thermal investigations relative to heating, ventilating, and air conditioning (and engine cooling, if no smaller and cheaper facility is available) A measuring precision of 0.5% can thereby be achieved. As an alternative it is also possible to take a photo from the vehicle; lenses with great focal lengths (1000 mm or greater) are used.

Using laser as a light source, frontal area measuring methods was developed that provide high precision results in small test room. Laser is mounted on a cross beam whose plane of movement is perpendicular to the vehicle's plane of symmetry. A laser-light detector is located behind the vehicle, which is also mounted on a cross beam and moves in a plane parallel to the plane. The movements of the laser and of the detector are synchronized; thereby, the outer contour of the vehicle can be scanned and the projected frontal area determined. If instead of the detector a CCD-array camera is mounted and a Marata screen is inserted between the vehicle and the camera the shadows forming on the Marata screen can be digitized and stored in a computer (ISRA method). The projected frontal area can then be integrated from these test data.

In another method instead of the laser light detector, a retro reflective screen is mounted behind the vehicle. The laser device, in whose optics the detector is simultaneously integrated, is situated on a transferring device. The outer contours of the vehicle are recorded when the laser beams reach the wall and are reflected there.

Road Tests

Road tests for the evaluation of the impact of aerodynamics on directional stability are mostly conducted in closed proving grounds. This is advantageous with regard to safety, reproducibility, cost, and confidentiality, especially for development tasks performed on early workhorses and prototypes. Additional tests on public roads are used to

gain ratings and standards for driving situations which cannot be simulated on the proving ground: stormy coastal roads, high bridges, passing manoeuvres.

Measurements in crosswind facilities are of particular importance for evaluating the correlation between aerodynamics and directional stability. In the open-loop test, no steering corrections are performed by the driver. Only the yawing reaction and the lateral course deviation of the vehicle under the effect of crosswind are measured.

Open-loop tests are generally conducted with the steering wheel held steady (fixed control). Comparative measurements indicate that tests with a released steering wheel have a slight tendency toward more pronounced course deviations. However, major differences between "fixed control" and "free control" were measured on a car-trailer unit. With the steering wheel fixed, this vehicle combination showed only a minimum course deviation; with steering wheel released, on the other hand, almost the same course deviation was obtained as for a "solo" car. These opposed results led to the conclusion that open-loop tests are insufficient for the assessment of the directional stability of cars towing a trailer, and that closed-loop tests are necessary.

The closed-loop method also includes the driver's reaction. When passing a crosswind facility, the driver has the task of keeping his vehicle on track by means of corresponding steering corrections. His steering activity can be measured, and the directional stability can be subjectively evaluated and rated.

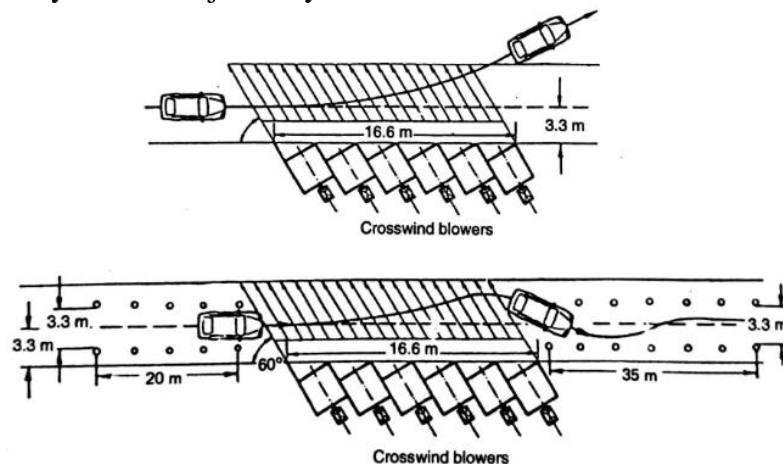


Fig. comparison of open loop and closed loop test methods.

Pressure Measurements

a) Pressure Probes

The simplest way to measure the dynamic and static pressure in a free airstream is to use a Pitot - static tube. The total pressure (or total head) g is measured at the opening in the probe's head and the static pressure p on the holes or slots farther downstream in the parallel part of the probe. The various types of Pitot-static tubes are in use. They differ mainly in the shape of their heads. Hemispherical, ellipsoidal and, occasionally, tapered "nose" are used as head shapes.

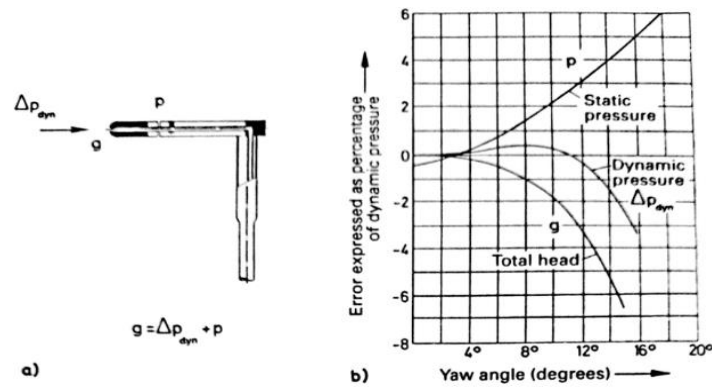


Fig. Error of Pitot tube due to Yaw

The Pitot-static tube provides accurate measurements in a free airstream. Its axis must coincide with the direction of the (local) flow, otherwise errors may occur. This error versus yawing angle is depicted for a semi-spherical head. It can be seen that up to 12° yawing angle the error in dynamic pressure is less than 1 %, which is acceptable for most measuring tasks.

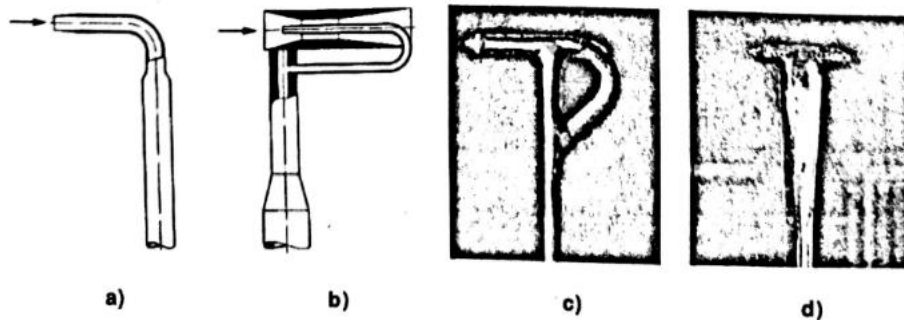


Fig. Types of probe: a) Pitot probe b) Kiel Probe c) 7 hole probe d) 14 hole probe

The sensitivity of the Pitot-static tube toward an oblique flow is greatly affected by the shape of its bead; ellipsoidal and semi-spherical heads. A special type of Pitot-static tube is the so-called total head tube which has no holes to measure the static pressure.

b) Pressure Transducers

The pressure probes are usually connected to pressure transducers by plastic hoses. Often the pressures to be measured are low, in the range of 10-1000 Pa. In most cases, the measurement of the differential pressures rather than the absolute values is required. The pressures measured in the wind tunnel operation very seldom exhibit constant values. Therefore, using test equipment with good dampening characteristics is advantageous if time-averaged pressure data are required. In the past, mainly liquid manometers were used. They are easy to handle. The risk of a defective operation is low due to the absence of signal conversion and, thanks to the inertia of the liquid columns, they possess good dampening characteristics.

The pressure transducers are mechanical or electrical types. Mechanical transducers operate with diaphragm or bellows to convert the pressure signal into a linear movement and transmit it to a gage. They are hardly used anymore in vehicle aerodynamics. Electric transducers convert the physical displacement, e.g., the bending of a membrane (diaphragm), into an electrical signal. Capacitive, inductive, or piezo-electric devices as well as strain gages are used as signal converters. Potentiometers are used more rarely. Electric transducers allow recording of data continuously by recorders or magnetic tape. Moreover, they offer the advantage of computerized data handling and

processing. They have almost completely replaced the "classical," U-tube-based test equipment.

The mechanical and electrical pressure transducers exhibit a clearly higher-frequency response range than liquid-column manometers. For this reason, additional dampening is required for most wind tunnel measurements to gain time-averaged data. This dampening can take place either on the pneumatic side, i.e., between the pressure sensor and the transducer input, or on the electric side, between the transducer output and the data recording.

To dampen the pressure oscillations prior to their conversion into an electrical signal, either resistance or volumetric dampening can be used. Resistance dampening is obtained by means of a long plastic hose with a diameter of 1 mm or less. Its length can be changed to achieve the desired dampening. Volumetric dampening is obtained in sections with large diameter which are inserted in the connection line between the sensor and the transducer. A combination of the two dampening types is advantageous when measuring very low pressures, as, for example, in the case of the measurement of the airflow through the passenger compartment. If signal dampening on the electrical side is preferred, an active filter between the transducer and data recording device enables the desired dampening to be obtained.

However, for certain tasks, for example, in aero-acoustics, the pressure oscillations must be resolved. In this case, the dampening of the pressure signal must be as small as possible. The use of a small, highly sensitive transducer very close to the measuring point without any connection hoses represents an effective test setup. Piezo-electric pressure transducers or measuring microphones are suitable for this type of measurement. If measurements are to be performed at many locations, as, for example, are needed for a pressure distribution on a vehicle body, a single pressure transducer can be used in combination with a scanner.

Each of the pressures to be measured is turned on the transducer for a preselected period. The pressures picked up by the individual pressure holes are led to the scanner via plastic hoses. The scanner, in turn, mechanically selects and connects each pressure hole to the pressure transducer. The advantage of using such a device is its ability to read a great number of pressure signals with only one (expensive) transducer. The disadvantage is that the mechanical component of the system wears out with time and thereby the system's reliability is reduced.

The alternative is to place miniature pressure sensors at each measuring point and, by the computer controlled scanning of these at a very high frequency (higher than 10,000 per second), a real-time recording of the pressure distribution (using up to several hundred measuring points) is possible. This type of electronic scanning does not have any mechanical-wear components, and in the case of a large number of points, can be very time efficient. However, due to the large number of transducers, it is extremely expensive.

c) Measurement of the Airflow Velocity

Velocity measurements in a wind tunnel include the determination of the (overall) wind tunnel operational air speed and (local) air speeds outside and inside a vehicle. In addition the measurement of velocity fluctuations, the "turbulence," may also be required. The airflow velocity can be determined by means of a Pitot-static tube (Prandtl-tube). Wind speed can be computed from the dynamic pressure as follows:

$$v = \sqrt{\frac{2}{\rho} \Delta p_{\text{dyn}}}$$

where

- v = the airflow velocity (m/s)
- ρ = the air density (kg/m³)
- Δp_{dyn} = the dynamic pressure (Pa)

The air density changes with temperature, atmospheric pressure, and humidity as follows:

$$\rho = \frac{349p - 131p_e}{T}$$

where

- T = the absolute temperature (K)
- p = the atmospheric pressure (bar)
- $p_e = U \cdot E/100$ is the partial pressure of the water vapor in the air (bar)
- U = the relative air humidity (percent)
- E = the saturation vapor pressure at T (bar)

d) Determination of the Airflow Velocity outside and Inside a Vehicle

The Pitot-static tube can be used to determine the airflow speed when the flow is steady and direction of flow is known. However, at low wind speeds the accuracy of this probe is not satisfactory, and other more suitable probes must be used below 3 m/s. A typical probe offering good service at low speeds is a miniature vane-type anemometer.

This vane anemometer consists of a small vane wheel (diameter 10 mm and above), which is mounted co-axially in a cylindrical housing. The rotational speed of the vane wheel is a measure of the wind speed. The conditions required for a correct reading are the same as for the Pitot-static tube: The airflow must be steady and the vane wheel axis must coincide with the direction of local flow. The tolerable yawing angle until 1 % accuracy impairment is approximately 5-7° for an anemometer furnished with a cylindrical housing. However, this tolerance limit can be increased up to a yawing angle of 15-30° if the anemometer housing is aerodynamically optimized.

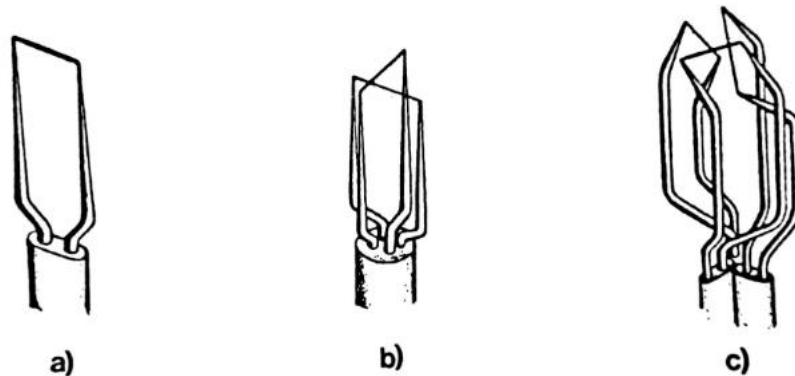


Fig. Hot wire probes for velocity measurements in one dimensional, Two dimensional, Three dimensional

On the other hand, housing shapes have also been developed which by intention are very sensitive to yaw. Due to their easy handling, vane anemometers are very popular in vehicle aerodynamics. The principle behind hot-wire anemometers is based on the fact that the heat loss of an electrically heated wire subjected to airflow increases with increasing wind speed. Since the electrical resistance of the wire depends on its temperature, the resistance variation of the wire exposed to airflow can be used to measure the airflow velocity. The wire normally is made of tungsten, plated either with gold or platinum.

Measurement of Flow Direction

A correct speed measurement in a free airstream requires that the flow direction at the measuring point be known. The simplest way to correctly position a speed sensor in the airstream is to determine the flow direction in the concerned area by means of a wool tuft attached to the end of a thin stick.

If a measurement of flow direction is to provide detailed information about a velocity vector. Special devices can be used for this purpose (yaw meters). These probes are divided into two main groups: The first group operates on the basis of measuring the pressure difference at symmetrically positioned measuring points of a sensor. The second type of sensor is the hot-wire anemometer with multi-sensor probes. In the pressure-difference measurement method, the pressures are measured in orifice pairs placed axial-symmetrically on a probe. Their pressure difference is zero when the flow direction coincides with the symmetry plane of both measuring points. Two different approaches are applied to determine the yaw angle:

- The probe is rotated around one or two axes as long as the pressure difference between the two orifices is equal to zero; the angle(s) is (arc) read on a scale. This zeroing method is very accurate but slow. Since the adjustment is generally done by hand.
- The yaw angle is determined by means of a previously established calibration curve showing the pressure difference versus yaw angle.

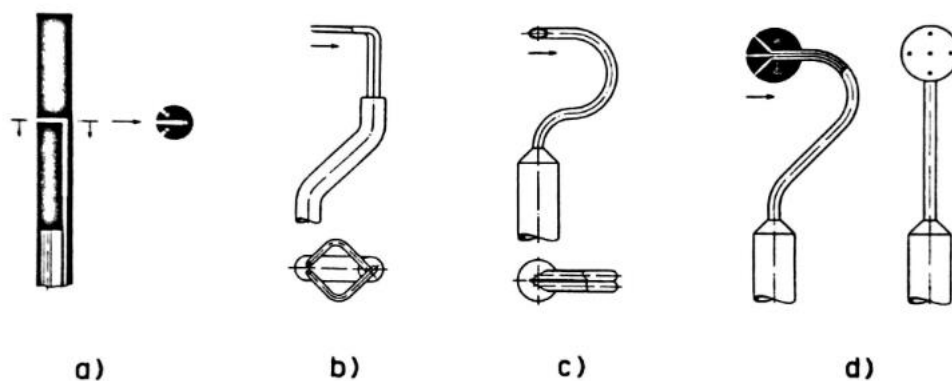


Fig. Measurement of air flow direction

Temperature measurement

Temperature measurements in vehicle aerodynamics have to meet two objectives:

- To determine the performance of vehicle systems such as engine cooling passenger compartment heating and cooling, as well as window defogging and defrosting.
- To investigate the temperature level of vehicle components such as brakes, plastic parts which may be damaged if exposed to high temperatures, etc.

Two types of investigation may be required:

- Measurement of the temperatures at individual locations.
- Measurement of the temperature differences between two locations.

The first type usually covers most test requirements. If, however, a heat balance has to be established during a performance test, it is necessary to measure temperature differences of air or coolant with great accuracy.

a) Temperature sensors

Thermocouples are the most common temperature sensors used for vehicle testing in a wind tunnel. The thermocouple consists of a pair of electrically conductive wires made of dissimilar metallic conductors, soldered or welded at both ends. When the two junctions are exposed to different temperatures, an electrical potential (electromotive force,

EMF) is set up between them which is approximately proportional to the temperature difference. A voltmeter in the circuit can thus measure the temperature difference. If one of the junctions is carefully maintained at a standard reference temperature, i.e., 0°C , the second junction can be used to measure the temperature at any desired point. The reference junction can also be simulated with an electrical compensation circuit.

The most commonly used thermocouples and their ISA (Instrument Society of America) identification codes are:

Base-metal thermocouples:	ISA code
Copper-Constantan	T
Iron-Constantan	J
Chromel-Alumel (equivalent to Nickelchrom-Nickel)	K
Noble-metal thermocouples:	
Platinum-10 % Rhodium Platinum	S

Copper-constantan and iron-constantan thermocouples are preferred for the temperature ranges of -200°C to $+500^{\circ}\text{C}$ and 700°C , respectively. Both these thermocouples produce high EMFs, but they tend to oxidize at high temperatures. Chromel - alumel thermocouple (corresponds to nickel chrome - nickel) can be used at Heat transfer by conduction occurs when the temperature on the surface or inside a solid body has to be measured. In a liquid or gas, the heat between medium and sensor is transferred by convection. If a high-temperature component is located close enough to the sensor, a measurement error due to the radiation of the hot object will occur. The error due to conduction or convection will be high, if high temperature difference exists between the sensor and its connection cable.

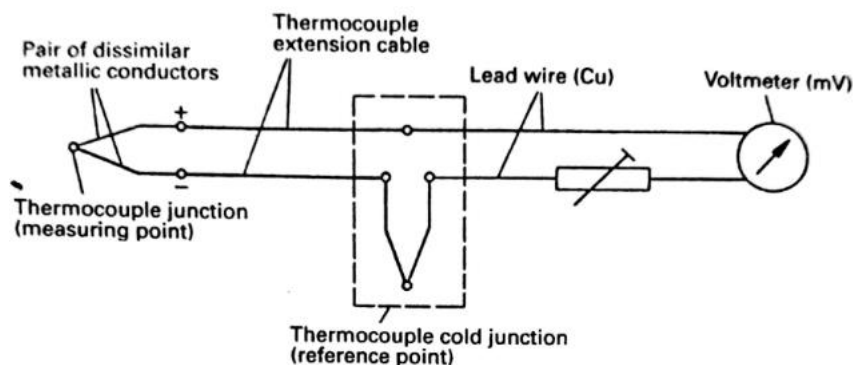


Fig. Temperature probe using Thermocouple

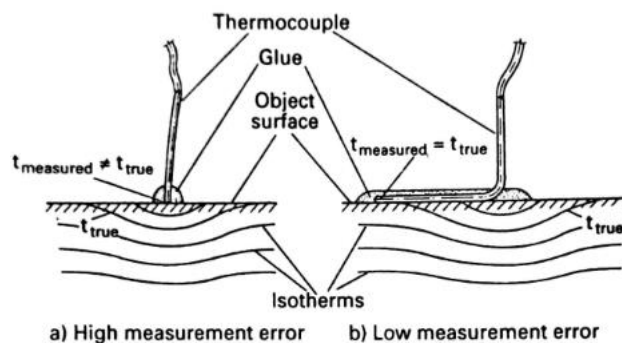


Fig. Error due to heat transfer between testing object and thermocouple

The error increases with lower thermal conductivity coefficient of the measured object, higher thermal conductivity and convective heat transfer coefficient (relative to the

air) of the sensor, and poorer contact between the sensor and the test object. In the measurement of the surface temperature of plastic or rubber components, each or all of these unfavourable conditions must be taken into consideration. If a certain length of the probe bead (or cable) is glued to the surface, the thermocouple junction which actually measures the temperature is still exposed to the actual surface temperature. The longer the glued piece is, the smaller the error. The heat conduction of the sensor increases with an increasing diameter. The thermal properties of the test object must not be changed by the measures introduced to improve the measuring accuracy. The thermocouple cable is glued onto a surface. The convective heat-transfer coefficient of the cable and adhesive should be as close as possible to that of the test object. This is especially important if the object to be measured is small. When temperatures of a solid object are to be measured, similar means to those described for surface-temperature measurements should be used to minimize any change of the initial isotherms of the test object.

Road Testing Methods

Drag measurements are generally performed in a wind tunnel. Therefore, various methods have also been developed to measure the C_D outside the wind tunnel i.e., on the road. However, due to uncontrollable environmental conditions on the road, the confidence in these measurements is limited. Furthermore, a precise separation of aerodynamic drag and mechanical resistances is difficult.

The test vehicle is first accelerated to high speed and then is made to coast freely by disengaging the engine. The change of the vehicle speed is continuously recorded. The deceleration occurs by means of the resistances acting on the vehicle, namely the aerodynamic drag and mechanical resistances.

$$m(1 + f) \frac{dV(t)}{dt} = D_M + D_A$$

Where

m = the vehicle mass (kg)

f = the effective mass increase of the vehicle taking into consideration the rotating masses

$V(t)$ = the vehicle speed versus time (m/s)

D_A = Aerodynamic Drag

$$f = \frac{\frac{I_d}{r_d^2} + \frac{I_o}{r_o^2}}{m}$$

Where

I_d = the moment of inertia of the rotating components of the driveline including the wheels of the driven axle (Nms^2)

I_o = the same value of the non-driven axle (Nms^2)

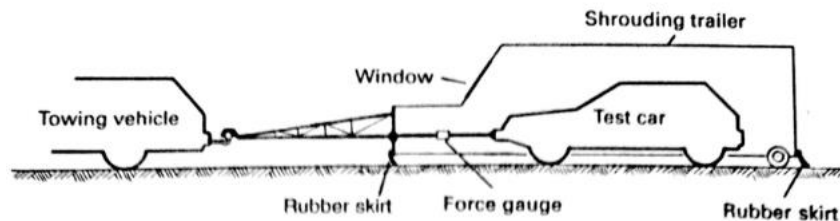
r_d and r_o = the dynamic rolling radii of the tires on the driven and non-driven axles, respectively (m)

One method to determine the mechanical resistance is to conduct laboratory tests. However, the confidence in this procedure is not satisfactory. The main difficulty consists in accurately measuring the rolling resistance of the tires. Considerable differences are found in measurements on drums outside or inside surface of a drum may be used) compared to level road. Furthermore, the additional tire rolling resistance caused by the vehicle suspension geometry (i.e., wheel camber, toe-in) must also be considered.

The shrouding trailer has wheels at the rear end and is connected to the tractor vehicle by a trailer hitch. The connecting rod to the test vehicle (inside the shrouding

trailer) has a sensor to measure the towing force. The side walls of the shrouding trailer are equipped with rubber skirts which are in contact with the road surface so that the test vehicle is fully enclosed, its aerodynamic drag thus being equal to zero.

This method eliminates all disadvantages of the previous one, if the measurement of the mechanical resistance occurs immediately after the coast-down test. However, a disadvantage is the fact that the driver of the test vehicle must perform some steering correction in order to not deviate from the course of the pulling vehicle. This necessarily increases the mechanical drag. Furthermore, for safety reasons, the test speed must be limited when driving two vehicles in a pair. To obtain reliable results, the entire test run should be repeated several times and the results averaged out.



Cross wind test

The crosswind sensitivity of a vehicle can be assessed if the vehicle is subjected to an artificially created crosswind gust during a straight-ahead drive on the road. The vehicle's lateral deviation from the initial straight-ahead direction is usually considered as a characteristic parameter. Crosswind tests can be performed in two ways:

- The driver does not apply any steering correction. During the entire test, the steering wheel is held either in its original position (fixed control) or it remains untouched by the driver (free control).
- The driver attempts to minimize the lateral deviation of the vehicle by steering wheel corrections.

The first method considers the reaction of the vehicle alone; therefore, it is well-suited for comparative tests. The second method includes the driver's reaction; thus the test result depends also on the driver. However, the second procedure has the great advantage that the closed control circuit made up by driver, vehicle, and road is reproduced and is very close to a real-life situation.

The vehicle lateral deviation can be measured in two ways:

- The driver enters the test track at a given orientation line, parallel to the battery of the crosswind generators. During the test, the position of the vehicle is marked on the road by a colour-spraying gun or picked up by sensors inserted under the road. Also, photography sequences of the front of the vehicle are used for this purpose.

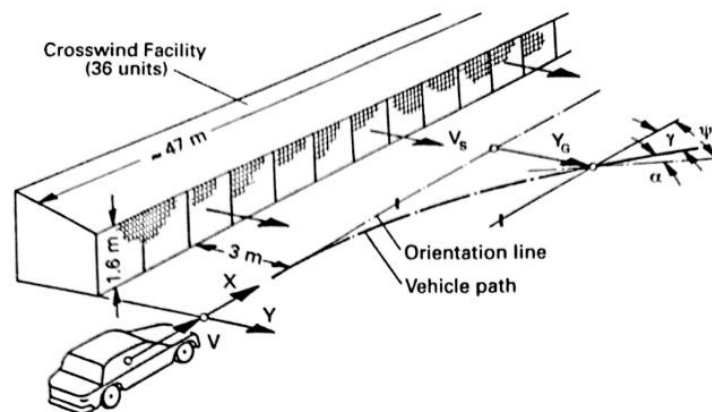


Fig. Cross wind test

- Measurement devices mounted in the vehicle record the course of the vehicle before and during the test. The equipment used to measure its lateral movement is based on the exact measurement of the vehicle lateral acceleration. The lateral deviation of the vehicle is found through the two successive integrations of the acceleration signal. In order to measure the lateral acceleration, tube accelerometer is mounted on a gyroscopically stabilized platform, i.e., during the entire test it maintains its original horizontal position in an earth-related coordinate system. Finally, the vehicle speed must be accurately recorded in order to define the vehicle lateral deviation from its original course parallel to the blowers.

Method (a) is quick, easy to perform, and does not need any complicated test equipment. However, it is less accurate than the second method. One source of error is the difficulty in entering the crosswind gust with zero yawing angles, due to the steering corrections of the driver immediately beforehand. This error does not occur when using a gyroscopically stabilized test device (method (b)); if recording of the lateral deviation is started before the vehicle enters the crosswind.

It can be easily demonstrated that the crosswind sensitivity of a vehicle does not depend only on its aerodynamic properties. Its behaviour is, for example, affected by changing the tire pressures front and rear in two consecutive tests. Although the aerodynamic coefficients do not change, the vehicle's Lateral deviation produced by the crosswind considerably increases when the vehicle has a greater tendency to oversteer; that is, for instance, when the tire pressures of the front wheels are higher and those of the rear wheels lower.

Flow visualization Techniques

Visualization of the flow on a vehicle body and the airflow patterns in the passenger and engine compartments is an effective method for optimization of these now fields. The flow pattern on the surface of the vehicle body can be very easily visualized with wool tufts. The areas of attached or separated flow are clearly visible. However, applying the wool tufts to a vehicle body is rather laborious; therefore this "classical" technique is hardly applied any more. Another possibility of visualizing the flow on the surface is the application of a surface oil film containing collared or luminescent pigments.

A frequently used device is the smoke generator. By blowing smoke into an airstream, the course of the airflow becomes visible. In the most commonly used smoke generators, an alcohol/water mixture is heated. A thick non-toxic vapour (wrongly called "smoke") develops, which is injected into the airstream with long thin stem. There are two methods: Either the smoke is introduced into the undisturbed flow ahead of the vehicle, which makes streamline patterns visible as, for example, depicted in or the smoke is introduced into the separated flow, where it fills the entire dead water up to the separation point. Good illumination is a prerequisite for flow visualization. Light of a high performance laser is first led through a cylindrical lens and then deflected with a mirror in such a way that the vehicle can be illuminated in each desired section in full width, length, or height. The thickness of the light sheet can be set between a few millimetres and several centimetres.

If the flow pattern in a region of separated flow is investigated, a bubble generator can be used. Helium-filled soap bubbles are introduced into the airflow and their movements photographed. If the exposure time is well chosen, the overlapping flow patterns are clearly visible.